INFORMATION TO USERS

This reproduction was made from a copy of a document sent to us for microfilming. While the most advanced technology has been used to photograph and reproduce this document, the quality of the reproduction is heavily dependent upon the quality of the material submitted.

The following explanation of techniques is provided to help clarify markings or notations which may appear on this reproduction.

1. The sign or "target" for pages apparently lacking from the document photographed is "Missing Page(s)". If it was possible to obtain the missing page(s) or section, they are spliced into the film along with adjacent pages. This may have necessitated cutting through an image and duplicating adjacent pages to assure complete continuity.

2. When an image on the film is obliterated with a round black mark, it is an indication of either blurred copy because of movement during exposure, duplicate copy, or copyrighted materials that should not have been filmed. For blurred pages, a good image of the page can be found in the adjacent frame. If copyrighted materials were deleted, a target note will appear listing the pages in the adjacent frame.

3. When a map, drawing or chart, etc., is part of the material being photographed, a definite method of "sectioning" the material has been followed. It is customary to begin filming at the upper left hand corner of a large sheet and to continue from left to right in equal sections with small overlaps. If necessary, sectioning is continued again—beginning below the first row and continuing on until complete.

4. For illustrations that cannot be satisfactorily reproduced by xerographic means, photographic prints can be purchased at additional cost and inserted into your xerographic copy. These prints are available upon request from the Dissertations Customer Services Department.

5. Some pages in any document may have indistinct print. In all cases the best available copy has been filmed.

University
Microfilms
International

300 N. Zeeb Road
Ann Arbor, MI 48106

Meller, Menachem M.

THE STRUCTURE AND OPERATING CHARACTERISTICS OF HIGH VELOCITY FLUIDIZED BEDS

City University of New York PH.D. 1985

PLEASE NOTE:

In all cases this material has been filmed in the best possible way from the available copy. Problems encountered with this document have been identified here with a check mark __√__.

1. Glossy photographs or pages __✓__
2. Colored illustrations, paper or print _____
3. Photographs with dark background __✓__
4. Illustrations are poor copy _____
5. Pages with black marks, not original copy _____
6. Print shows through as there is text on both sides of page _____
7. Indistinct, broken or small print on several pages _____
8. Print exceeds margin requirements _____
9. Tightly bound copy with print lost in spine _____
10. Computer printout pages with indistinct print _____
11. Page(s) _____ lacking when material received, and not available from school or author.
12. Page(s) _____ seem to be missing in numbering only as text follows.
13. Two pages numbered _____. Text follows.
14. Curling and wrinkled pages _____
15. Other _____

THE STRUCTURE AND OPERATING CHARACTERISTICS OF HIGH VELOCITY FLUIDIZED BEDS

by

MENACHEM M. MELLER

A dissertation submitted to the Graduate Faculty in Engineering in partial fulfillment of the requirements for the degree of Doctor of Philosophy, The City University of New York.

1985

This manuscript has been read and accepted for the Graduate Faculty in Engineering in satisfaction of the dissertation requirement for the degree of Doctor of Philosophy.

11/19/84
date

Professor Herbert Weinstein
Chairman of Examining Committee

11/19/84
date

Professor Paul Karmel
Executive Officer

Professor Alberto I. LaCava

Professor Reuel Shinnar

Professor Gabriel Tardos
Supervisory Committee

The City University of New York

Abstract

THE STRUCTURE AND OPERATING CHARACTERISTICS
OF HIGH VELOCITY FLUIDIZED BEDS

by

Menachem M. Meller

Adviser: Professor Herbert Weinstein

An experimental investigation of the parameters that determine local solids holdup in a transported gas-solid fluidized bed is reported. Knowledge of the local solids holdup is necessary both to predict the axial pressure gradient in the fluid bed as well as to evaluate the performance of the fluidized bed for a particular process. Such information is essential to assure smooth operation of the equipment, good contact between gas and solid, and have some measure of the system power consumption.

The experimental system consists of an 8.5 meter high, 15.2 cm. I.D. recirculating bed. Two different silica-alumina cracking catalysts were used, which differ mainly by a density ratio of 1.4. Gas velocities ranged from 0.65 to about 6.0 m/s and solid rates approached 150 Kb/m^2 sec for the heavier catalyst. Axial solid density profiles were measured using a series of differential manometers. A method

for measuring radial solid profiles using X-ray absorption was explored. The radial density distribution measurement was based on inverting side-on absorption data using a chordal absorption technique.

The axial solid fraction profile often exhibits, for either solid, a variation from a relatively high value in the bottom section of the bed (dense phase) through a transition region in the middle of the bed which contains an inflection point, to a low value (dilute phase) in the top section of the bed. The position of the point of inflection is shown to depend upon the pressure drop imposed across the bed as well as gas and solid rates. Raising the imposed pressure drop, raising the solid rate or decreasing the gas rate all have the effect of raising the inflection point in the density profile.

Experiments have shown x-rays to be suitable for non-disruptive solid density variation measurements. These experiments confirm the existence of a core-annular radial density profile. Preliminary experiments indicate that this type of profile applies for both turbulent and fast fluidization. The X-ray images at three axial positions in the fast fluidized bed, corresponding to the dense phase, dilute and inflection point positions show relative agreement with the densities determined from the axial pressure gradient.

Acknowledgments

I would like to express sincere gratitude and appreciation to my friend and mentor Professor Herbert Weinstein for his help and guidance.

I would also like to thank the entire faculty and staff of The City College - Chemical Engineering Department without whom this project could not proceed.

Special thanks to my fellow graduate student Manjun Shao who helped in obtaining the experimental results.

The following organizations supplied materials or funds needed to carry out the experimental work.

1. Exxon Research and Engineering
2. W. R. Grace and Company
3. National Science Foundation - Grant CPE-8103627

Table of Contents

List of Figures

List of Tables

Nomenclature

A - Cross sectional area of the bed.

d - Distance from x-ray source to bed centerline.

d_p - Volume-surface mean diameter; $d_p = 1/\sum(x_i/d_i)$

d_i - Particle diameter in a given size cut.

ELR - Energy Loss Ratio - defined on page 29.

G_a - Galilleo number

G_s - Solid rate per unit bed area.

g - Acceleration due to gravity

h_i - Inflection point height or pressure "head".

I - Inventory height.

$I(\lambda)$ - X-Ray intensity.

I_0 - Reference x-ray intensity.

L - Length of bed.

ΔP_f - Frictional pressure drop.

ΔP_s - Slow bed pressure drop.

$\frac{\Delta P}{\Delta L}$ - Pressure drop per unit bed length.

r - Radial coordinate of the bed.

U_o - Superficial gas velocity.

U_c - The velocity at which the pressure fluctuations across a bubbling bed begin to diminish from their peak value.

U_k - The onset of the turbulent regime.

U_{slip} - Slip velocity.

U_t - terminal velocity of a particle of size $\bar{d}_p$

U_{tr} - Transport velocity.

U_{pt} - Velocity of onset of pneumatic transport.

V_s, U_s - Mean solid velocity

x - Chord distance coordinate.

Greek Symbols

α - Chord angle.

ℓ - Path length in "ring method" of chordal absorption technique.

ϵ - Void fraction

$\bar{\epsilon}$ - Average void fraction.

ϕ - Sphericity of particles.

ρ - Density.

$\bar{\rho}$ - Bed density.

μ - Absorption coefficient.

1.1 - Introduction

Fluidization is a unit operation for contacting fluid and solids in which the solids are suspended or buoyed in the fluid stream. Specifically, the interest herein is in gas-solid systems. These systems exhibit what is known as aggregative fluidization. Many of the important properties of a gas fluidized bed, such as fluidlike character, enormous surface of contact between gas and solid, high thermal conductivity, and high gas treating capacity were recognized from the onset of its development. A statement to this effect can explicitly be found in Lewis and Gilliland's historic patent on hydrocarbon catalytic cracking in (downflow) bubbling beds (patent number 2,498,088).

Since then however the fluidization field has expanded to include other applications of the bubbling bed as well as to other modes of operating the cracking operation. This work is concerned with the high velocity (upflow) mode of fluidization. However, it is useful to briefly trace the development of fluidization, the various modes of operation of fluidized beds, as well as how choice of mode may have been made in the past.

Much of the early work of Gilliland and coworkers, on the fluidization of fine particles in a gas stream (1940), focused on measuring voidage and slip velocities for a particular set of operating parameters. The urgency of the war effort to produce high octane aviation fuel left them either uninterested or unable to offer a more general

understanding of such phenomena. It may have been this incomplete understanding which shortly thereafter caused the catalytic cracking industry (Esso et al., 1942) to alter their design from upflow to downflow mode, i.e. high velocity to bubbling beds, after only three such upflow mode units (SOD model 1) were constructed. This incomplete understanding was specifically cited as the cause for poor reactor performance of the SNG to gasoline plant at Brownsville, Texas in the 1950's. More global understanding must be found in order that such disasters do not recur in the presently proposed coal to hydrocarbon fluids processing schemes.

This work is focused on upflow or transported fluidized beds. Fast fluidization or high velocity fluidization are names which have been coined to describe this type of operation. In designing a transported fluidized bed system it is important to be able to predict the pressure gradient in the bed. This problem is a two phase analogy of fluid flow in a pipe. Unlike a fully developed pipe flow however, the two phase pressure gradient is found to depend on equipment parameters as well as the flow parameters.

The purpose of this investigation is to experimentally measure the solids holdup in a fast fluidized bed as a function of axial and radial location for various values of particle density, solid inventory, and gas and solid rates. These data are used to develop a better understanding of the physical phenomena governing these flows.

The experimental measurements of axial and radial variations of solids holdup (solids fraction) in the high velocity fluidized bed were carried out by totally different procedures. The former was obtained from differential pressure measurements while the latter was obtained from x-ray absorption density measurements. However, this thesis work was concluded with the radial density variation measurements only measured in an approximate manner. The methodology for making these measurements quantitatively is outlined. Although axial solids holdup measurements were made previously, most were done on bubbling beds. The other studies on transported beds are seen to be in disagreement with each other.

The second chapter of this thesis reviews the history and development of fluidized bed processes. This is followed in chapter 3 by a presentation of the analytical methods used in presenting the data. Chapters 4 and 5 present previous work followed by the experimental data for axial and radial density profiles respectively. Finally, the two data chapters are brought to a close with the discussion and conclusion chapters, 6 and 7.

This work demonstrates some of the important parameters that determine local solids holdup in a high velocity fluidized bed. These parameters have been shown to be solid and gas rates as well as system inventory. The need to include these variables in a fluidized process design is being emphasized here. Disagreements between previous

investigators can be traced to their lack of consideration of the pertinent inventory parameter.

1.2 - Scope

This work was carried out in an 8.5 m high recirculating high velocity fluidized bed system. The fast bed and companion bed inside diameters were 15.2 and 34.3 cm. respectively. Ambient air was used as the fluidizing medium. The experiments were performed using two types of silica alumina cracking catalyst, HFZ-20 and FCC catalyst, with mean particle diameters of 49 μm and particle densities of 1.45 and 1.07 g/cc respectively. Velocities used spanned the entire range of turbulent fluidization through pneumatic transport, about 1-5 m/sec, with emphasis on the high velocity regimes. Axial pressure gradient profiles were measured using a series of differential manometers which were aligned so that the profiles could be seen on obsevation. Radial density distributions were approximated by inverting side-on x-ray absorption data using a chordal absorption technique.

2.1 - History and Development of Fluidization

Fluidization (bubbling) was first used intentionally by Winkler in his historic patent (1922) on gasification of coarse (3 mm.) particles. He described the motion of solids as flowing freely, and the bed character as a bubbling liquid. Frazer and Yancey [10], working on an air-sand process for beneficiating coal (removing ash) at the Bureau of Mines, used the term "fluidized" to describe this expansion of fine particles as "boiling uniformly on the surface - feeling much like a liquid." We presume that with their term feeling they were well aware of the unusual transport properties - the high thermal conductivities, and the heat capacities the bed experiences. Odell [21] also worked with Frazer and Yancey extending this work to coarse particles and patented this process. It was his patent (1934) that was to become one of the legal claims for the developers of hydrocarbon cracking.

The development work for the fluidization technology of coarse and fine particles has taken two distinct paths. Coarse solids were associated with the above mentioned Odell patents, Winkler's gasifiers and Houdry fixed bed catalytic crackers, while fine solids were connected with the circulating beds developed later by Lewis and Gilliland. In order to understand what kept these technologies separate, and how each matured, it is necessary to have some knowledge about the metamorphosis of fluidization.

Eugene Houdry empirically discovered the catalytic

properties of natural silica-alumina, bentonite clays, on the cracking reaction [9]. He pelletized this catalyst and fed it to three fixed bed reactors which were operated cyclically for reaction and regeneration. Although these reactors gave essentially the same conversion of gas-oil as a thermal cracker (40%), the high octane produced motivated the effort. Commercialization of his first plant was achieved in 1938 with the aid of the Socony Vacuum (Mobil) and Sun Oil (Sunoco) companies.

A number of companies lacking the license rights to the catalytic process decided to try and develop a comparable process of their own. Their first attempt was with some experiments with a similar cyclic fixed bed unit. It immediately became apparent that a continuous mode of operation would be desireable to simplify operation and improve safety and product quality. The result was a moving bed process, a bed of solids gravitating countercurrent to air and/or gas-oil streams. This operation was scrapped due to the unwieldy operation of mechanical conveyors and to particle attrition.

In an attempt to circumvent the above problems, operation of the catalytic reactor was chosen in the horizontal pneumatic conveying mode. Particle size was now in the 100 micron range. Dilute powder suspensions 1-2 lb./ft^3 were fed to a coiled tubular reactor. In order to meet the required contact times the reactor length imposed a very large pressure drop. This in turn necessitated the use

of a screw feed pump to pressurize the catalyst powders. The result was agglomeration of the catalyst and the accompanying loss in activity and surface area. The new vertical pneumatic conveying mode was chosen due to the problems encountered in horizontal conveying.

It is unclear who was responsible for the transition to vertical conveying. Ghor [12], reports that Lewis and Gilliland were "asked" to carry out studies on flow properties of powdered solids suspended in gases, simultaneously with the coiled tube work. Squires [35], paraphrases a letter from Edwin Gilliland in which Lewis and Gilliland suggested this mode in response to a coil plugging problem. Also recounted is Keith's, of Kellog, fabrication of a glass coil reactor and his observation of saltation flow. Squires suggests that it was Keith who promoted a fluidized bed. Finally, Jhanig et al. [14] reports how Standard Oil Development Co. (SOD) itself chose to borrow large particle Winkler Technology for the processing of catalyst powders. In doing so they were making use of the Odell patents they had purchased as discussed earlier. They were well aware of the greater catalyst concentration in upflow compared to downflow as a result of slippage. This slippage increased the solid concentration (holdup) so that the necessary catalytic surface area could be stored in a reasonably sized vessel.

In spite of the uncertainties in the development of fluidization, the experimental work of Lewis and Gilliland

is quite clear. Their graduate students Walker and Chambers showed that particle slip velocities in fluidized beds were greater than that given by the terminal velocity of single particles. These experiments may be viewed as early evidence of the complicated nature of the solid flow patterns in fluidization.

Commercialization of the first upflow mode, Standard Oil Development Co. (SOD model 1 - riser standpipe combination), was achieved in 1939. However before the first unit came on stream, engineers were already redesigning for SOD model 2 downflow or bubbling bed unit. The difficulties with model 1 were given as excessive reactor length and poor dust collection. It is somewhat unfortunate that the upflow mode was discarded before the improved contacting was explored. The improved contacting was demonstrated by Massimilla (1973) [20], in an experimental study on the ammonoxidation of polypropylene.

As a mature process Houdry evolved into a pair of gravitating beds for reaction and regeneration with either dilute (riser) or dense phase (mass lift) solid recycle. These are the so called Houdriflow and Thermophor Catalytic Cracker (TCC) reactor units respectively. The combined capacity of Houdry and TCC exceeded Fluid Catalytic Crackers (FCC) until 1947 [35] and remained competitive well into the 1950's.

A mature FCC plant is embodied by an SOD model IV, where side by side reaction and regeneration are carried

out. Solids transfer is effected through the connecting risers and standpipes. Simplification in solids flow control through aeration rate rather than slide valve opening is given as a major process improvement in this model. The relationship between solids rate and aeration rate, with imposed pressure as a parameter will be seen in chapter 3.

Houdry large particle processes and FCC small particle processes are remarkably similar in morphology. In the former process the large particles force reaction and regeneration to take place in the dense gravitating mode. Recycle of solids is carried out in a riser tube. In the FCC process however smaller particles and their increased slip allow for the proper contact time so that reaction is in the bubbling mode. In this process it is the regeneration which is in the standpipe or gravitating bed. In spite of the different patent positions there is a certain amount of convergence in the design trends.

Terminology is another issue which has persisted in keeping the technology of large and small particles distinct. Fluidization and fluidized beds were routinely associated with a dense, bubbling bed, [45]. Dilute phase and transport processing was concerned with high gas throughputs with voidages in the 95-99% range. Zenz describes it as "uniformly distributed, dilute suspension ranging from 1-5% by volume of solids which flow along with the gas at a particle velocity only slightly less than the fluid velocity." It appears that the denser transported beds

were not considered until later. Present day riser type catalytic cracker reactors, with voidages from 75-95%, now operate in this range. This denser transported mode of operation is now considered as a separate regime of fluidization. It is the subject of this thesis.

2.2 - Fluidization of Large vs. Small Particles

Following the historical development, present day analysis of gas-solid fluidization is still carried out along two distinct paths. A flow chart for the two different types of behavior that a gas-solid suspension can exhibit is seen in Figure 2.2-1 (after Leung 1979 [17]). The right branch depicts a system where decreasing gas velocity at constant solid rate causes the suspension to collapse sharply, or choke, from dilute phase pneumatic transport into a slugging (fluidized) dense phase flow and thereafter into a packed bed (not fluidized). This sort of behavior is normally associated with class B/D solids of Geldart's classification [11], as well as historically with Winkler's 1-3 mm lignite particles. Geldart's classification is in fact a measure of the ability of a solid to imbibe (entrain) gas, or conversely, the ability to choke.

In contrast to the above system, the left branch of the flow chart depicts a system associated with fine powders where decreasing the gas velocity at constant solid rate does not collapse the suspension but merely allows the

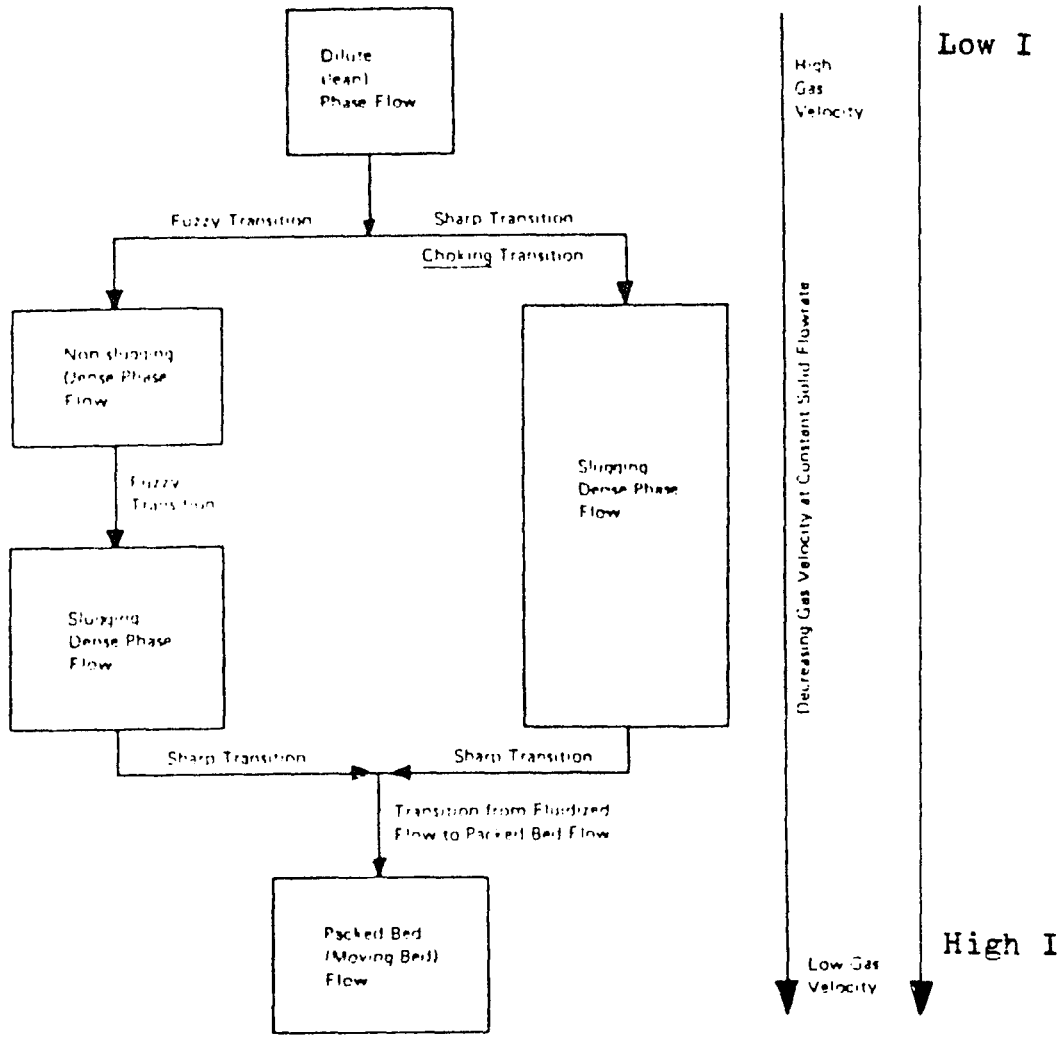

Fig. 2.2-1 . Possible flow patterns in vertical pneumatic conveying showing two types of system: the choking system (right-hand branch) and the non-choking system (left-hand branch). **(From: Leung (17), with permission).**

fluidized density to increase. This state is termed by Leung as "non-slugging dense phase flow." As shown on the diagram the transition is rather fuzzy and, in fact, Gajdos and Bierl claim it does not exist. Yerushalmi and coworkers [41], have referred to this region of fluidization as fast fluidization. Yerushalmi's terminology refers to the transition from slugging dense phase flow, to fast fluidization as occuring at the transport or flooding point velocity. Yerushalmi makes distinctions between bubbling, slugging and turbulent regimes which Leung lumps in his slugging dense phase flow box.

The disagreement and confusion in results and terminology so apparent in the literature indicates that the parameters which have been used to date to define the state of the system are insufficient in number to do so. It is one of the purposes of this work to show how gas and solid rates alone do not comprise a complete set of variables with which to define the flow. The solid inventory in a recirculating solids system or the imposed pressure drop on the system will be shown to be another variable which must be specified to define the system's operating point.

2.3 - Regimes of Fluidization

Avidan [2] has restated the work of previous CCNY workers and has reviewed the literature with regard to the mapping of regimes of fluidization. As they pertain to our

studies gross features of each regime as well as the transition conditions between them will be mentioned here. This discussion is limited to Geldart's class A fine powders and the left branch of Leung's phase diagram. A brief discussion for the analogous condition for coarse particles will follow.

In packed beds the solids are resting on one another and the gas follows the tortuous passages between the particles. Pressure drop for these beds is correlated by the Ergun equation for a packed bed of fine particles. On the flow map of log ΔP vs. Uo this is the linearly increasing portion of the map.

Fluidization begins where the pressure drop is such as to balance the weight of the entire bed of particles. The point where the two are equivalent is termed incipient fluidization; the voidage at this condition is ϵmf, the minimum fluidization voidage and the gas velocity is termed Umf, the minimum fluidization velocity. Shortly above this velocity, the structure of the bed exhibits two phases. One phase is the dense, solid filled emulsion region with voidage approximately equal to ϵmf. The other phase is given by large bubbles or voids percolating through and shortcircuiting the emulsion region. The oscillatory nature of bubble bypassing sets up vibrations which are quite evident in both the bed pressure fluctuations as well as movement of the bed structure. For heat transfer processes in bubbling beds the temperature is fairly uniform

throughout the entire bed due to high solids backmixing and the inherently high solids heat capacity.

On a log pressure gradient vs. Uo map this regime is given by $\Delta P/\Delta L = W/AL$ the region of approximately constant bed pressure drop. This means that the axial density profile in the bed is flat. The total ΔP across the bed is essentially independent of gas velocity except for the small frictional loss at the wall.

Visual observation of the bed shows a clearly defined bed top, and little carryover. Of interest are the observations made by previous investigators and the photographs and x-ray recordings of this investigation regarding the preferred paths of bubbles up the center of small diameter laboratory sized beds. The gas velocity giving rise to the bubbling condition is bounded by Umf on the lower end and either Uc or Uk on the upper end.

	Umf	Uc	Uk	Ut	Utr	Upt (m/s)
FCC	9x10-4	0.61	0.61	.078	1.2-1.5	>5
HFZ-20		0.91	1.37	.106		

Table 2.3-1 Characteristic velocities for the two powders investigated

At the higher extreme of the bubbling regime a somewhat different behavior of the system can be seen. Depending on a number of solids-system properties such as particle density, bed aspect ratio or solids inventory, slugging may set in. This is the condition where the bubbles have had enough time

to grow as they travel up the bed so that their diameter is the same as that of the tube. Under these conditions the bed can be seen to consist of striations of alternate dense and dilute regions. What was previously minor vibrations due to bubble passage has now been amplified to the point where there is real danger in fracturing the vessel. Pressure drop measurements still have the same mean as for a bubbling bed but the deviations are much larger. On a flow regime map Figure 2.3-1, this condition is still given by the constant pressure gradient region of a bubbling bed. Notice however that since slugging depends intrinsicly on bubble growth it is quite possible for a deep bed to slug at the top and bubble at the bottom. This is of course due to bubble coalescence and growth up the bed.

Transition to turbulence was first studied by Lanneau [16] and later by Kehoe and Davidson, Massimilla [20], and Turner [38] for fine particles. The transition has been characterized by Turner by U_c and U_k the velocities at which the slugging vibrations peaK and then decay and begin to level off respectively. In these terms Uc and UK are system dependent and it is uncertain how one would translate these criteria to another sized bed. For this purpose the criterion of Kehoe and Davidson appears to have greater predictive capability.

$$Ug > 3U_t \text{ min.}$$

Visual observation of the bed shows a fluidized bed

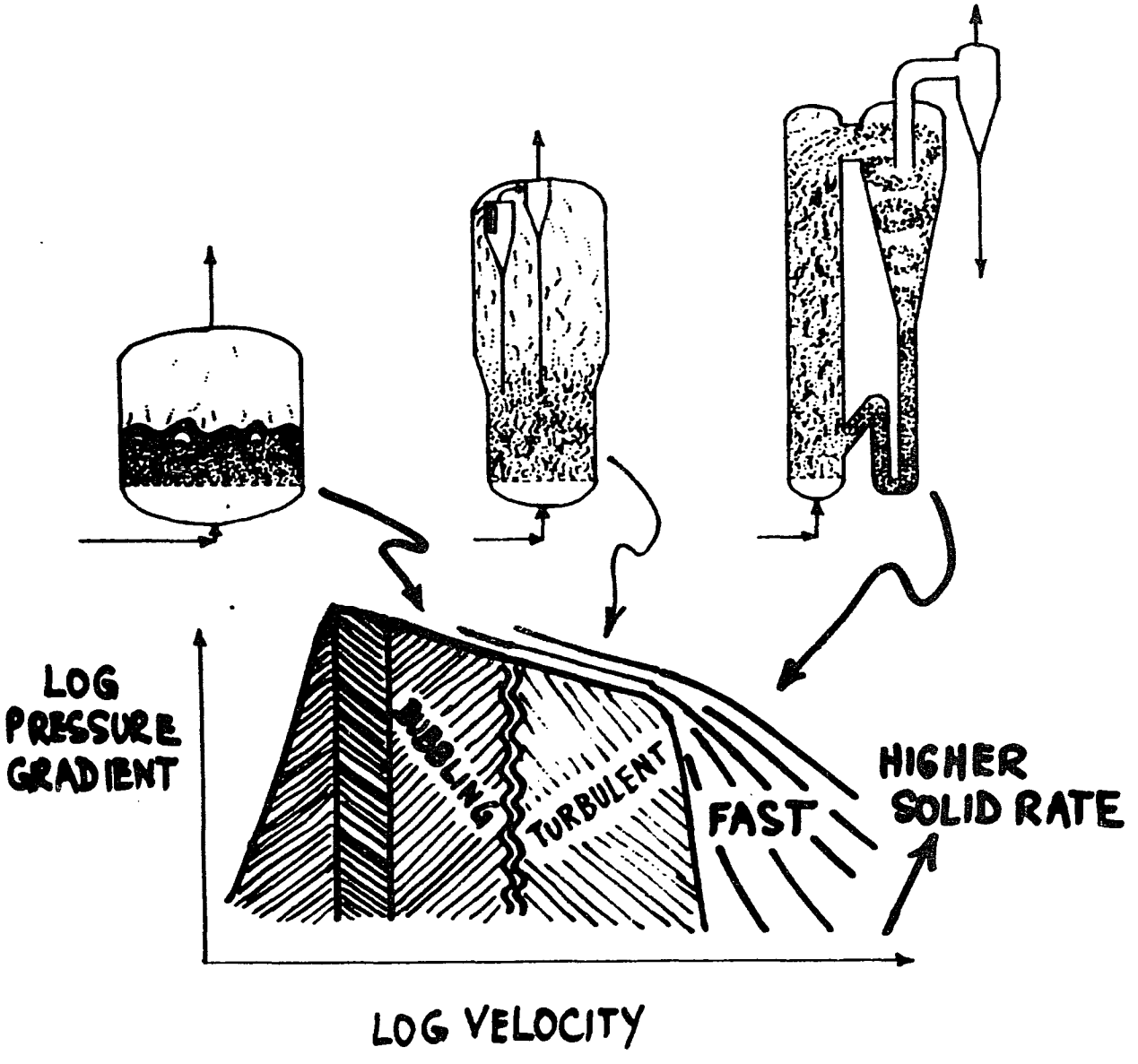

Figure 2.3-1 Flow Regime Map: log pressure gradient vs. log velocity.

with a distinct bed top although it is considerably more diffuse than before. Large voids in the form of bubbles are dissapearing and more intimate contact between gas and solids are seen at the tube wall. In spite of considerable freeboard activity the bed is still quite dense. This is because the gas velocity for the particles of Canada et al. is still $0.3U_t$ - $0.35U_t$ below the single particle terminal velocity. For fine particles Avidan and Yerushalmi have invoked the concept of clustering so that even though the gas velocity is $10U_t$ - $20U_t$ of a single particle the clustering phenomenon has increased slip and holdup. The gas velocities which bound the turbulent regime are given by Uc and Uk at the lower limit and U_{tr}, the transport velocity, which is the gas velocity at which solid carryover sharply increases, at the upper end.

In addition to the decay of pressure fluctuations in the turbulent regime the mean bed density begins to decrease as well. On the flow regime map of log pressure gradient vs. Uo this occupies the portion of the curve where voidage is decreasing from that of a packed bed.

Recent data of Abed [1], lent another explanation to the increased slip exhibited by a turbulent bed. His radial density profiles (capacitance probe data) show how the bed voidage is larger in the center than at the wall of the tube. Video recordings made in the course of this investigation confirm this profile. This profile appears to be a natural extension of the preferred centerline paths for

bubbles in a small diameter bubbling bed. The increased average slip in this regime can be attributed therefore to high solids concentration in a relatively stagnant or backflow region at the wall. The axial density profile for the turbulent bed is relatively flat in the solids dense region, similar to that of a bubbling bed.

As described by Yerushalmi [42], The situation changes entirely as one crosses the Transport Velocity. As this velocity is approached there is a sharp increase in bed carryover and the bed would empty quickly if not for solid recycle. The average solid fraction in the bed can be as high as 0.2. The dense phase portion of this regime has been referred to by Yerushalmi as fast velocity fluidization. He has compared the transport velocity to the flooding point velocity of sedimentation. Yang [40], has given the criterion for the onset of this regime in general as $Fr > 140$. Further increase in the superficial velocity at constant solids rate has the effect of leaning out the bed and approaching the pneumatic transport regime, (solid fraction < 0.05). Whether fast fluidization and pneumatic transport are in fact separate regimes is at present being disputed [6].

A high velocity, or fast fluidized, bed operating above the transport velocity has at least one other important distinguishing feature. The bed voidage is no longer a unique function of gas velocity but now depends on solid rate as well. On a flow regime map of log pressure gradient

vs. gas velocity this regime may be represented by a family of curves for various values of solids rate. This alteration in solids rate cannot be related to a uniform change in overall fluidized density. Rather, the experimental work of Gajdos and Bierl [6] and of Li and Kwauk [44] has shown that the character of the bed is often stratified i.e. a dense phase region exists below a dilute phase region with axial pressure gradient (proportional to solids fraction) exhibiting an inflection point which separates the two regions. Also the x-ray photographs given in chapter 5 show how the radial profile is not uniform either. The purpose of this work can be restated and amplified to relate one of the bed characteristics, the imposed pressure (system inventory) to the gas and solid rates.

3 - Analytical Developments

The system considered in this thesis deals with dense (0.80-0.95 void fraction) transported fluidized beds. Analytic methods to describe the operation of such a bed are discussed in this chapter. Each method is a separate macroscopic approach which relates gas and solid rates to the gross structural characteristics of the bed. In each section of this chapter a technique or mode of analysis, to be used in presenting the data of chapters four and five, is developed. In section 3.1 the pressure balances in a circulating system and the impact of imposed pressure drop are discussed. In section 3.2 the gas and solid rates are related to the pressure drop across the bed. It is thereby shown that the pressure gradient is a measure of the fluidized density. Section 3.3 discusses methods of plotting the fluidized density as a function of operating variables and thereby introduces the axial pressure gradient variation. In section 3.4 the gas and solid rates are related to give a measure of the mechanical energy efficiency of the fluidized bed. This measure is given by the Energy Loss Ratio (ELR). Section 3.5 adapts the chordal absorption technique for measuring radial solid density profiles in fluidized beds. In this section gas and solid rates were not related to a particular radial profile as the emphasis of this work is to demonstrate the feasibility of this method for such measurements.

3.1 - Pressure Balances in a Circulating System

Within each section of this chapter are the principles which govern pressure balances in a fluidized bed. Figure 3.1-1 is a schematic of the solid circulation system with a typical pressure loop given on the right. This figure can be used to demonstrate many of the important concepts that can be used in describing such systems. The denser bubbling companion bed is represented by the left, higher gradient leg of the pressure profile. For illustrative purposes the right, fast bed leg, is represented by two possible types of axial density profiles. One type has a constant pressure gradient for the entire height of the column. This axial density profile will be seen to be most often associated with the lighter FCC catalyst. The other type is represented by a two zone region, each with constant axial density gradient. This latter type of profile will be seen to be most often associated with the heavier HFZ-20 catalyst although both types of profiles are possible for either solid examined. The point where the density gradient is considered to change is termed the Point of Inflection. The variation in height of this point of inflection as well as the particular values of density in both the dense and dilute regions are given in the next chapter.

Each of the two possible fast bed density profiles cannot be considered in isolation because of the inherent dependence upon the complete pressure balance. Again, for illustrative purposes, the transition between the two

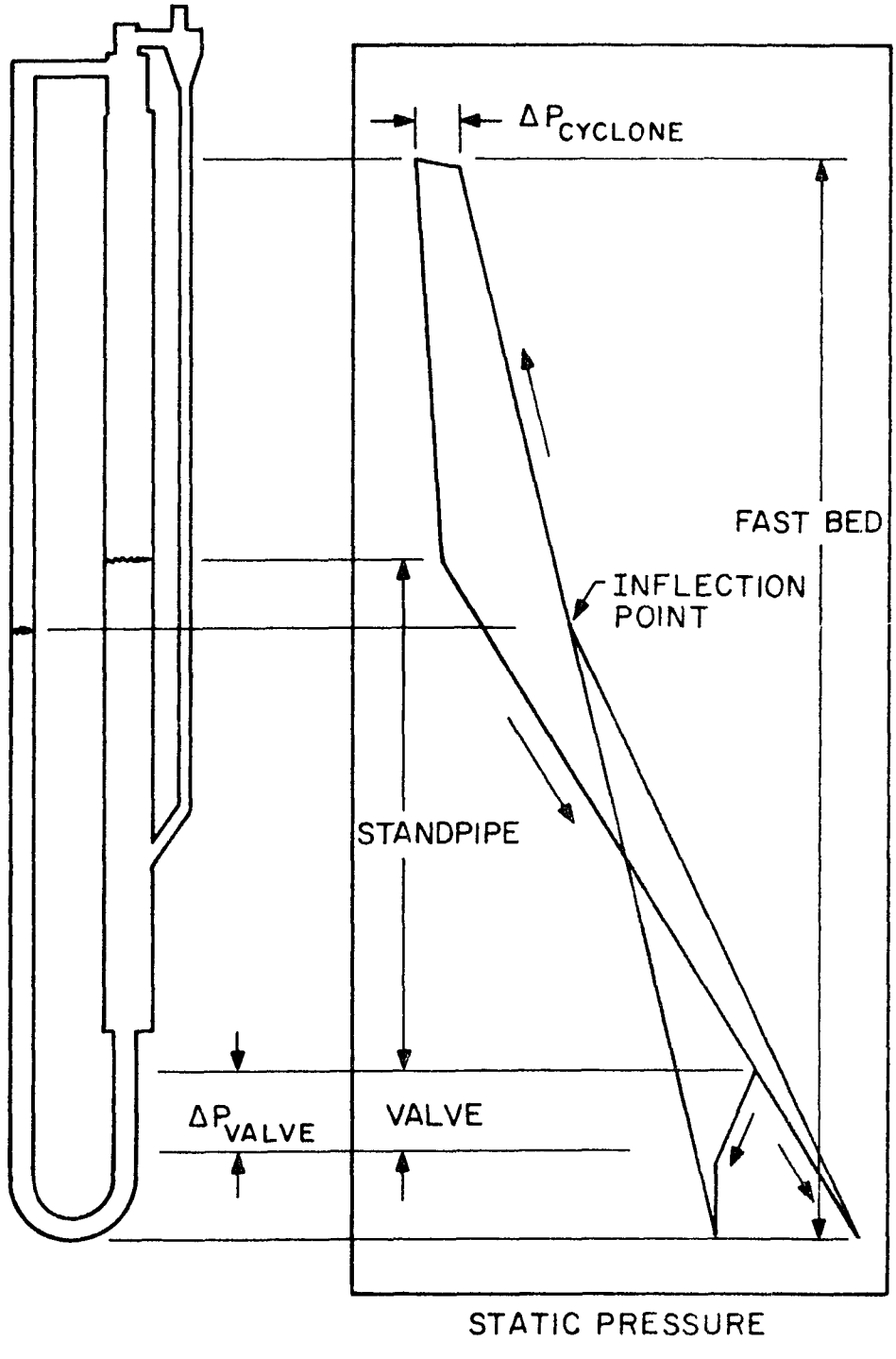

Figure 3.1-1 Typical pressure loop of the circulating system.

profiles is shown to come about by varying the solid feed valve opening. In fact, it can also be effected by varying the gas and solid rates as well as the solid invantory, I. If the solid feed valve is fully open, frictional pressure drop across the valve is negligible and the static pressure continues to rise unabated from the bottom of the bubbling companion bed through the bottom of the "U" tube. The "U" tube under these conditions is filled with fluidized solids. Upon closing the solid feed valve to some critical value the frictional pressure drop becomes large enough to break the fluidized bed at the valve and the static pressure falls. Under these conditions solid flow past the valve is insufficient to maintain the inventory in the "U" tube and the solids are in free-fall to the bottom of the U-tube. The two modes of operation just described result in two different aggregation states in fast bed operating conditions. The data of the next chapter shows how the different aggregation states can occur for a given solid even at the same gas and solid rates.

The fact that the system being considered is closed and recirculating with respect to solids means that the pressure profile must be a closed loop as well. Any changes in pressure on the inventory side must be met on the fast bed side either by changes in inflection point height or by changes in slope above and/or below the inflection point. The two "legs" of the system are therefore not unlike a manometer in which the pressure in both legs must be

balanced. The main effect on pressure in altering the solid inventory in the system is to shift the right end of the entire profile to the left or right.

In this particular manometer-type system not only is the balance of pressure in both legs essential, but the pressure level which is set by the solid inventory level in the companion bed is important as well. This pressure level sets the solid holdup in the fast bed and is being termed imposed pressure drop. It is given by the value of fast bed pressure drop, ΔP_f which can be seen for a closed recirculating system to be equal to the sum of the companion bed, cyclone, and solid feed valve pressure drops. At a fixed value of gas and solid rate, increases in ΔP_f result from increasing frictional losses with increased internal solid recirculation and/or holdup.

An estimate of the magnitude of the solid recirculation rate can be obtained as follows. If one were to approximate the solid velocity with the gas velocity, since Ug is so large compared to Ut, an estimate of the minimum solid fraction can be obtained.

$(1-\epsilon) = G_s/\rho_s V_s = 117.4/3.0 \times 1450 = 0.02$ (from data of run 011d)

Experimentally for that run a mean solid fraction $(1-\epsilon)$ of 0.16 was measured. Thus this larger holdup than

necessary can be considered to be ascribed to the adjustment of the fast bed to the imposed pressure drop.

3.2 - Analysis of a Circulating Fluidized Bed System

A fundamental concept in the design of many gas-solid transported fluidized bed systems is the creation of a continuous pathway for solids so that they may be recycled from bed top to bottom in a smooth, continuous manner. Kunii and Levenspiel best illustrate this concept with an analogy to water-air systems. It can be seen from the diagram that if the air rate to section C-D is sufficient to decrease the fluid density in that section to 0.5 g/cc then the driving force for circulation is 50 cm H_2O

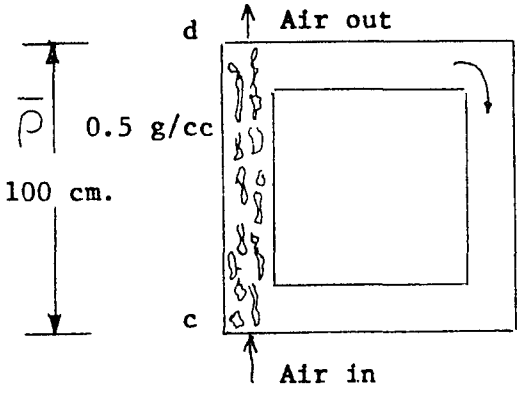

$$P_c - P_d = 50\text{cm } H_2O + P_{fcd}$$

$$P_d - P_a = P_{fda}$$

$$P_a - P_b = -100\text{cm } H_2O + P_{fab}$$

$$P_b - P_c = P_{fbc}$$

Figure 3.2-1 Pressure changes around a circulating system.

Checking the static pressure around the loop starting with point C, we find

$$\Sigma\Delta P_f = (P_c - P_d) + (P_d - P_a) + (P_a - P_b) + (P_b - P_c) = 0$$

$$\text{or: } \Delta Pf = 50 \text{ cm } H_2O$$

Thus, the density differences between the vertical sections cause a driving force which is consumed by frictional resistances in all sections of the loop. The resistance in each leg may not be equal. The underlying principle in creating stable circulation around a loop is to have density differences between parallel vertical sections in the loop.

In a gas-solid fluidized system the calculation of pressure drops around the loop can be done in a similar manner. Figure 3.1-1 illustrates pressure changes around a recirculating system. As given by Kunii and Levenspeil [17], the rate of steady state circulation is given where the sum of the static head terms just balance the sum of all frictional resistances, including solid circulating beds, cyclones, constrictions or acceleration.

$$-\Sigma\overline{\rho}h_i \, g/g_c = \Sigma\Delta P_{fi}$$

In practice both $\overline{\rho}$ and ΔP_{fi}, the fluidized density and friction of the gas-solid mixture are unknown. In fact, the frictional term of the gas-solid mixture is actually a sum of gas-wall, particle-wall, interparticle, and acceleration pressure drops. Rather than separating these terms in the above equation, we assign the left term to be the fluidized density ("head") and the right frictional pressure term to be that given by a differential manometer. This is the basis for equating the fluidized density to the pressure gradient.

3.3 - Axial Pressure Gradient

Intuitively, one might be led to believe that the fast bed "loads up" or fills uniformly so that the axial pressure gradient is flat. A large part of this work consists of measuring the pressure gradient experimentally and examining the stratification properties of the fluid bed. The bed usually contains a more dense zone at the bottom followed by a more dilute region on top. In the next chapter two sets of data are used in examining this behavior. One set plots the axial pressure gradient (void fraction) as a function of axial location in the bed. In this set the variation in density of the bed can be seen as a function of solid inventory, gas velocity, and solid rate for both solids examined. The first six figures in this set are a group of profiles corresponding to the maximum possible solid rates for a given superficial gas velocity for each solid and each of three solid inventories. The remaining figures in this set are profiles showing where either the gas velocity, or solid rate have been kept constant for each solid and each of three solid inventories. In these the isolated effects of each rate are examined to determine its effect on inflection point height and mean solid holdup.

The second set of data illustrates how three particular void fractions, dilute phase, dense phase and mean value, vary with either solid mass or volumetric rates. This method is used to demonstrate the convergence of the dilute and dense phase void fractions at either high or low values

of solid mass rate. It is also used to demonstrate how two solids with densities of 1.45 and 1.07 g/cc show similar void fractions at the same volumetric rates.

3.4 - Energy Loss Ratio

Recently a number of competing processes for solids conveyance have been presented. In such systems, such as the dense phase hyperflow arrangement or the more conventional pneumatic transport it is important to have a quantitative measure of the gas and power requirements of each alternative. Towards this end Sandy et. al. have fluidized 70-80 mesh particles in air in 1/2 - 3/4 in. diameter tubes operated under dense and dilute phase conditions. Their conclusions for these experiments were that although the dense phase required 10 times the dilute phase power the corresponding gas rates were only 1/20. This conclusion was arrived at by performing an energy balance on the gas and solid streams. The difference between the two is attributed to gas-solid friction and is considered lost energy.

The above analysis is fine where the pressure drop in the bed and its corresponding energy loss is single valued for any given set of gas and solid rates. In the system of this thesis however, with recycle of solids through a solids return leg, the lost energy can have a number of such values depending upon the solids density and inventory. Under such circumstances it is deemed beneficial to map out such energy

loss variations as a function of such operating parameters rather than attribute their loss to any specific cause. This consideration led to the development of the Energy Loss Ratio (ELR) as a measure of energy efficiency of solids conveyance.

Energy Loss Ratio (ELR) is defined as being the difference between the kinetic energy given up by the gas and the potential energy gained by the solids in traversing the column per pound of solid per foot of column height.

$$ELR = \Delta PUo - GsL[(g/gc)]/G_{sL}$$

ΔPUo = power input to column per unit area ft-lbf/ft^2-sec

$GsL(g/gc)$ = power gained by solids per unit area "

GsL = mass flow per foot of column

The data indicate, Figure 3.3-1, that the transport of FCC solids is carried out quite efficiently with the lost energy to potential energy gain ratio equal to about 2. The result is different for HFZ-20. In figure 3.3-2, it is seen that the loss ratio is almost double for HFZ-20. The trend in both cases seems to be downward at low solid rates and upward at high solid rates. At the time these plots were constructed the effect of solid inventory was not accounted for.

Although not evident from the figures, examination of the defining equation for ELR demonstrates that a plot of ELR vs. Gs must be multivalued. In a bubbling fluidized bed the kinetic energy input from the gas has a finite value

Figure 3.3-1

LOSS RATIO VS. SOLIDS RATE FOR FCC

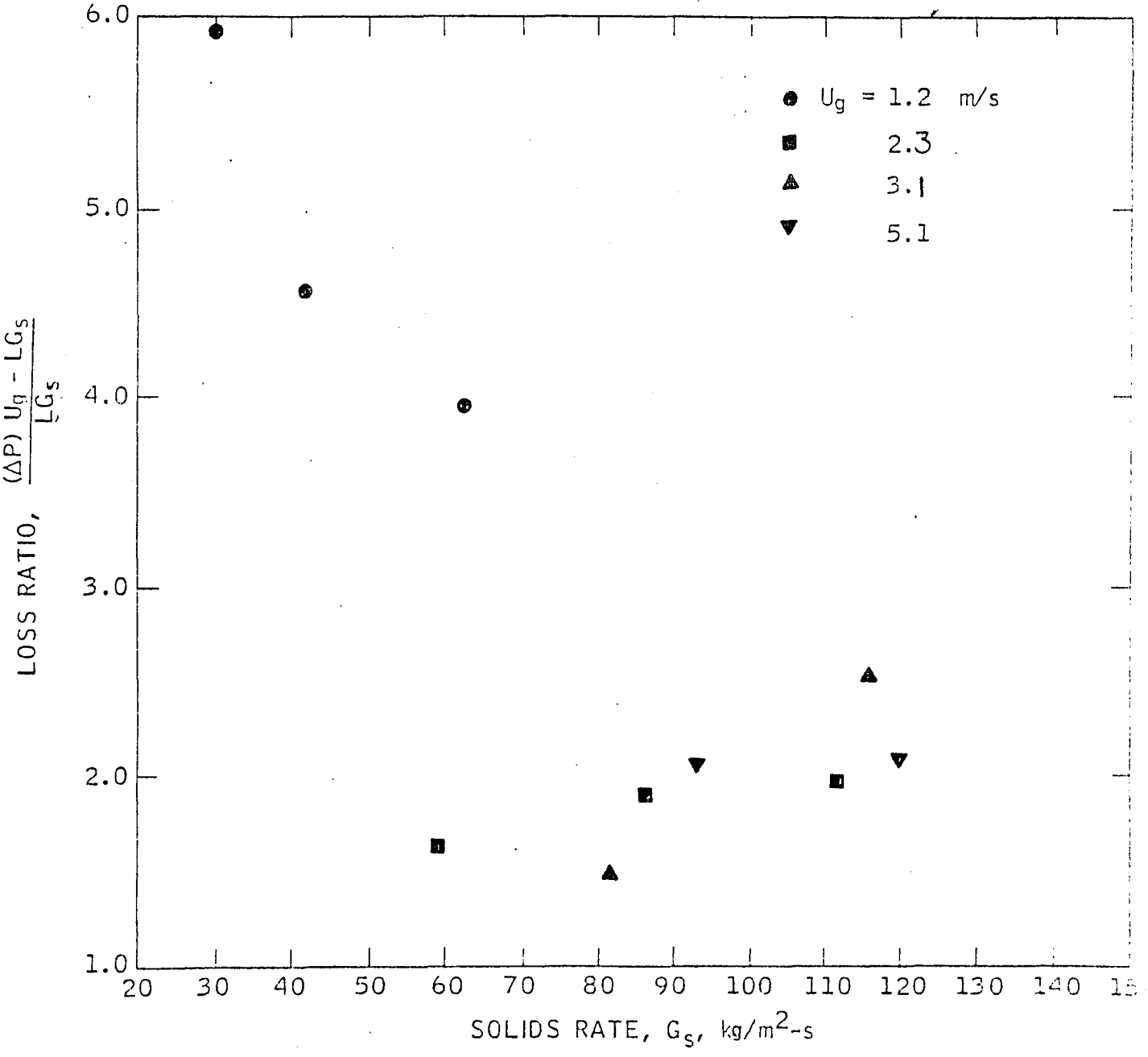

Figure 3.3-2

LOSS RATIO VS. SOLIDS RATE FOR HFZ-20

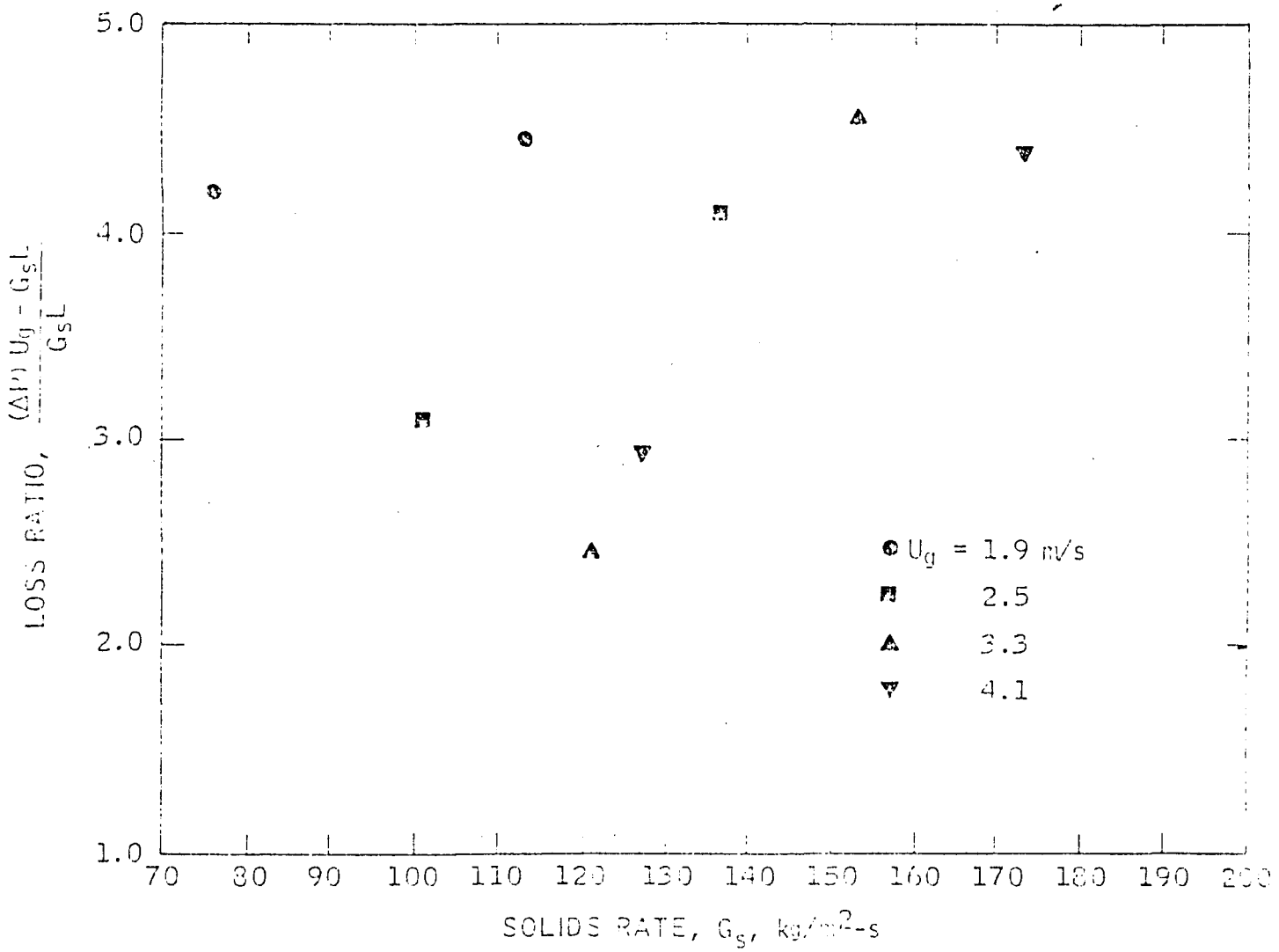

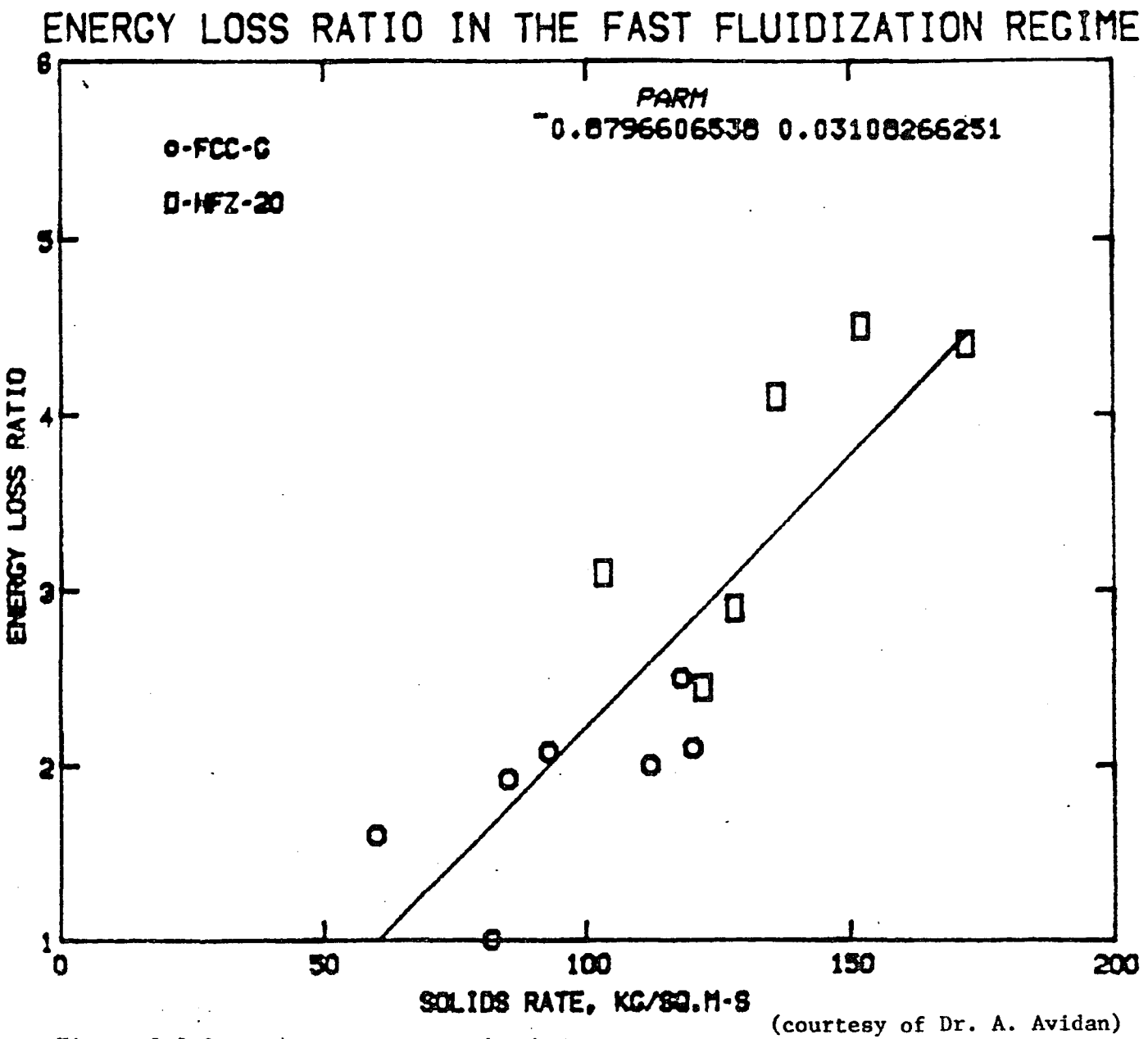

(courtesy of Dr. A. Avidan)

Figure 3.3-3 Energy Loss Ratio (ELR) for both FCC and HFZ-20 catalysts vs. solid rate.

whereas the solid rate is zero. The loss ratio is therefore almost infinite, or in other words all the gas kinetic energy goes into recirculating the solids. In dilute phase transport the solid rate is again very low only this time the pressure drop across the bed is low as well. The loss ratio for the dilute phase transport is therefore a small but finite value.

3.5 - Chordal Absorptometry Technique

Chordal absorptometry has been used in the past to determine the radial distribution of physical properties in an inhomogeneous axially symmetric plasma from line probe data. Originally it was used for high temperature plasmas where internal probes could not be used. The technique is ideally suited for our purpose, determining the radial mass density distribution in a fluidized bed as no disruption of flow takes place.

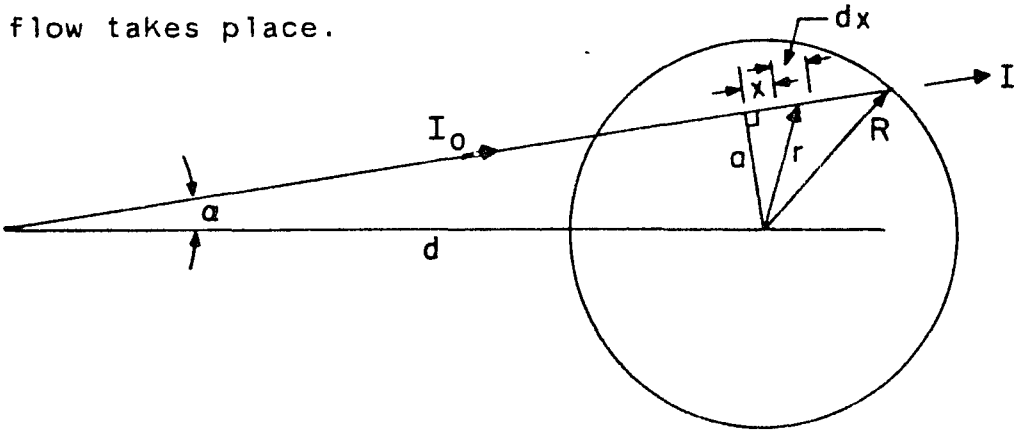

Figure 3.5-1 Geometry of Chordal Absorptometry Technique

The relationship between the x-rays absorbed by the solid in a fluidized bed along the chord distance dx is:

1. $$dI(\lambda) = I(\lambda)\,\rho(x)\,dx$$

Therefore the light transmitted through a chord length 2x can be determined by the following equation:

2. $$\ln I/I_0 = -2\int \rho(x)\,dx$$

In this experimental investigation the radial solid density profile was measured in an approximate manner using a "ring method". This method was chosen because of its simplicity which was in keeping with the quality of the data. As the work developed it became clear that much additional work needed to be done in order to calibrate the absorption method. This additional work was beyond the scope of this investigation.

The "ring method" involves dividing the vessel cross section into equally spaced annular rings. Each annular ring is imagined to consist of a region of constant solids density. The four chords shown in Figure 3.5-2 are seen to pass through regions with different constant solid densities. If equation 2 is solved in discrete form for each chord the following equation allows for the evaluation of the arbitrarily selected four solid density values by successive substitution.

3. $$\ln I/I_0 = \sum \rho_n \ell_n$$

Specifically, beginning with the outermost ring, chord 4 passes through a region of constant density ρ_4 with length ℓ_4. ρ_4 is simply determined by dividing the experimentally determined $\ln I_4/I_0$ by ℓ_4. The successive densities can be

calculated from the relationships given in Table 3.5-1. In Figure 5.3-2 the length subscript refers to the chord number and the superscript to the annular ring. These lengths are likewise included in the table.

Experimentally I/I_0 measurements were made on the x-ray exposures with the aid of a Macbeth Transmission Densitometer, Model TD-902. I_0 is given as the undisturbed field exposure given by the x-rays.

Each chord measurement was corrected for the increasing thickness of the plexiglass with increasing angle α, Figure 5.3-2. For each set of plate film exposures an eqivalent empty tube exposure was made. This quantified the x-ray absorption of the plastic. For the high intensity x-ray exposures e.g. 95 kV and above, the empty tube exposures saturated the film. I was close to I_0 everywhere and it was judged that the relative x-ray absorption by the tube was minimal.

The redundancy due to the axial symmetry was used by averaging the measurements made on either side of the line of symmetry. For each experimental run the empty tube I/I_0 ratio was subtracted point by point. The final ratios I/I_0 were used in the "ring method" to evaluate the densities.

Table 3.5-1 Geometric constants used in the "ring method".

$$\rho_4 = \frac{\ln (I4/I_o)}{\ell_4}$$

$$\rho_3 = \frac{\ln (I_3/I_o) - 2\rho_4 \ell_3^4}{\ell_3}$$

$$\rho_2 = \frac{\ln (I_2/I_o) - 2\rho_4 \ell_2^4}{\ell_2}$$

$$\rho_1 = \frac{\ln (I_1/I_o) - 2\rho_4 \ell_1^4 - 2\rho_3 \ell_1^3 - 2\rho_2 \ell_1^2}{\ell_1}$$

r_5 = 7.6 cm. (I. D.)

r_4 = 6.7 cm. ℓ_4 = 7.4 cm.

r_3 = 4.4 cm. ℓ_3^4 = 1.1 cm. ℓ_3 = 9.8 cm.

r_2 = 2.2 cm. ℓ_2^4 = 1.0 cm. ℓ_3^3 = 1.9 cm. ℓ_3^2 = 7.7 cm.

r_1 = 0.0 ℓ_1^4 = 0.9 cm. ℓ_1^3 = 2.2 cm. ℓ_1^2 = 2.3 cm. ℓ_1^1 = 4.4

4 - Axial Pressure Gradient

Recent laboratory invenstigations [5],[6],[44], reported in the literature have indicated that there often exists an axial variation in solids loading or pressure gradient along a fast fluidized bed. These reports show considerable disagreement in the nature of the variation as well as in the average solids loading obtainable in the fast bed. In this chapter the literature is evaluated with respect to the data obtained in this investigation and a discussion of the disagreement as well as some of the parameters which govern holdup and fast fluidization is presented.

4.1 - Review of Previous Work

A number of experimental axial pressure profiles for fluidized beds have been recently reported [6], [44]. Fast bed profiles always exhibit at least a slight decrease in solids fraction upward along the bed. However, when the difference between the lower and upper bed solids fraction is large, it is implied that an inflection point exists in the bed. If the bed-average value is close to the upper bed value the inflection point is close to the bottom of the bed, and conversely, if it is close to the lower bed value the inflection point is close to the top of the bed. The position of the point of inflection has been shown by Li and Kwauk [44], to be dependent upon gas velocity. In general

agreement with those of Li and Kwauk are the axial profiles reported by Gadjos and Bierle [6], although there is a disparity between the shapes of the profiles given in each report. Also there is disagreement between the values of solids fraction, $(1 - \epsilon)$, even for similar solids fluidized under similar conditions. Additional work was undertaken to explain how such differences come about. The present work also shows the additional dependence of both holdup and inflection point position on solids rate, solid particle density, as well as on the additional parameter of imposed pressure drop.

Bakker and Heertjes [3][4], were probably the first to apply a three zone model to describe a fluidized bed. These zones are acceleration (I), dense (II), and dilute (III) regions, respectively.

In performing their analysis for bubbling beds Shumkov and Ivanov (1977) [34], examined the effects of gas velocity, static bed height and column diameter on these three voidage regions. Although our interests are in an entirely different regime of fluidization, the conclusions of Shumkov and Ivanov provide a foundation for fast fluidization:

a. Gas Velocity - an increase in gas velocity tends to decrease the solids concentration in the dense part of the bed (zones I and II) and to increase the solids concentration in the dilute phase. This dilute

phase is synonymous with freeboard, exponential decay of solids and dispersed phase. Note that for the bubbling bed the total area under the pressure gradient profile must remain almost constant and is in fact given by the weight of solids in the bed. An apropos description of the effects of increasing gas velocity, as given by Shumkov and Ivanov is to flatten the $\epsilon(h)$ profile. From their data it seems as if the inflection point remains at a fixed bed height although not at a given ϵ. The density profile pivots about this inflection point. How this inflection point can be shifted in a transported bed will be dealt with below.

b. Bed Depth - changing the depth of the stationary bed does not alter the shape of the density profile but merely changes the height of the dense section (II) in the same direction.

c. Bed Diameter - increasing the bed diameter decreases the voidage in the dense region and increases it in the dilute region. In effect, it does the same thing as decreasing gas velocity.

d. Radial Profile - for small diameter columns (less than 0.14 m), an increase in density of 15% at the wall is observed. The data was collected using capacitance probes. It was clearly recognized that for larger scale columns the descending motion of the solid phase which occurs at the wall in small columns is observed at various positions over the cross-section of

the bed. For fast beds Yerushalmi has speculated on the shape of the solids velocity profile [42], but definitive measurements of this profile for large diameter equipment are not available.

For the more general case of profiles in a fast bed, and specifically for a closed loop system, a number of additional effects must be taken into account.

Fast beds can similarly be divided into three distinct zones. These zones are I - acceleration, II - dilute in the core and dense phase at the wall, III - dilute phase transport, with the inflection point being the division between zones II and III

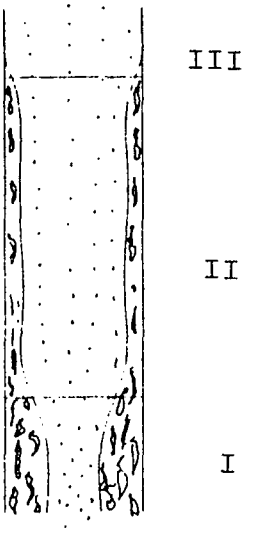

Figure 4.1-1 A Three Zone Model for a Fast Fluid Bed

Figure 4.1-1 is a three zone model for a fast fluidized bed. Evidence for this model comes from the axial density profile of Li and Kwauk [44], the x-ray photographs of Gadjos and Bierle [6] as well as the negative wall shear

stresses of Van Breugel [39]. The measured quantities in these studies were: x-ray absorption and sampling/momentum probe measurements of Gadjos and Bierle [6], from which they claimed downflow at the wall in zone II, differential pressure measurements for Li and Kwauk [44] and wall force measurements for Van Breugel et al. [39]. In addition to these measured quantities the physical appearance of the bed above and below the inflection point (interface) are markedly different. As reported by Gadjos and Bierle [6, page 78] and as observed in The City College test stand, significant downflow in the form of strands or clusters at the wall is not apparent above the inflection point.

The basic features of this model can be summarized. In zone III, the dilute phase region, the bed approaches a solid concentration similar to pneumatic transport. The density of solids in this region can be approximated according to Gadjos and Bierle as $(1 - \epsilon) = Gs/Ug\ \rho p$ which implies no aggregative phenomena at this dilution of solids. From their data a solids fraction of 0.03 can be calculated from the pressure gradient of about 3 lb/ft^3 which they reported. In zone II, again from the Gadjos and Bierle data, about 90% of the radius contains a region with solids density similar to that in zone III. In a region close to the wall a much denser region contains most of the solids holdup and at the junction of this zone and the wall downflow of solids is reported. Zone I may contain the same core-annular structure as zone II but in addition the solids

are accelerated from rest around the "U" bend. Although the actual densities of the core and annular regions are as yet unknown the present work measures relatively sharp changes in pressure gradient at the interface between the three postulated zones.

4.2 - Experimental Apparatus

All the experiments have been conducted in the City College Fast Fluidized Bed Facility [42]. A schematic of the circulating system is shown in Figure 4.2-1. High velocity fluidization is maintained in the 15.2 cm I.D. column shown on the left. It is 8.5 m tall. On the right is a 24.3 cm I.D. round vessel in which the test solid is maintained in low-velocity, bubbling fluidization. This so-called "slow" bed doubles as a standpipe and as a storage for the solid. Fluidizing air to the 15.2 cm column is provided at its bottom at room temperature from a 1400 cfm, 10 psi blower.

The solid powder to be fluidized is charged to the slow companion bed before a series of runs is undertaken. The slumped height of solids in the companion bed can be varied from about 1.2 m to 4 m giving a maximum range of solids inventory of about a factor of 3. Solid can be maintained in the 15.2 cm column at any desired fluidization condition through independent control of the gas velocity and of the solid rate from the slow bed to the bottom of the 15.2 cm column. The solid rate is controlled by a butterfly valve

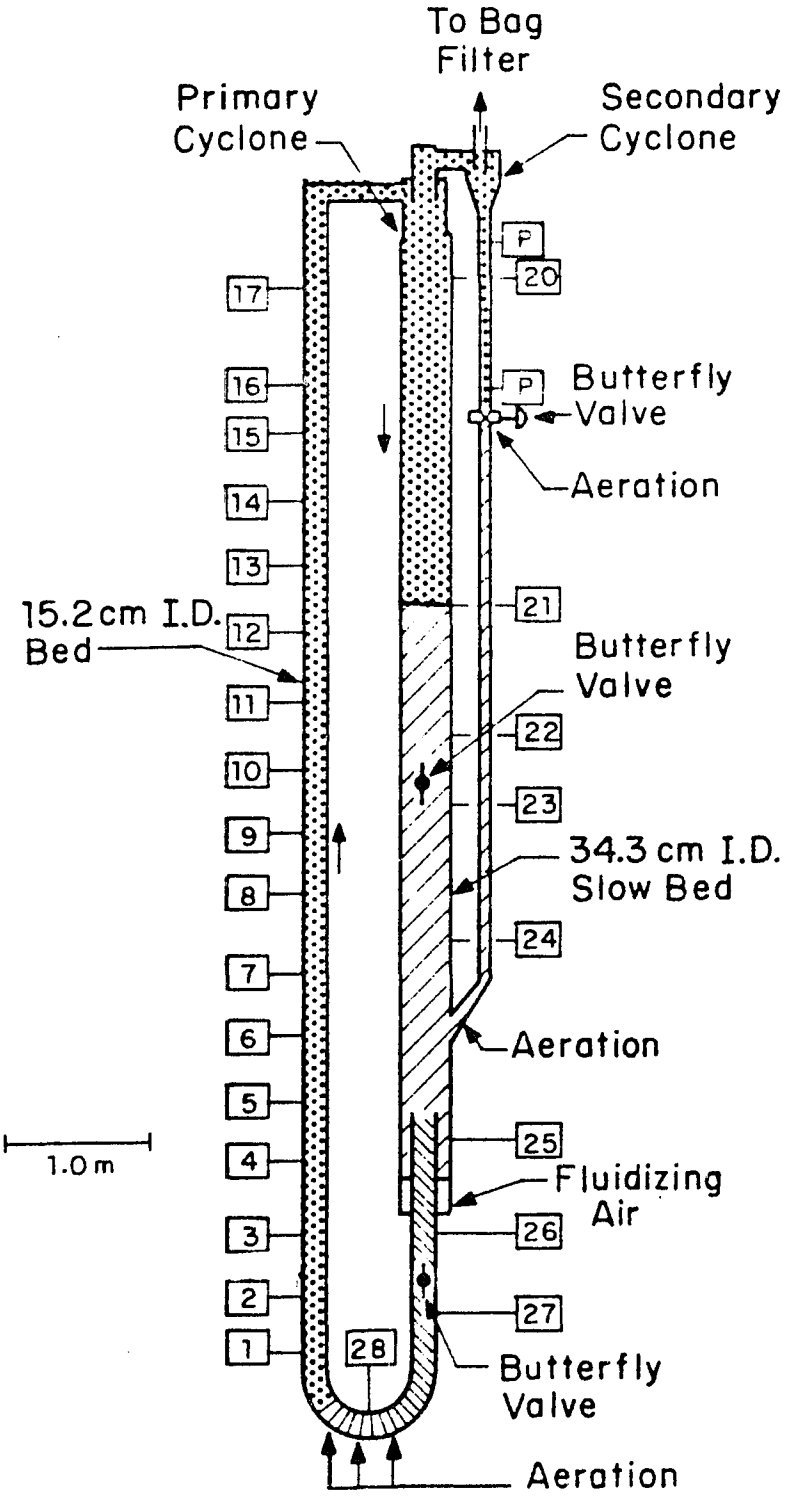

Figure 4.2-1 The 15.2 cm. I.D. Circulating System

installed in the U-tube just below the bottom of the slow bed.

Solid traversing the 15.2 cm column is separated from the gas in a primary cyclone which forms an extension of the vessel that houses the slow bed. The primary cyclone does not have an inverted conical bottom. A smaller cyclone acts as the secondary cyclone, and gas leaving it flows to a bag filter. Pressure taps are installed around the system with 17 located along the 15.2 cm column. Previous work has shown solid friction to be less than 10% of the total pressure drop in a given section for the turbulent and fast fluidization regimes [38]. It was therefore assumed that the pressure gradient at an axial position is equal to the density of solids at that position.

Solid circulation rates are measured as follows with the aid of a sintered plate butterfly valve installed in the middle of the 34.3 cm I.D. slow bed. At a given moment, the valve is closed and the rate of descent of bed level just below the valve is timed. The solid rate in the fast bed is calculated from this information. During this measurement solid returning to the slow bed forms a fluidized bed on top of the butterfly valve, acting as a distributor. Apart from some pressure drop due to the valve itself, the pressure head due to solids in the slow bed remains constant throughout this procedure.

All the runs were made with either FCC or HFZ-20 fluid catalytic cracking catalysts. The characteristic properties

of these solids both of which belong to Geldart's Class A, are shown in the following table.

Table 4.3-1 Properties of Powders Used (after Avidan 1980)

	Size range	$\overline{dp}$	density	sphericity	Umf	ϵ_{mf}	Ga x 10^{-8}
HFZ-20	0-130μ	49μ	1.45	1.0	0.12	0.48	2.49
FCC	0-130μ	49μ	1.07	1.0	0.09		

Table 4.3-2 Size Distribution of Powders Used

FCC Particle Diameter (microns)	Vol%
0 to 16	0.6
16 to 20.2	0.4
20.2 to 25.4	1.4
25.4 to 32	5.5
32 to 40.3	12.9
40.3 to 50.8	22.4
50.8 to 64	27.1
64 to 80.6	19.7
80.6 to 101.6	7.5
101.6 to 128	1.6
> 128	0.9

HFZ-20	Weight %
0 to 1	1.1
20 to 40	20.1
40 to 64	47.5
64 to 80	22.0
80 to 130	9.0
> 130	0.3

4.3 - Axial Density Profiles - Experimental Results

An experimental investigation of the axial density profile for each powder was carrried out using superficial gas velocities over a range of 0.65 m/s to about 5.0 m/s, solid rates from the maximum capacity for the equipment down to a bubbling bed with almost zero solids throughput (carryover), and three different slow bed heights or inventories. The axial pressure distribution is shown as apparent average void fraction between two pressure taps and the distance along the bed has been made dimensionless. The apparent void fraction, ϵ, is taken as one minus the ΔP per unit bed length divided by the particle density. A precisely predetermined gas velocity and solid rate are difficult to obtain for a number of reasons. The operating procedure was to chose a volumetric gas rate, correct it for temperature and pressure and then measure the prevailing solid rate. Because solid rate was then adjusted to the desired value the pressures and therefore, the gas rate changed as well. Essentially the entire process was a trial and error procedure. If an excessive length of time was taken to get precise values, attrition of solid would also drop the solid inventory and therefore change the gas rates. Therefore the data are "lumped" over small ranges of gas velocities for comparisons. This apporoximation should not be important enough to negate the important conclusions which can be drawn from the data.

Figure 4.3-1a shows density profiles for FCC catalyst

as the gas velocity to the fast bed is raised. Gas velocities are given in m/s, and solid rates, Gs, in Kg/m^2-s based on fast bed cross sectional area. In this figure the solid inventory in the slow (companion) bed is low, the solid feed valve is fully open and therefore the imposed pressure drop is low (1 psi). Gas superficial velocity is seen to range from that of the turbulent fluidization regime (Gs=low, ϵ = 0.7) to the maximum velocity possible in this equipment. Run 141 has a gas velocity of 0.65 m/s, just above the 0.61 m/s value for Uk for FCC, the transition velocity to turbulent fluidization. The entrainment rate is so low that an actual measurement of it could not be made. This is reflected in the shape of the pressure gradient profile where the dense turbulent bed has a brief acceleration zone at the bottom, followed by a constant density zone which falls off rapidly to zero at the bed top. The area under the density gradient profile when multiplied by the bed cross sectional area yields the weight of solids in the bed. For FCC catalyst the pressure drop required to suspend the bed of catalyst fixes the mean bed voidage at about 0.70. The position of the inflection point in the density gradient profile is a measure of the height of solids in the turbulent bed.

Run 142 is operating at the lower end of the range of transition to fast fluidization, at 1.2 m/s (Utr for FCC = 1.2-1.5 m/s). As expected for this condition carry-over rises sharply, the bed expands and the density profile tends

to flatten. Flattening occurs by both the lower dense region becoming more dilute and the upper region becoming more dense while the inflection point rises in the bed. Under these conditions the bed is no longer static but rather exists because of a continuous recirculation of solids from the accompanying standpipe. The total inventory in the bed is no longer fixed but depends upon a balance between entrainment and replenishment rates. As will be discussed later this balance depends on gas and solid rates as well as imposed pressure drop.

Contrary to what was previously believed to be typical of FCC catalyst, Run 143 clearly denotes an inflection point in the axial density profile. Conditions of low velocity and low solid inventory are necessary for this to occur.

The remaining three runs on the figure are all well above the transport velocity and their density profiles are quite flat. Aside from a very gradual thinning out of the bed as the top is approached no sharp changes in the gradient are observed. These profiles are a reflection of the smooth fluidization characteristics of FCC catalyst.

By comparing the consecutive series of gas and solid rates it may be shown that raising the gas velocity of the fluidized bed, with all else held constant, raises the solid rate as well. An explanation for this behavior may be that the solids velocity is increasing as fast as the gas velocity while the area for solids flow remains almost constant ($Us = Ug - Ut$). The solids rate increase with

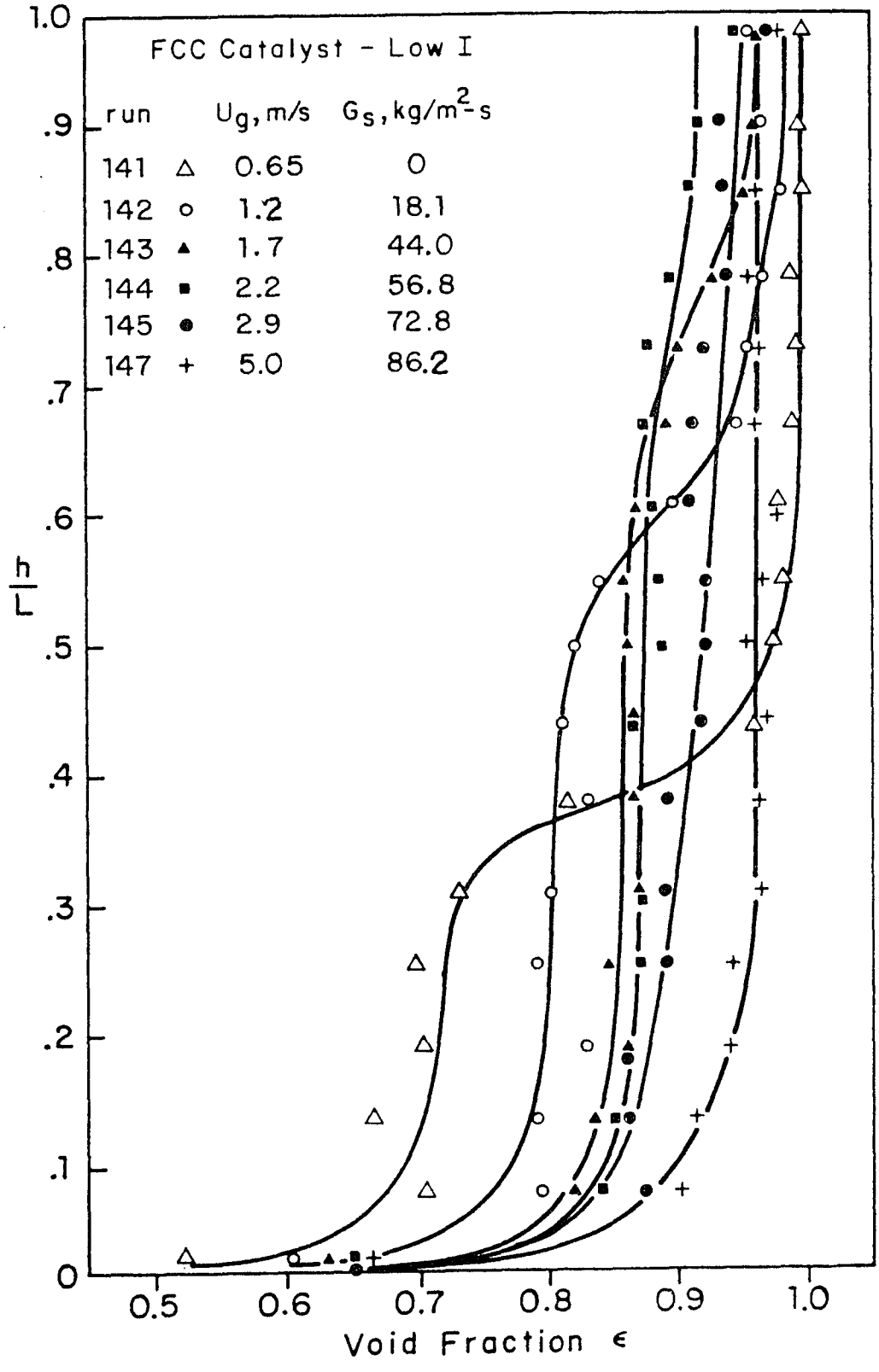

Figure 4.3-1a Void fraction vs. dimensionless bed height for FCC catalyst with a low solid inventory, (1.25m) - solid valve is fully open.

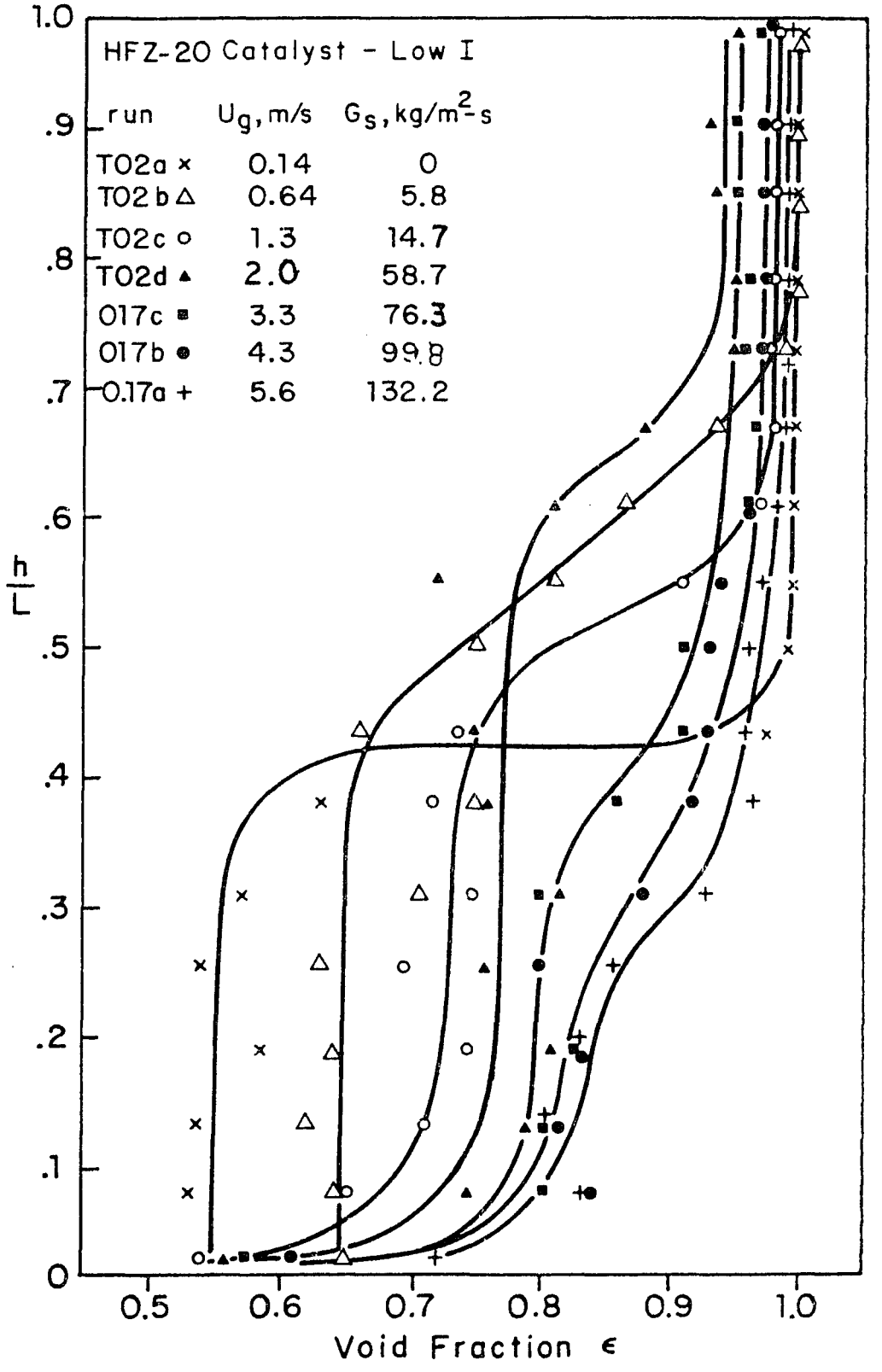

Figure 4.3-1b Void fraction vs dimensionless bed height for HFZ-20 catalyst with a low solid inventory, (1.25m), - solid valve is fully open.

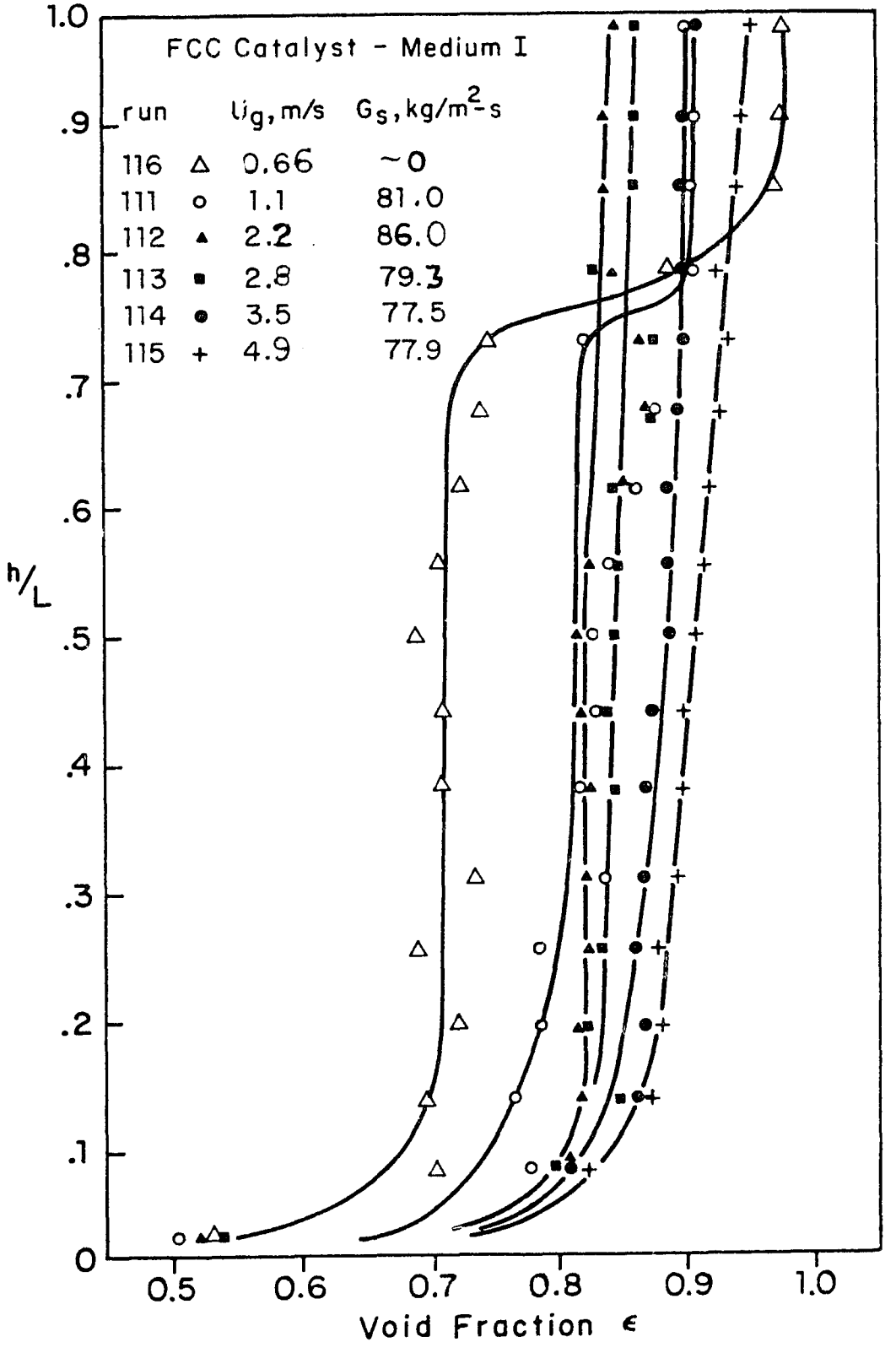

Figure 4.3-2a Void fraction vs. dimensionless bed height for FCC catalyst with a medium solid inventory, (2.5m), - solid valve is fully open.

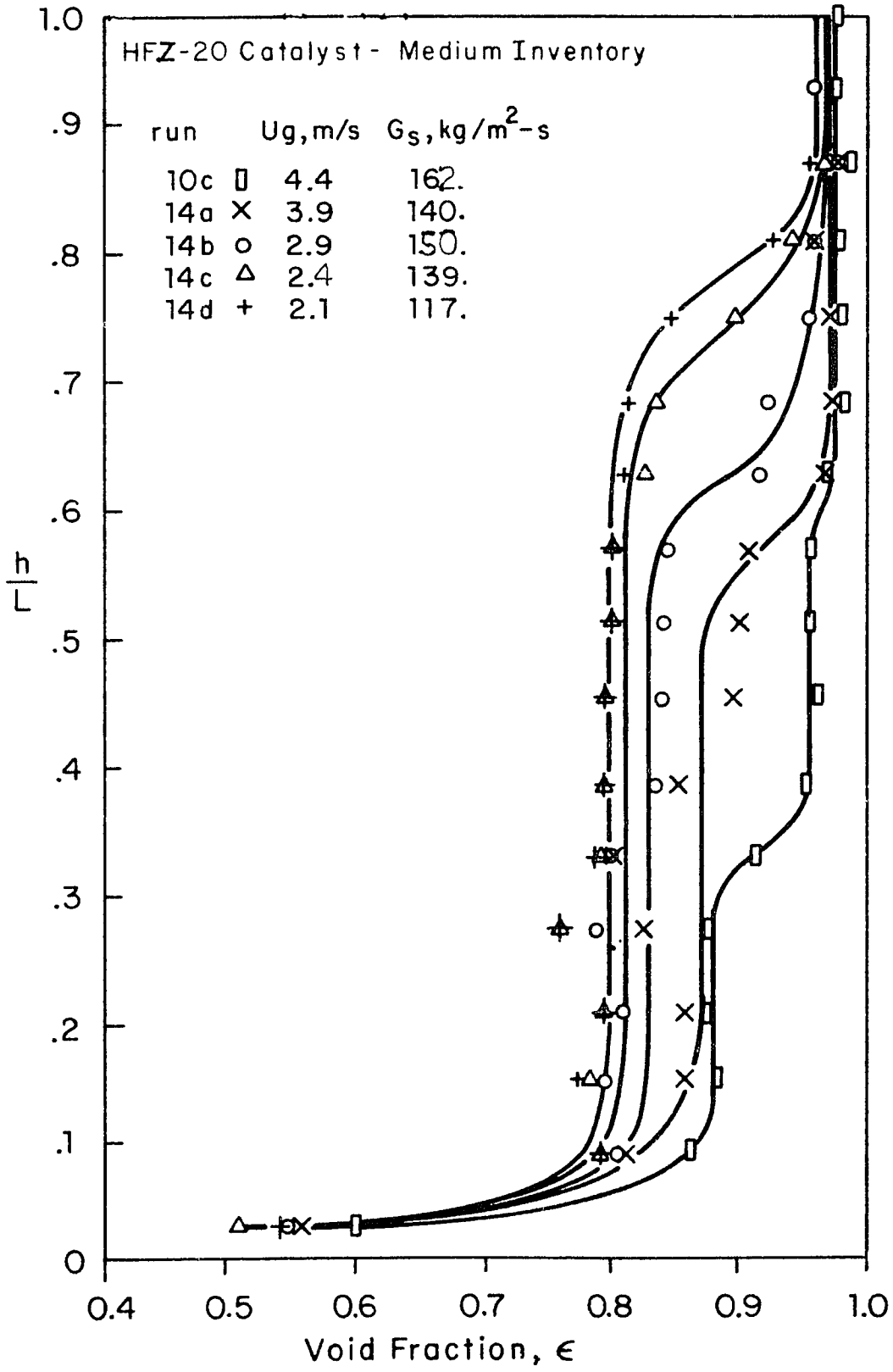

Figure 4.3-2b Void fraction vs. dimensionless bed height for HFZ-20 catalyst with a medium solid inventory, (2.5m), - solid valve is fully open.

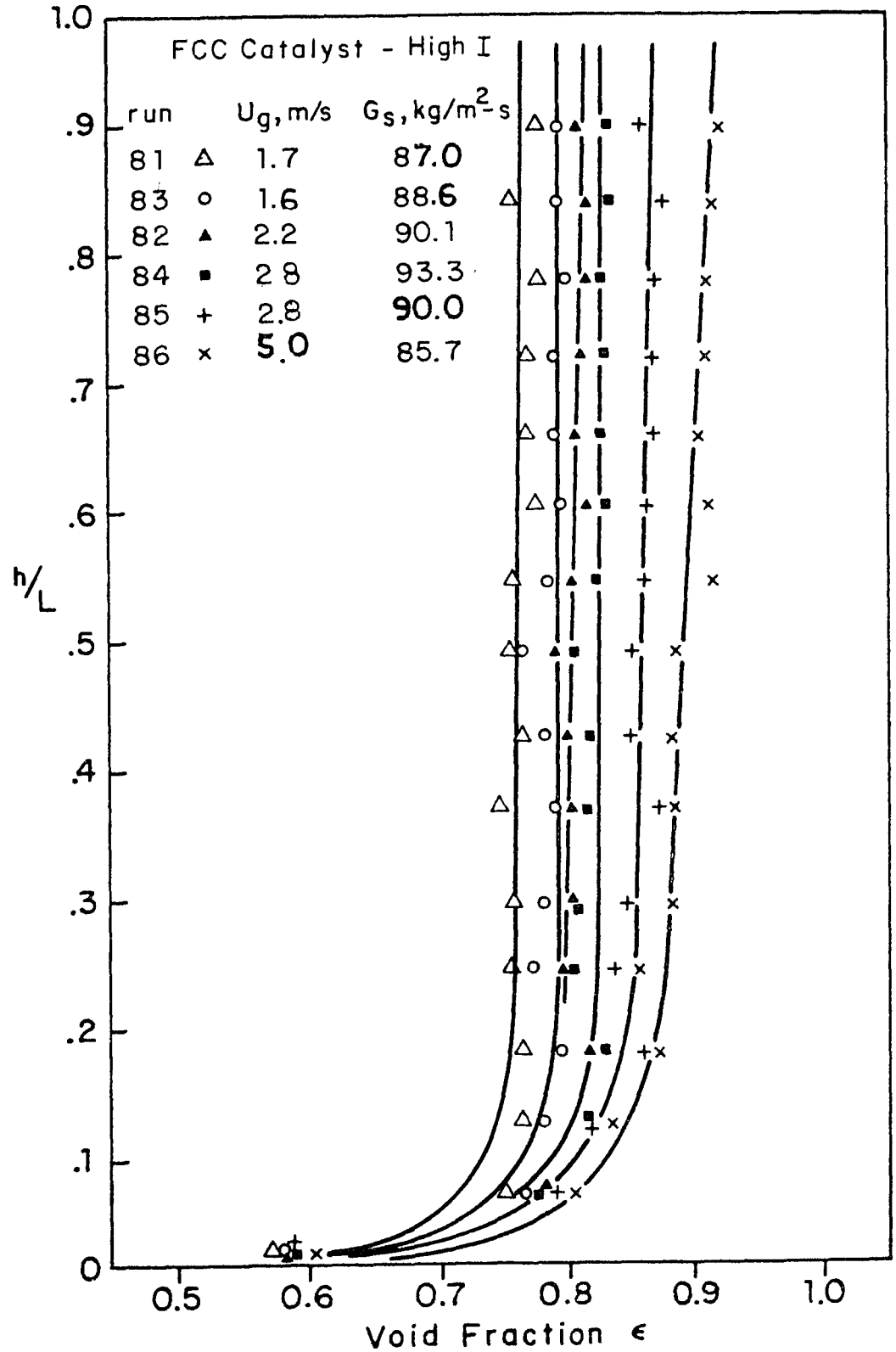

Figure 4.3-3a Void fraction vs. dimensionless bed height for FCC catalyst with a high solid inventory, (4.1m), - solid valve is fully open.

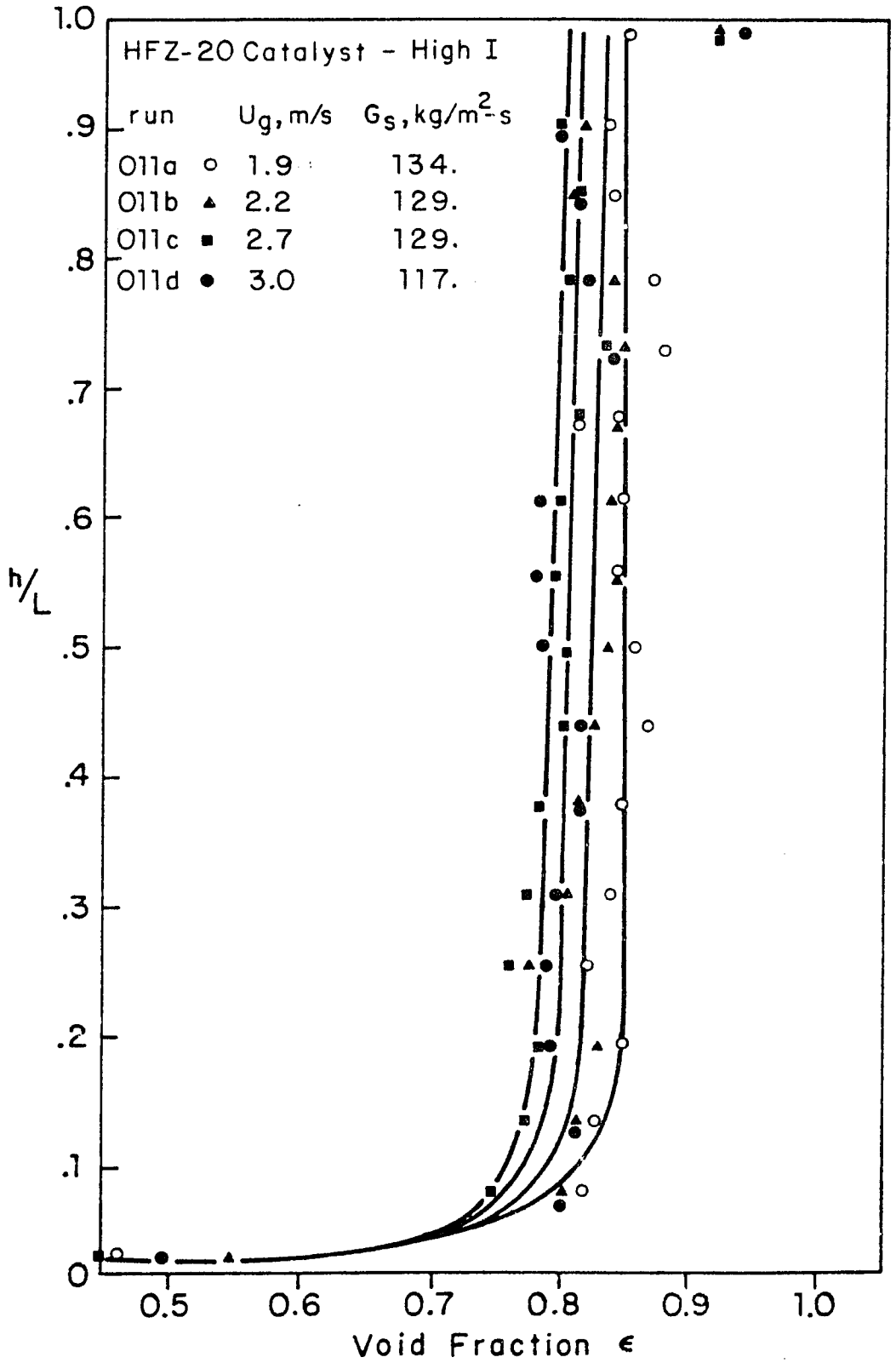

Figure 4.3-3b Void fraction vs. dimensionless bed height for HFZ-20 catalyst with a high solid inventory, (4.1m), - solid valve is fully open.

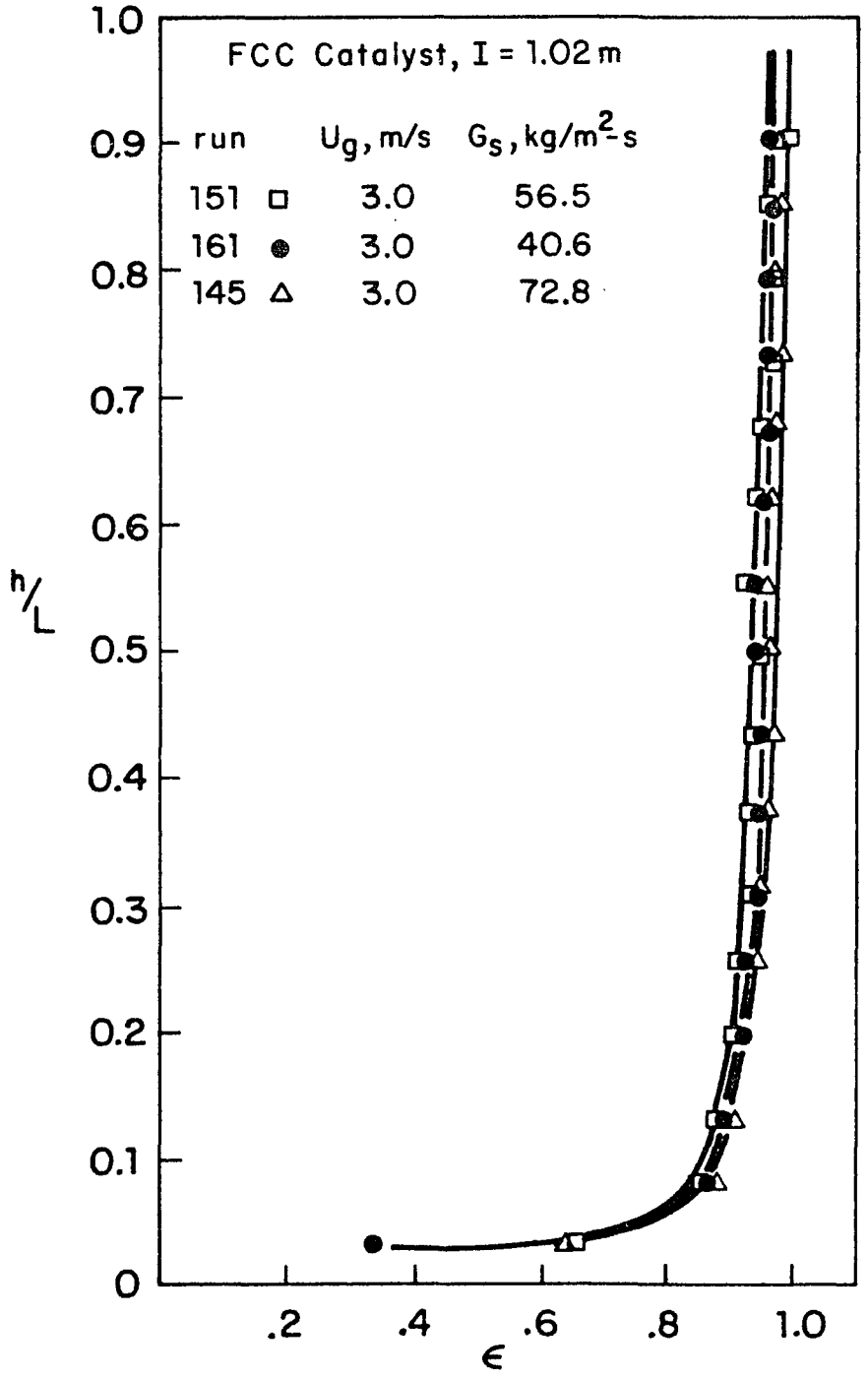

Figure 4.3-4a Void fraction vs. dimensionless bed height for FCC catalyst with a low solid inventory, (1.25m), for a constant gas velocity of 3.0 m/s and solid rates at less than maximal values as given.

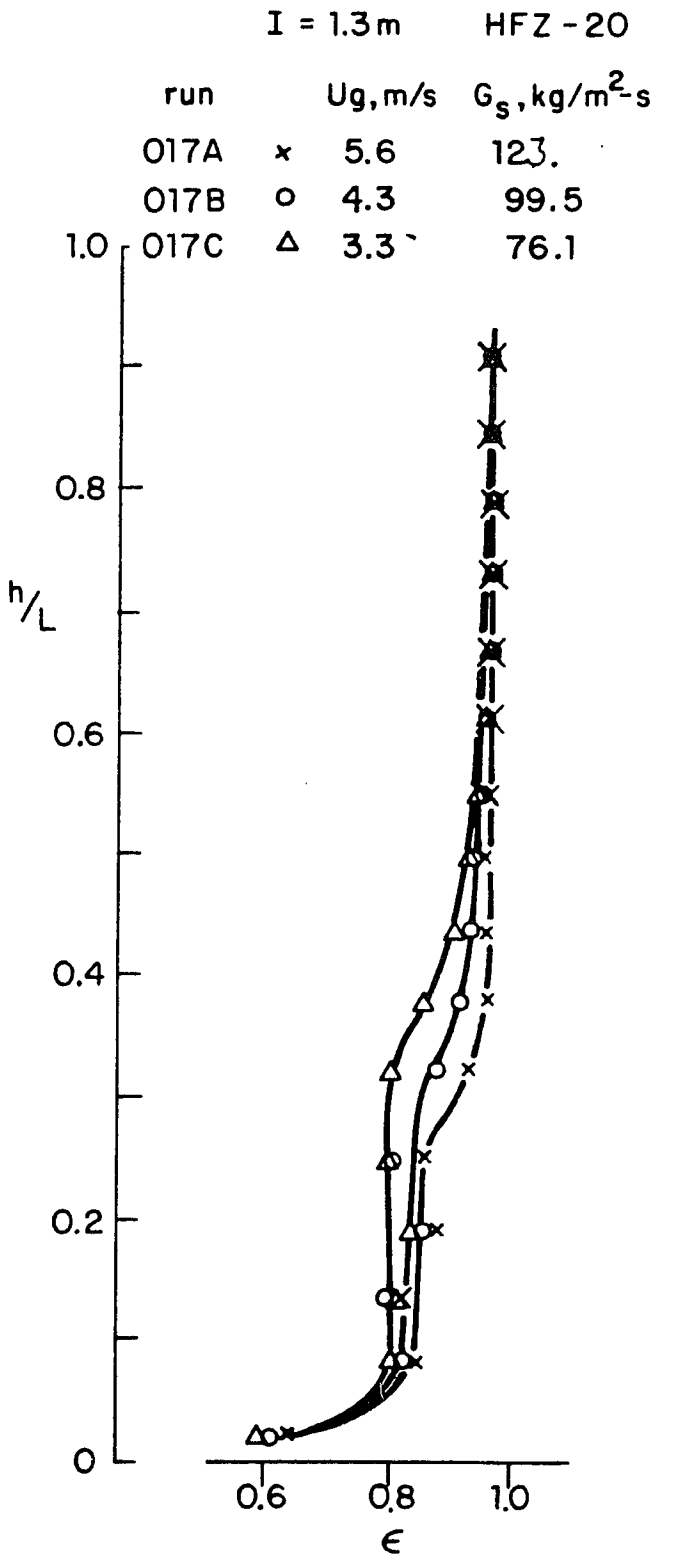

Figure 4.3-4b Void fraction vs. dimensionless bed height for HFZ-20 catalyst with a low solid inventory, (1.25m), at less than maximal solid rates and varying gas velocities.

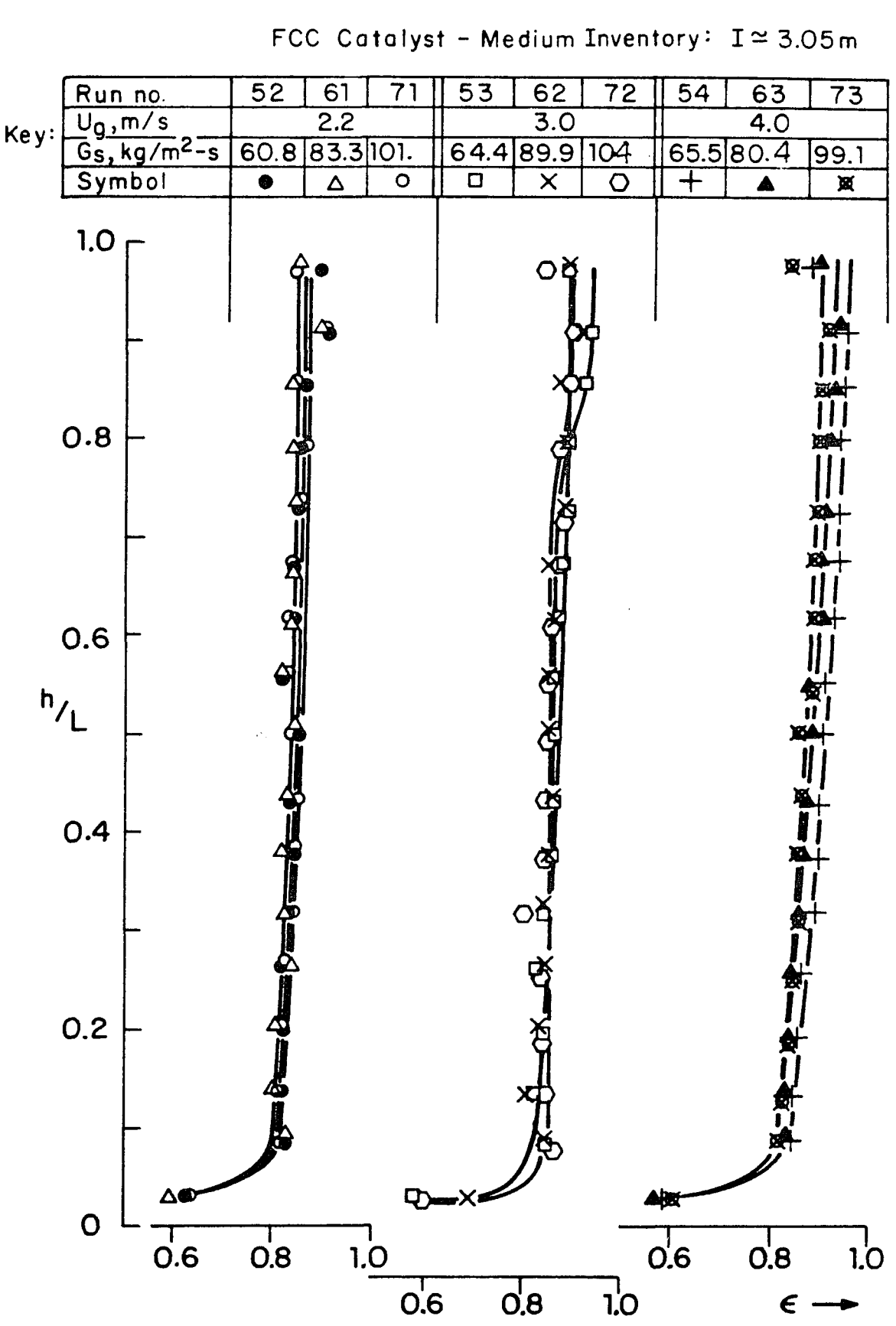

Figure 4.3-5a Void fraction vs. dimensionless bed height for FCC catalyst with a medium solid inventory, (2.5m), for each of three gas velocities and varying solid rates.

HFZ-20 Catalyst - Medium Inventory: I ≃ 2.5m

Key	Run no	14d	15d	16c	14c	15c	16b	14a	15a	16a
	U_g, m/s	2.9			3.4			5.7		
	G_s, kg/m-s	117.	107.	74.7	139.	105.	70.3	141.	111.	70.3
	Symbol	×	o	△	×	o	△	×	o	△

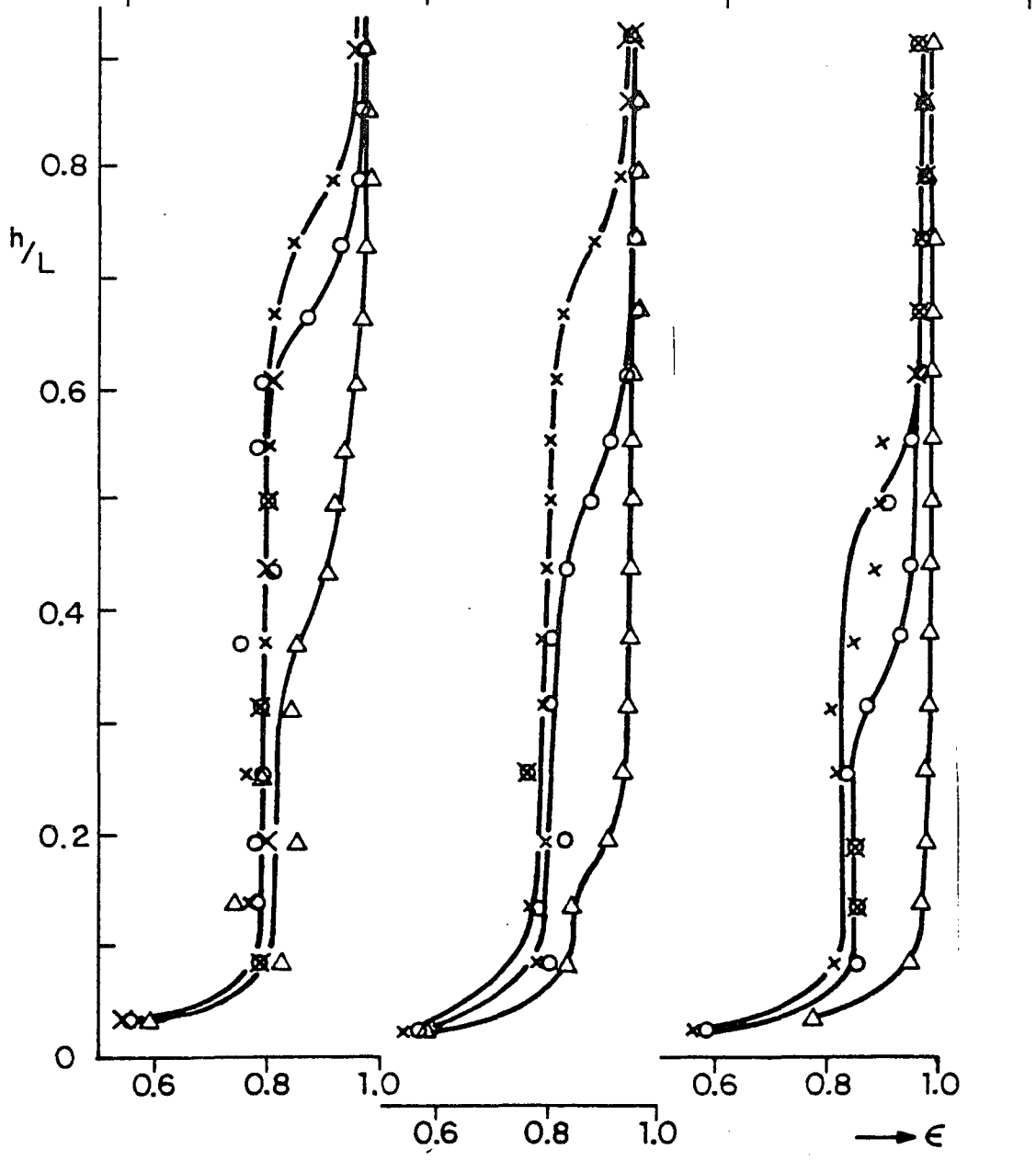

Figure 4.3-5b Void fraction vs. dimensionless bed height for HFZ-20 catalyst with a medium solid inventory, (2.5m), for each of three gas velocities and varying solid rates.

FCC Catalyst - High Inventory: I ≃ 4.32 m

Key:

Run no.	92	102	82	93	103	84	94	104	85
Ug, m/s	2.2			3.0			4.0		
G_s, kg/m²-s	65.7	87.9	90.1	64.1	86.6	93.3	64.7	80.0	88.5
Symbol	○	□	△	○	□	△	○	□	△

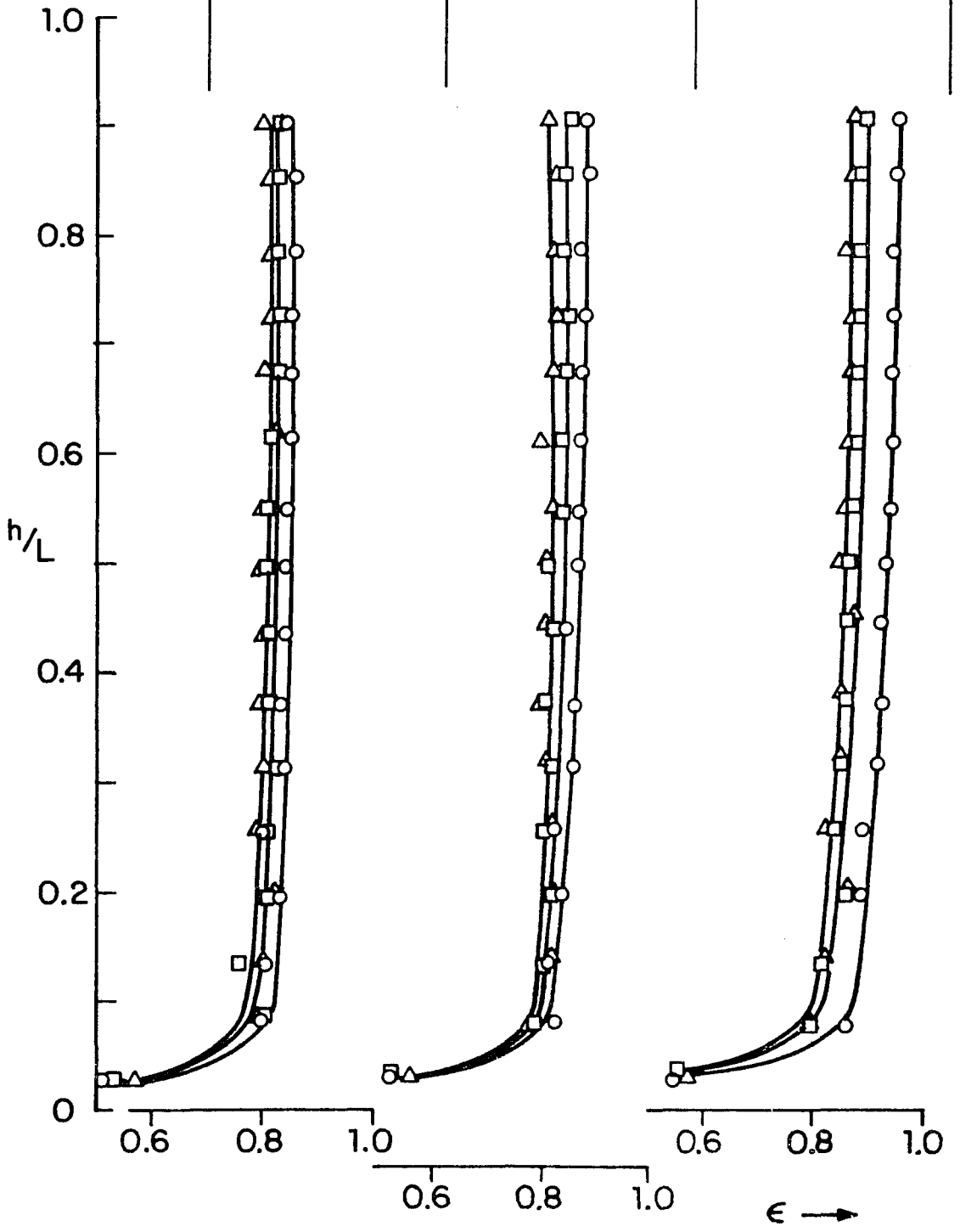

Figure 4.3-6a Void fraction vs. dimensionless bed height for FCC catalyst with a high solid inventory, (4.1m), for each of three gas velocities and varying solid rates.

HFZ - 20 Catalyst - High Inventory : I ≃ 4.1 m

Key	Run no.	11d	11h	13c	11c	11g	13b	11b	11f
	U_g, m/s	2.9			3.4			4.0	
	G_s, kg/m - s	117.	105.	73.2	129.	111.	79.1	129.	105.
	Symbol	×	○	△	×	○	△	×	○

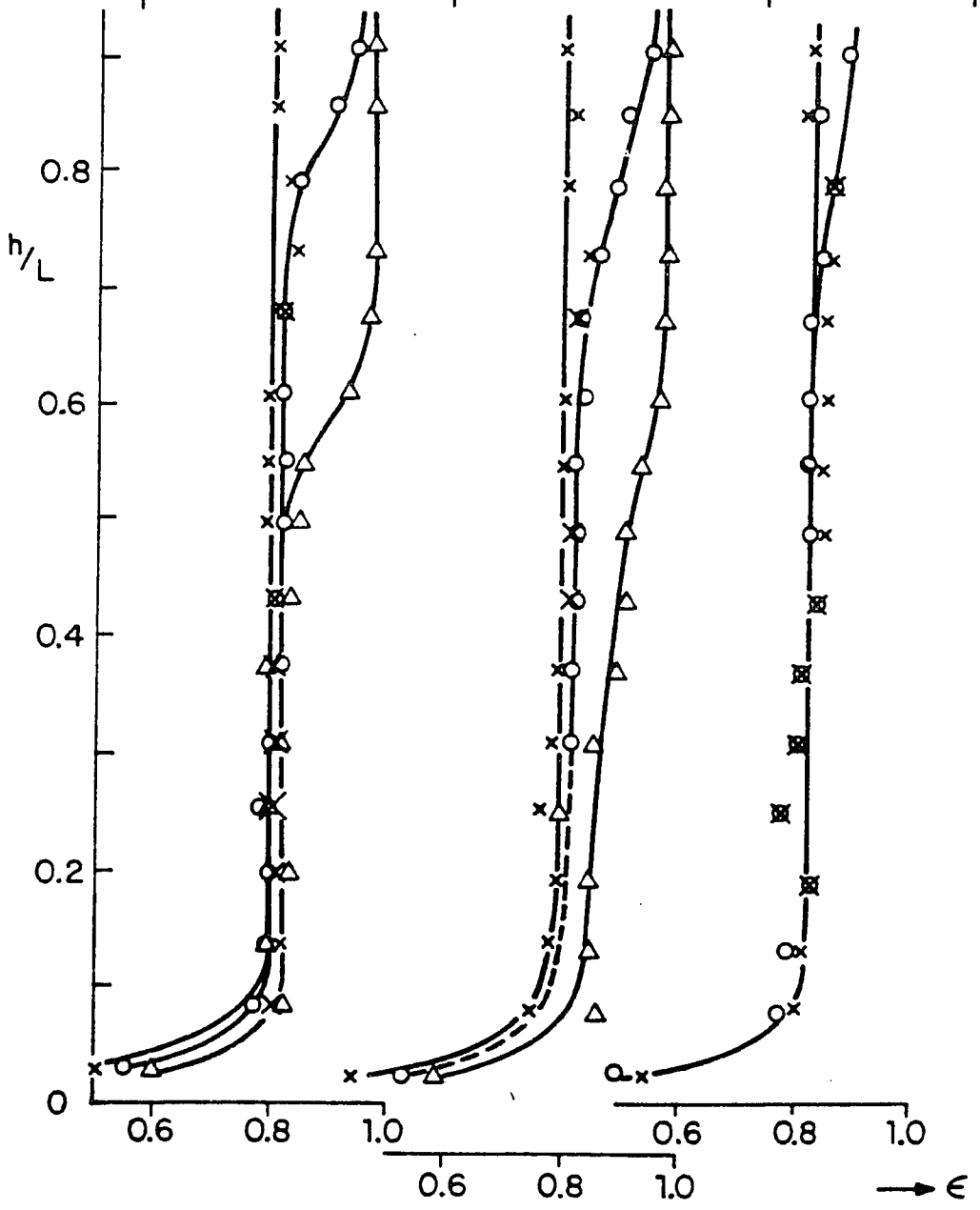

Figure 4.3-6b Void fraction vs. dimensionless bed height for HFZ-20 catalyst, high solid inventory (4.1m), for each of three gas velocities and varying solid rates.

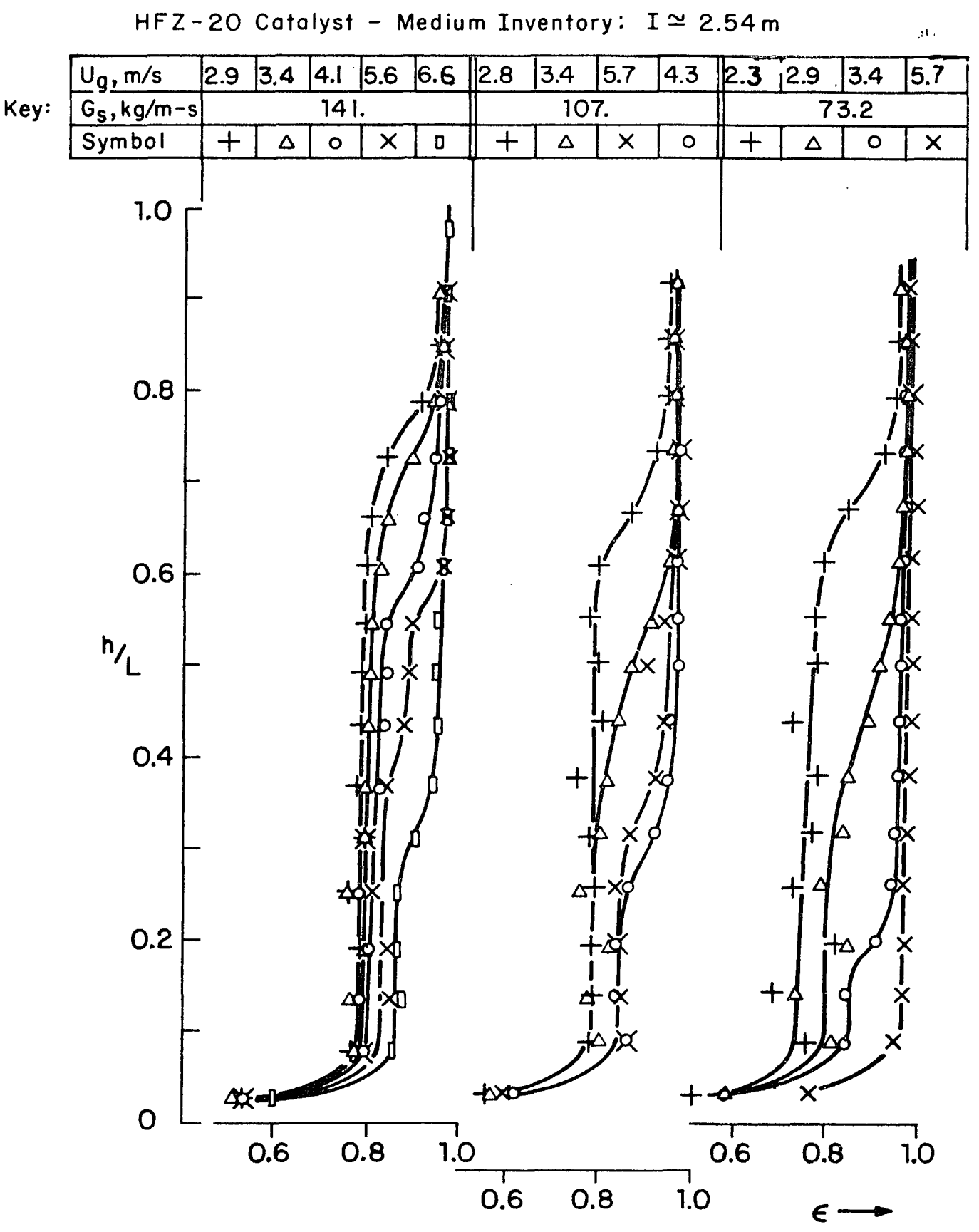

Figure 4.3-7 Void fraction vs. dimensionless bed height for HFZ-20 catalyst, medium solid inventory (2.5m), for each of three solid rates and varying gas velocities.

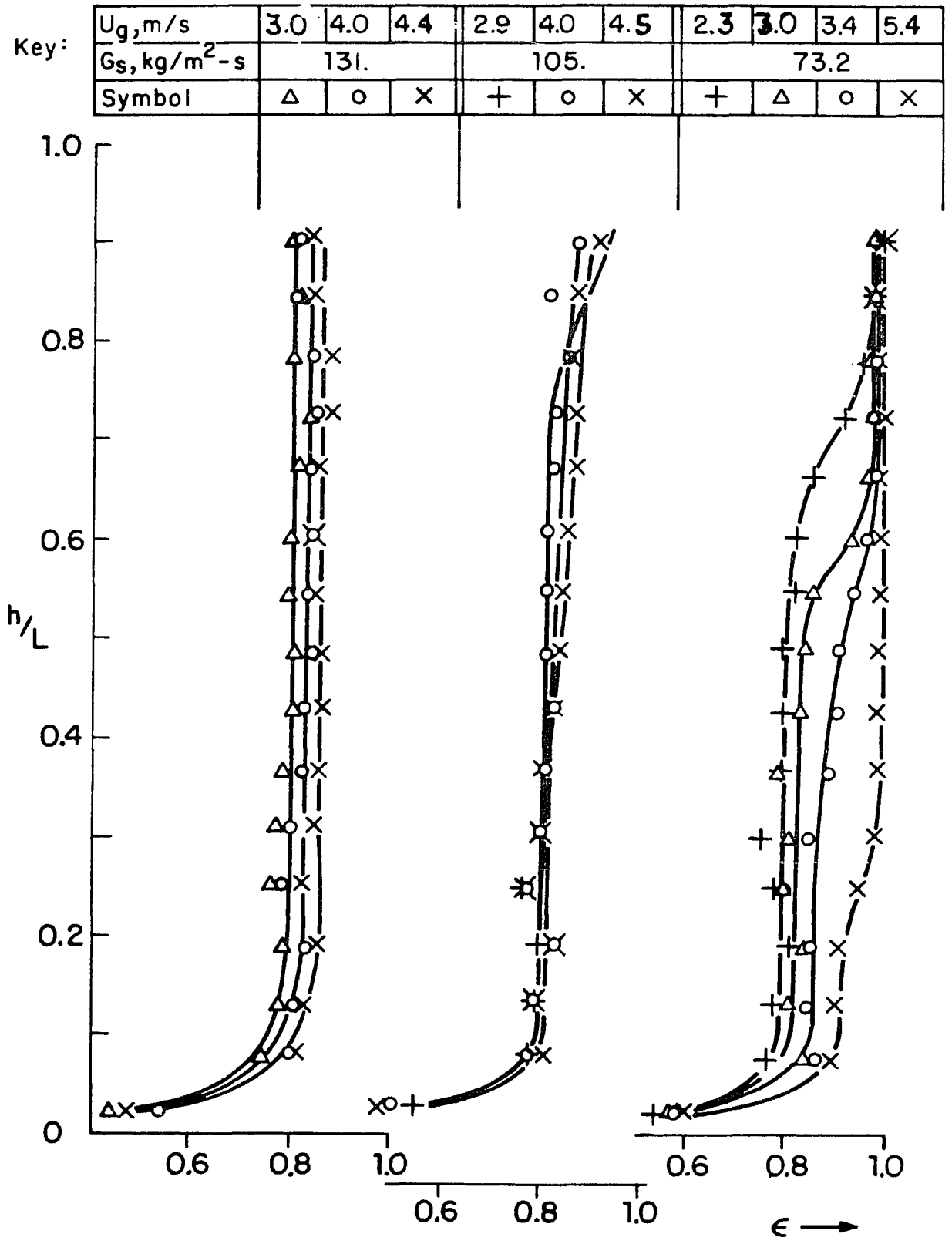

Figure 4.3-8 Void fraction vs. dimensionless bed height for HFZ-20 catalyst, high solid inventory (4.1m), for each of three solid rates and for varying gas velocities.

increasing gas velocity agrees reasonably well with this explanation.

Figure 4.3-2a was prepared from data collected on a bed operating under conditions identical to those of 4.3-1a with only the imposed pressure (solid inventory) changed to a medium inventory. In this figure only the runs with the lowest two gas velocities show any inflection point at all. Note that the bed top of the turbulent bed has moved to a higher position in the bed than given in Figure 4.3-1a. This is a reflection of the manometer type of balancing out of the solids in the fast and slow beds. Whereas in the previous diagram the remaining profiles showed some hint of an inflection point, in this figure only the very gradual thinning out of the bed towards the top is evident.

Each point on the axial density gradient profile is time-averaged by eye over the pressure fluctuations that are always present in a given bed interval. Thus, the lower velocity runs can be seen to show more scatter because the amplitude of their fluctuations are much greater. The smoother operating characteristics of the high velocity regime can be witnessed on these plots by the regular arrangement of the points on these profiles.

Figure 4.3-3a represents measurements similar to those used to construct the previous two figures except that the imposed pressure is at its highest value, 4.1 m. The large solid inventory did not allow operation in the turbulent regime and was therefore omitted. The most outstanding

characteristic of this figure is the flatness of the profiles of all the runs. For this set of runs Gs, the solid rate, did not increase with gas velocity as did occur in the low inventory case. 90 Kg/m^2-s is the maximum rate which can be achieved for FCC catalyst in this equipment and raising the gas velocity merely serves to decrease the holdup of solids in the fast bed as is evidenced by the rightward shift in axial density profiles.

The three figures examined thus far constitute a study of the variation of the axial density profile for FCC catalyst for the three solid inventories given. The low, medium and high inventories, refering to 1.2, 3.1, and 4.1 m respectively were chosen to give the maximum range attainable in the equipment. This threefold increase in inventory is judged sufficient to give meaningful results. The differences in the shape of the profiles at these inventories is quite unmistakeable. Yet, the dependence of axial density profiles on imposed pressure has not been previously recognized.

Figure 4.3-1b,4.3-2b and 4.3-3b constitute a similar study to the one just discussed using HFZ-20 as the catalyst. HFZ-20 has a particle density of 1.49 g/cc which is 1.36 times that of FCC. This higher density is reflected in the higher pressure drop of the bubbling bed of Figure 4.3-1b. The higher particle density is also reflected in the higher UK of 1.37 m/s which puts runs T02a, T02b and T02c well into the bubbling regime. The Utr for this catalyst has

not been given. Run T02d with the very erratic pressure profile must be in the range of Utr because above and below it profiles characteristic of turbuluence and fast fluidization can be seen. That HFZ-20 has poorer fluidization characteristics than FCC is evidenced by its more rapid defluidization characteristics. However these defluidization characteristics are only poor relative to the FCC and both catalysts are in the Geldart class A category.

Above the transport velocity the fluidized bed is operating in the fast fluidized mode. Unlike the flat profiles of FCC at a comparable inventory level the HFZ-20 profiles exhibit a sharp falloff in solids fraction after a short high-density zone. An inflection point in the axial density profile exists at the position in the bed dividing the dense and dilute regions. The dense phase region exhibits the solids density level that is characteristic of fast fluidization ($\sim$0.20 solids). The dilute phase region shows a solids density which borders on the dilute phase level ($\sim$0.04 solids). A column-average value of solids fraction is about 0.10, which is not characteristic of either the dense phase region or the dilute phase region in the bed. It would be unproductive to correlate any of the three solids fractions, dilute, dense or column-average, with gas velocity and solids rate unless we could predict a priori, the distribution of phases in the bed.

Figure 4.3-2b is the medium inventory set of profiles for HFZ-20 catalyst. All of the profiles shown are for high

velocity fluidization. The inflection point on each profile was previously thought to be characteristic of HFZ-20. Because the solid valve was fully open during these runs raising the gas velocity increased the solid rate as well. It is therefore not possible to distinguish from these runs which of these variables is responsible for the movement of the inflection point. Note that the dilute phase voidage is about fixed for all the runs at about 0.04 solids fraction. In the dense phase region however the two highest velocities tend to show dense phase solid fractions slightly below the 0.20 solids fraction characteristic of the lower velocity. It would appear from this figure that the inflection point rises with gas and solid rate.

Figure 4.3-3b shows axial density profiles for HFZ-20 under conditions of the highest imposed pressure drop for varying gas velocities. In all of these cases the bed density is about 0.20 solids fraction typical of that given for fast bed conditions. It might be said that the inflection point has moved above the top of the column thereby filling the bed. The slight decrease in solids rate with increase in gas velocity might possibly be explained in terms of incomplete fluidization of the slow bed. At the conditions of high flow rates of gas simultaneously with the highest slow bed inventory, hangup of solids in the slow bed is occasionally seen at the position of shrinking cross sectional area of the slow bed. This occurence would impose a ΔP across the fast bed which is less than the highest

inventory of solids would impose if the slow bed was totally fluidized.

The three figures with the axial density profiles for each solid can now be compared and contrasted. Figure 4.3-1a shows that the flat profiles are not characteristic of FCC since inflection points can be observed at the low end of high velocity fluidization. Conversely, Figure 4.3-3b shows that the curved profiles are not characteristic of HFZ-20 since these profiles are quite flat. The differences in the profiles are observed in the middle inventory range. Previous investigators using this equipment who did not vary inventory filled the bed to this level. Note that the maximum mass solid rates are different for the two solids, being much greater for the denser solid. However, the ratio of the maximum rates is approximately equal to the ratio of the mass densities, 1.36.

In the high velocity regimes, for both solids examined, the dense region tends towards 0.20 solids fraction while the dilute regions tends towards 0.04. The inflection point height sets the relative amounts of dilute and dense phase regions of the bed and thereby the column average. This height is so far seen to depend upon the solid inventory in the slow bed. It is also seen to depend in an as yet indeterminate way on gas and solid rates.

In order to separate the dependence of the inflection point on gas rates from its dependence on solid rates another set of experiments has been performed where one of

these rates is held constant while the other is varied and the dependence noted. These experiments are performed for each solid at each of the three slow bed inventories. For FCC catalyst at less than maximal solid rates the axial density profile is quite flat and cannot be used for this purpose. This data is included for completeness in Figures 4.3-4, 4.3-5, and 4.3-6. HFZ-20 catalyst profiles have inflection points which are both very pronounced as well as easily manipulatable in the range of interest. This is the data from which our conclusions are drawn.

Three sets of data with a middle inventory (2.5 m) are shown in Figure 4.3-7. Each plot presents the axial profiles for three different gas velocities at a given value of solid rate. Within each set the inflection point is seen to rise with decreasing gas velocity. Comparison of the three data sets shows how inflection point rises with increase in solids rate. The lowest inflection point is therefore given by the combination of highest gas velocity and lowest solid rate. In this case (Gs = 73.2, Ug = 5.76) the inflection point has merged with the acceleration zone so that the entire column exhibits the dilute phase.

An equivalent plot for HFZ-20 catalyst at the highest, 4.1 m, inventory Figure 4.3-8, shows the effect of that parameter. If the gas and solid rates are held constant raising the solid inventory has the effect of raising the inflection point. Intuitively this can again be explained in terms of the two legs of a manometer. If the slow bed leg is

filled to the higher inventory, the level of the denser, lower region in the fast bed leg must rise. At the high inventory level the denser region of the fast bed usually fills the column except at the lowest solid rates.

In the cross-plots, Figures 4.3-4b, 4.3-5b, 4.3-6b it apppears that two independent effects may be in conflict. Figure 4.3-5b contains three sets of axial profiles for three gas velocity values. Within each set the inflection point rises with solid rate as concluded earlier. However when comparing the series the set with the intermediate Ug should clearly have the intermediate inflection point positions. Note should be taken however of the higher solid rates for this set. It appears that in this case the solid rate has an overiding effect in pushing the inflection point up.

The data for HFZ-20 can now be used to summarize the effects that varying different system parameters have on inflection point position, and thereby mean solids loading in the fast bed. Raising the gas velocity, decreasing the solids rate and lowering the inventory of the slow bed all have the effect of decreasing the inflection point height and thereby decreasing solid holdup in the fast fluidized bed.

Figures 4.3-9a and 4.3-10a are plots of the three solids fraction values for both solids at the three inventories as functions of solids mass rate, Gs, for superficial gas velocities of about 3 and 4 m/s, for FCC

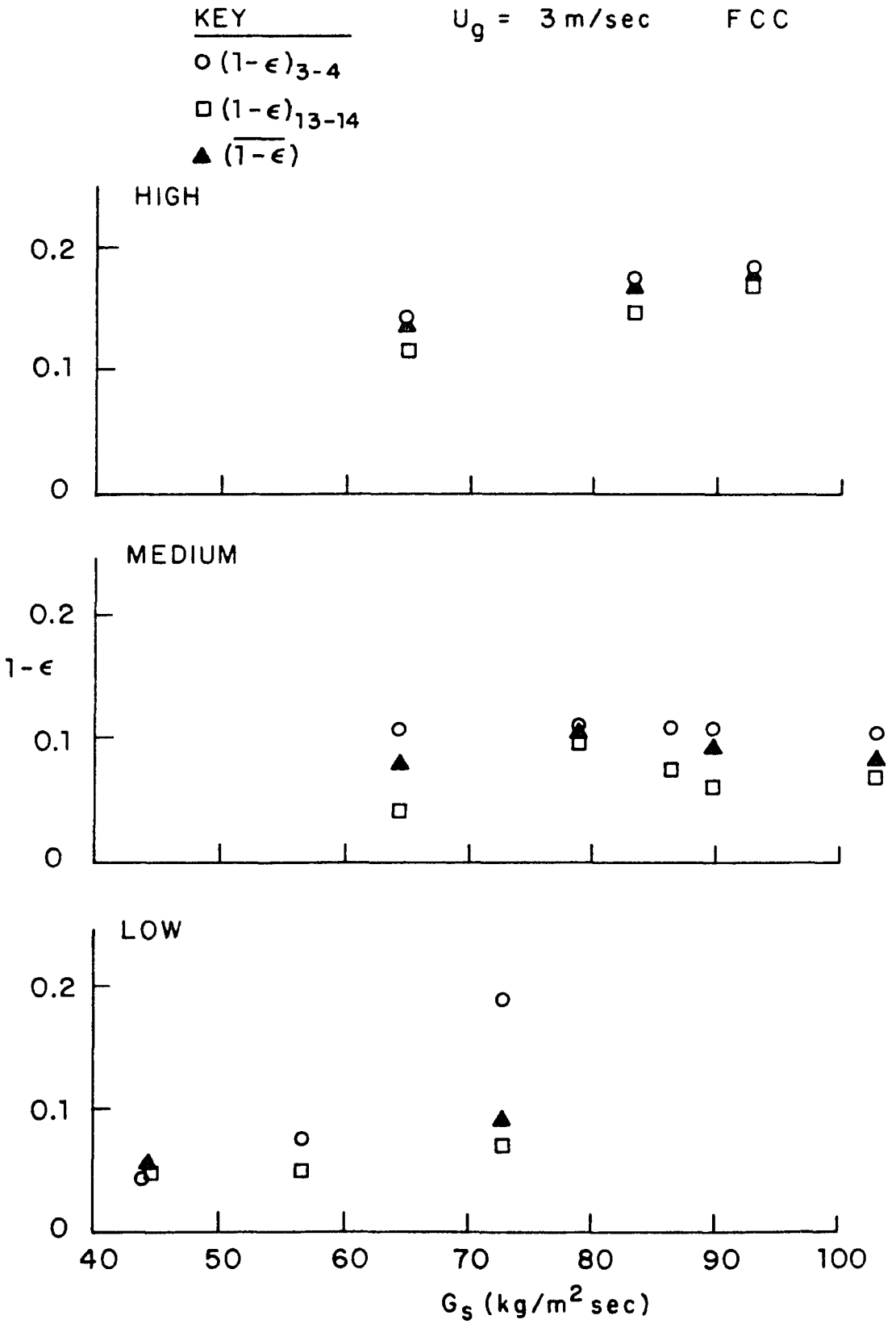

Figure 4.3-9a Solid fraction values for FCC catalyst at 3 m/s, corresponding to the bottom, top and mean of the bed for each of three solid inventories vs. Gs.

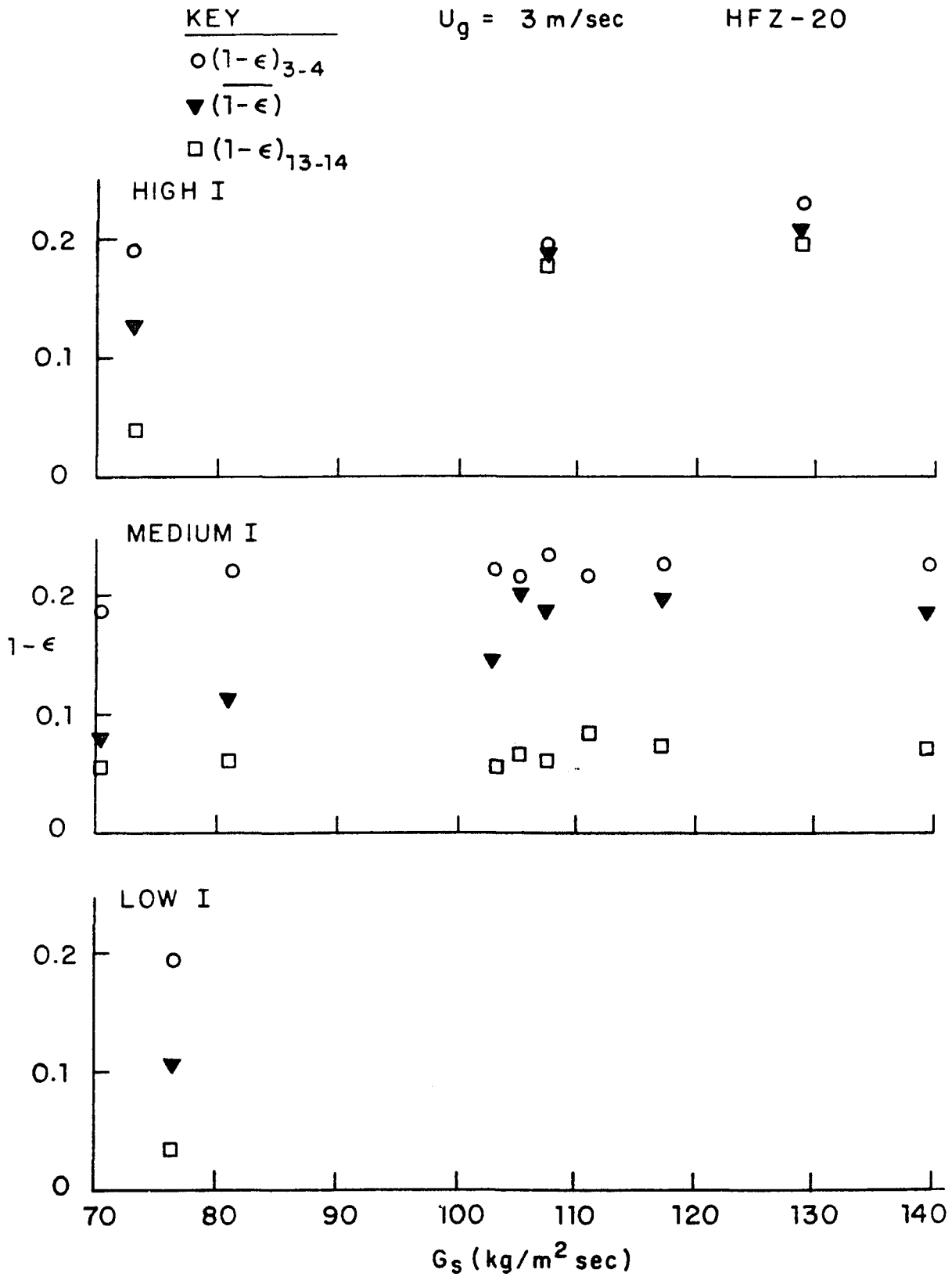

Figure 4.3-9b Solid fraction values for HFZ-20 catalyst at 3 m/s, corresponding to the bottom, top and mean of the bed for each of three solid inventories vs. Gs.

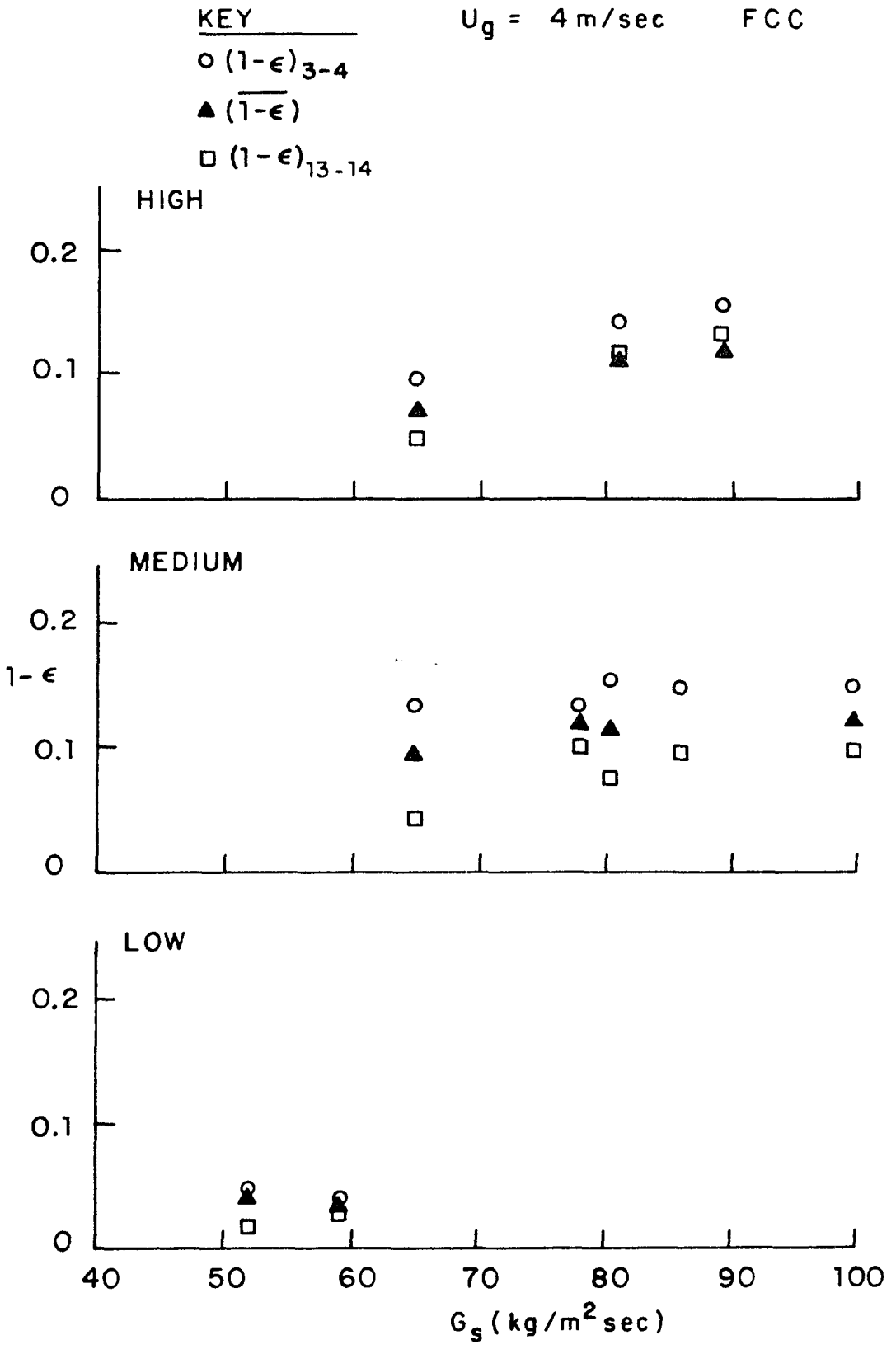

Figure 4.3-10a Solid fraction values for FCC catalyst at 4 m/s, corresponding to the bottom, top and mean of the bed for each of three solid inventories vs. Gs.

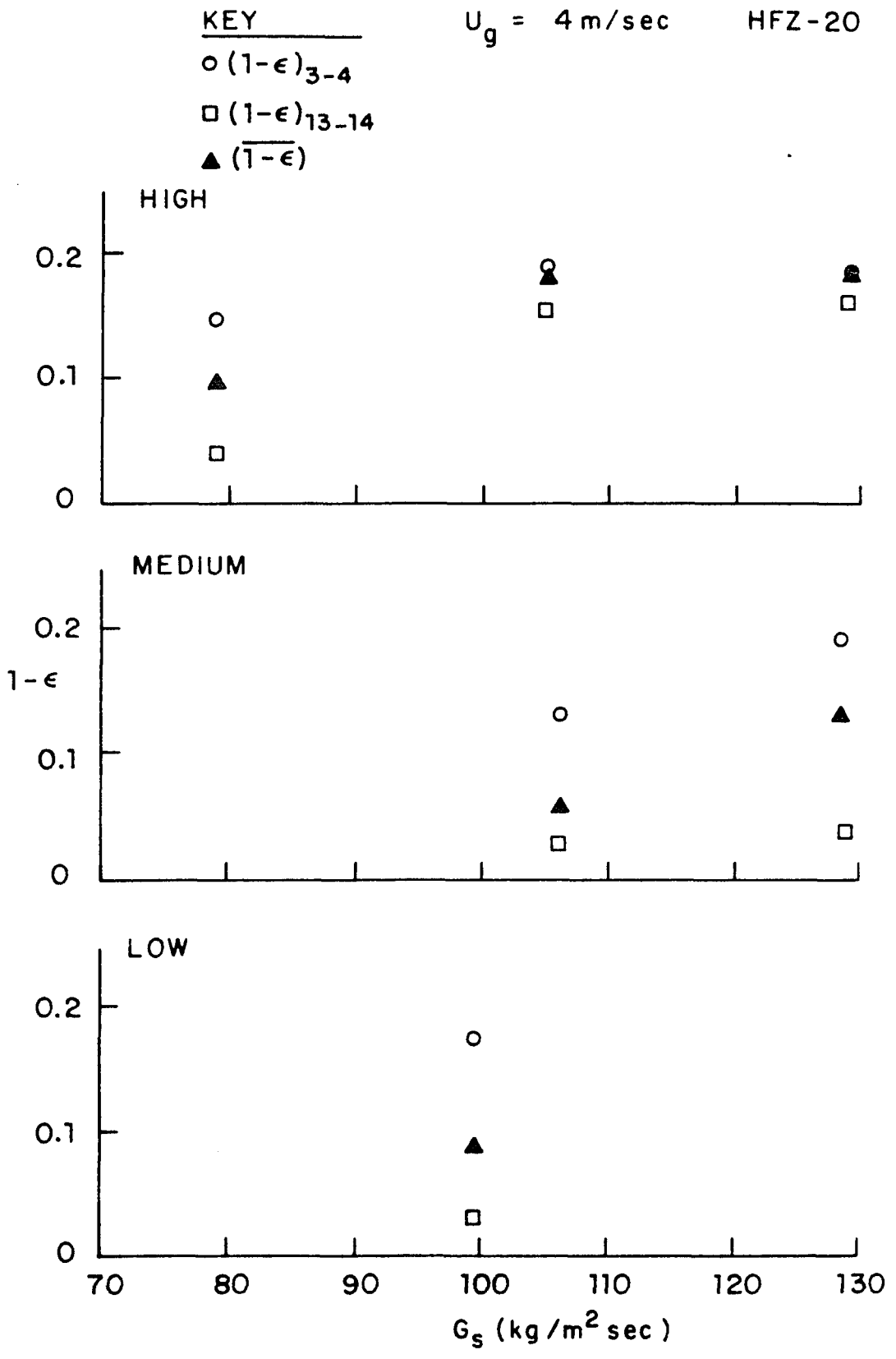

Figure 4.3-10b Solid fraction values for HFZ-20 catalyst at 4 m/s, corresponding to the bottom, top and mean of the bed for each of three solid inventories vs. Gs.

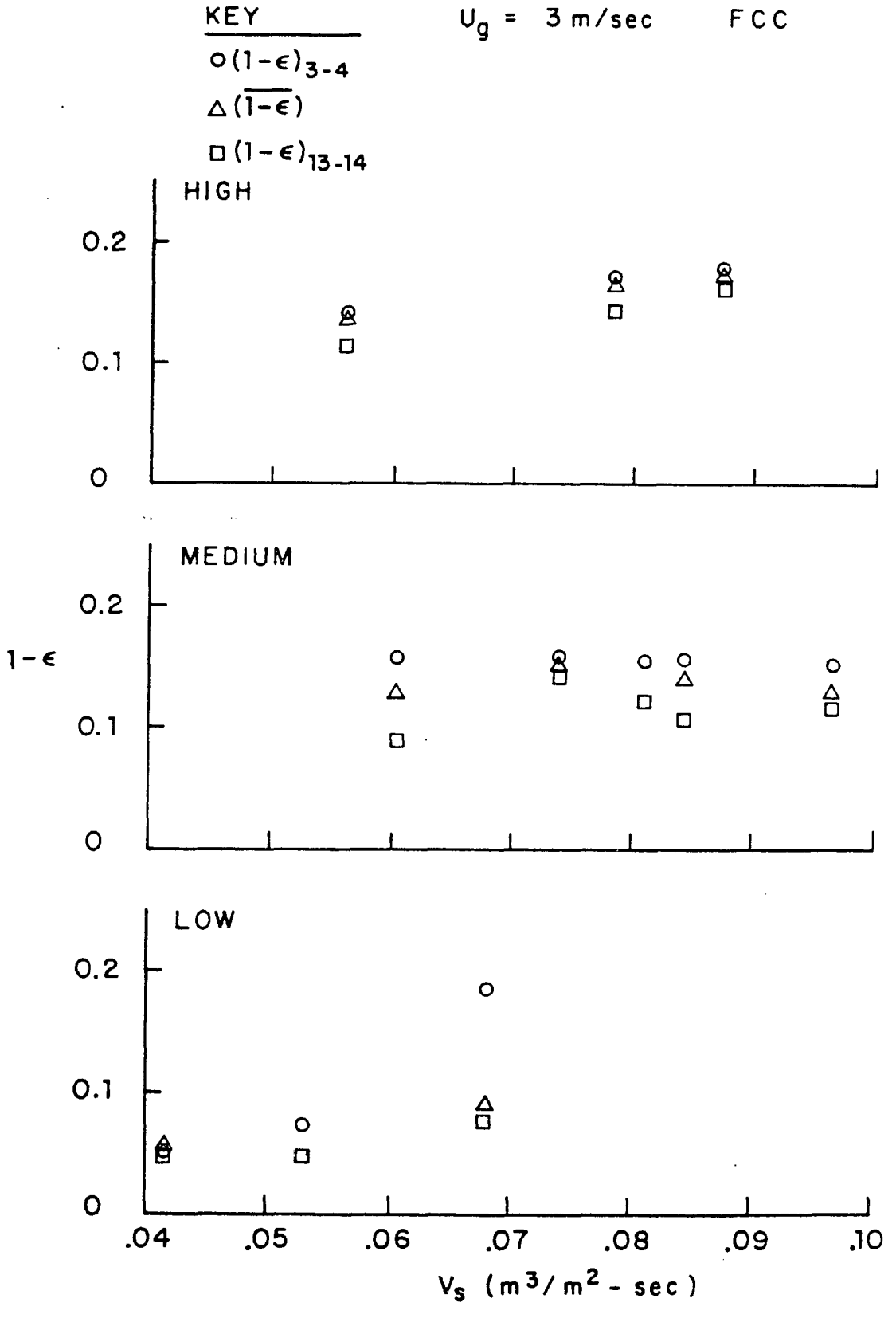

Figure 4.3-11a Solid fraction values for FCC catalyst at 3 m/s, corresponding to the bottom, top and mean of the bed for each of three solid inventories vs. Vs.

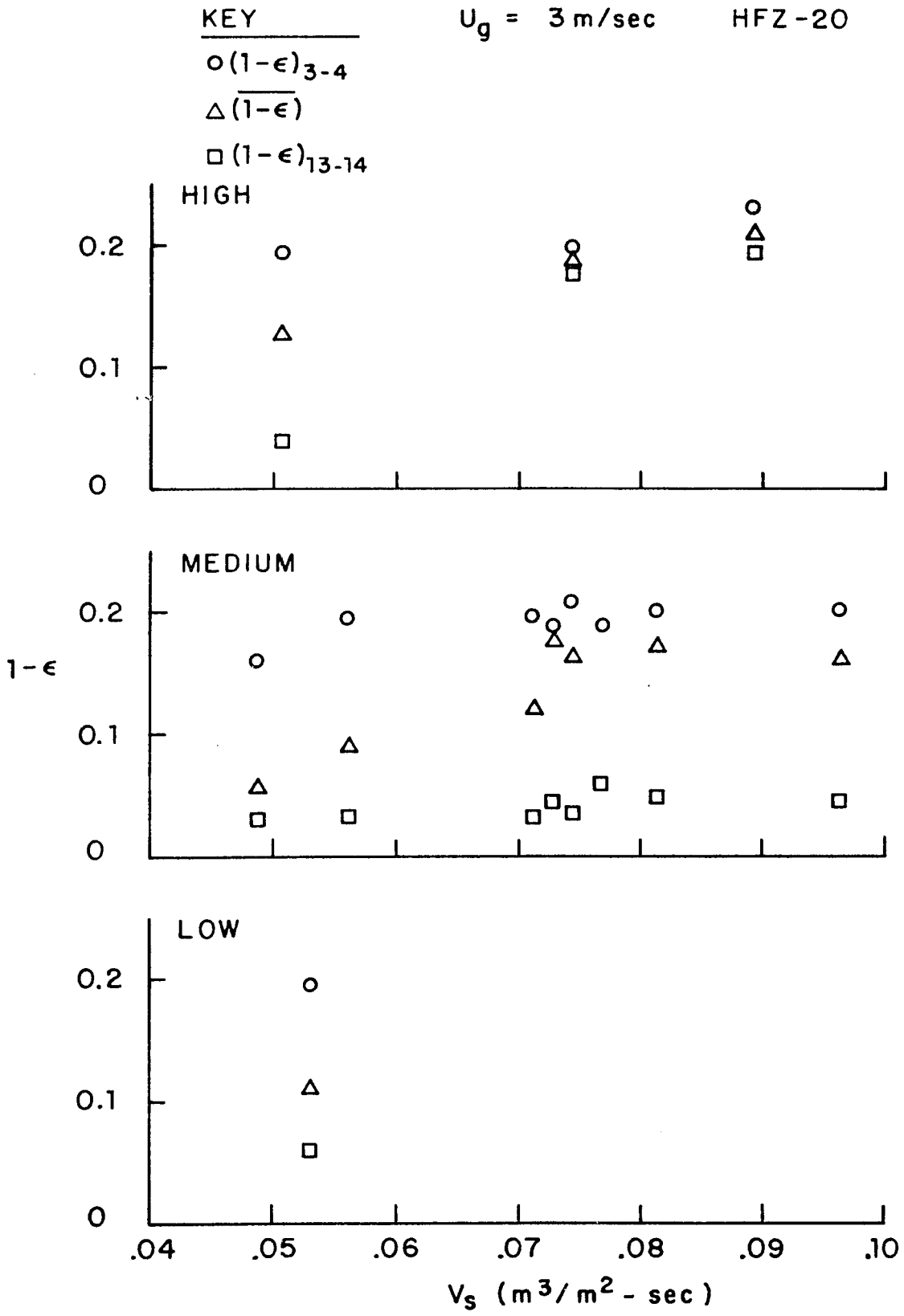

Figure 4.3-11b Solid fraction values for HFZ-20 catalyst at 3 m/s, corresponding to the bottom, top and mean of the bed for each of three solid inventories vs. Vs.

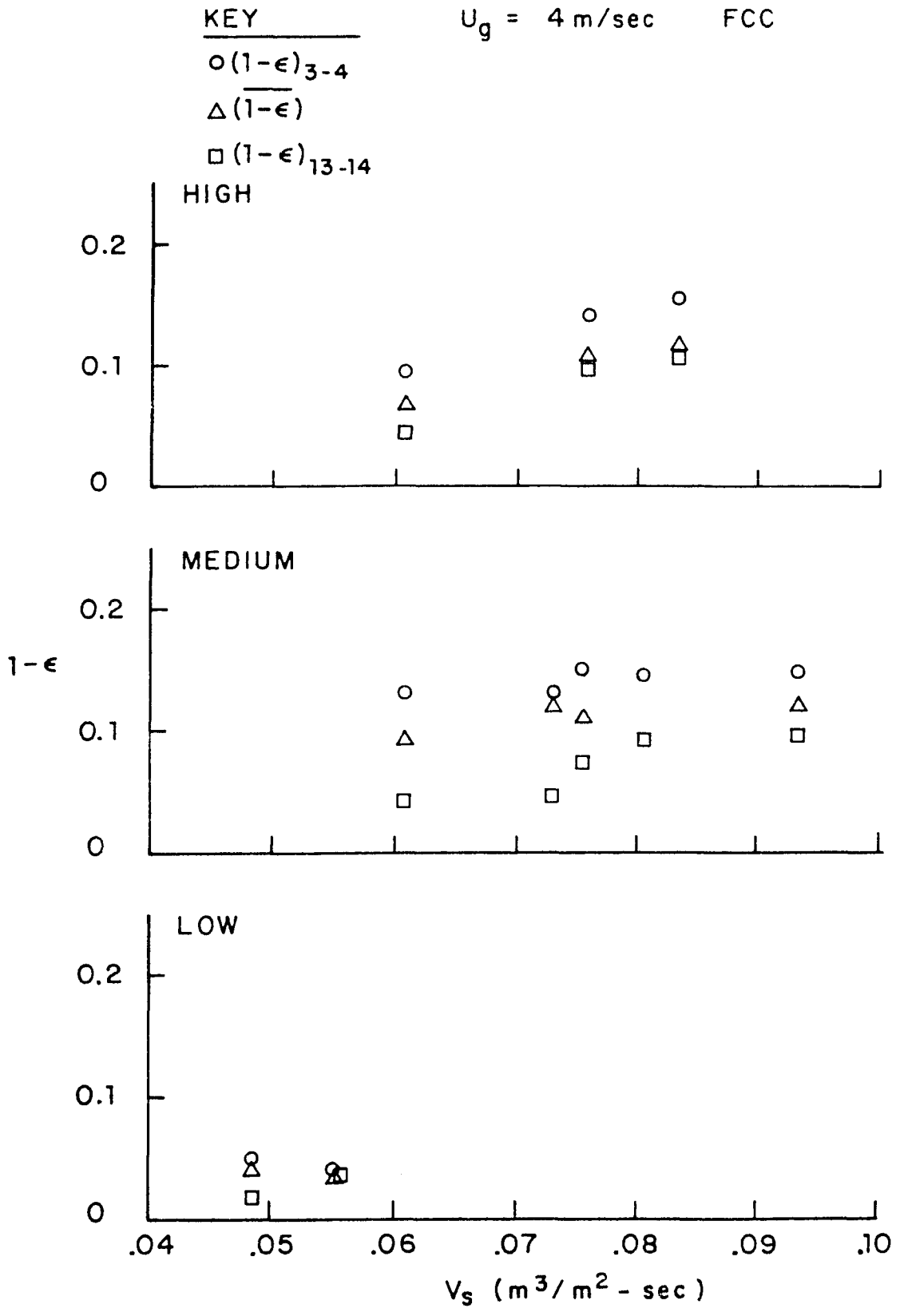

Figure 4.3-12a Solid fraction values for FCC catalyst at 4 m/s, corresponding to the bottom, top and mean of the bed for each of three solid inventories vs. Vs.

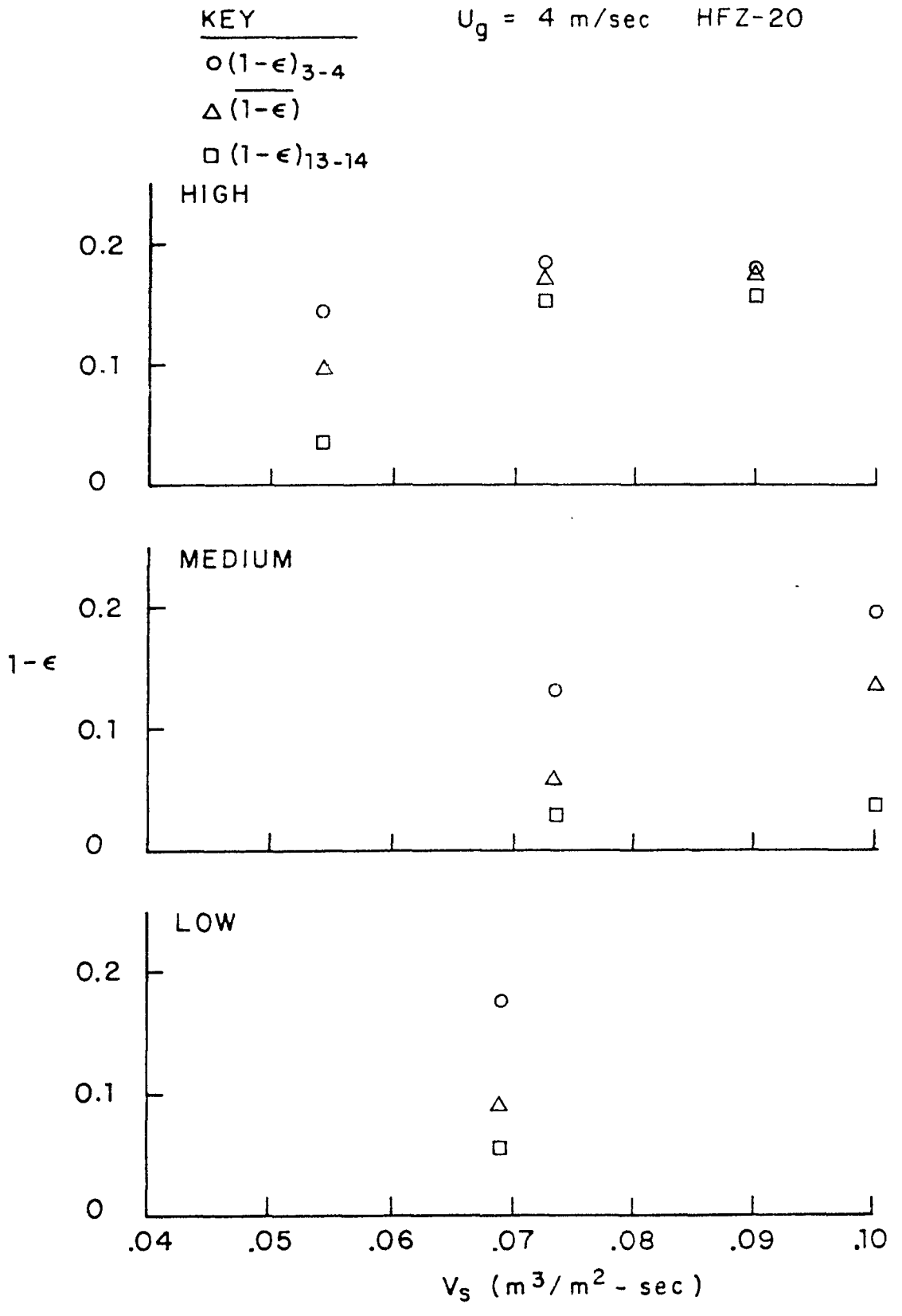

Figure 4.3-12b Solid fraction values for HFZ-20 catalyst at 4 m/s, corresponding to the bottom, top and mean of the bed for each of three solid inventories vs. Vs.

catalyst. The comparable plots for HFZ-20 catalyst are shown in Figures 4.3-9b and 4.3-10b. The observations made from the axial density profiles are confirmed in these plots as well. Also confirmed is the observation that solids fraction decreases with increasing gas velocity, all else held constant.

Plots of the three solids fractions as functions of volumetric solids rate, $Vs = Gs/\rho s$, for a superficial gas velocity of about 3 m/s are shown in Figures 4.3-11a and b, for FCC and HFZ-20 catalyst respectively. It can be seen how the average solids loading in the fast fluid bed is almost independent of solid particle density at the same volumetric solids rate and superficial gas velocity, and solids return leg volume, for the two particles considered.

The rationale behind the collapse of the data for both particles when plotted against volumetric solids rate can be given as follows. Consider two different solids each in a fast bed system at the same gas velocity, solids volumetric flow rate, and slow bed inventory. If there were no losses or pressure drops through the cyclones and solid valves which are not proportional to solids density, the two solids should have identical fast bed solid fractions, assuming that the less tangible fluidization characteristics of both solids are the same. Identical height of solids in the slow bed for each solid would yield pressure drops in the ratio of their particle densities. The solids energy gains on the fast bed side as well as the energy inputs from the

compressor would also all be proportional to the solids particle density. The frictional loss terms, however should not be proportional to the particle density. It would therefore be expected that the solids fractions in the fast bed would be close for the two different solids but not identical.

Energy Losses

In trying to define the differences in behavior between the two solids considered, a calculation was made of the ratio of energy loss from the gas ΔPUg minus the rate of potential energy gain of the solids, GsL per pound of solid per foot of column. This quantity has been defined earlier in section 3.3 as the Energy Loss Ratio, ELR. This ratio is shown as a function of solid rate for FCC and HFZ-20 in Figures 3.3-1 and 3.3-2 respectively. It should be understood that this ratio approaches infinity for a static, bubbling, fluidized bed. The FCC results Figure 3.3-1 show a trend downward with increasing solid rate at a low gas velocity, approximately the transport velocity. At higher gas velocities there appears to be a trend to increasing values of the ratio with increasing solids rate. Each set of data at a given gas velocity show this trend.

5 - X-Ray Density Studies

In this study x-rays were used as a tool for measuring radial density profiles as a function of axial position in the high velocity fluidized bed. Four previous investigations in any type of fluidized bed using x-rays have been reported in the literature. These are described below.

1. Grohse (1955)[13] x-rayed a bubbling bed of Si-Al catalyst and obtained instantaneous axial density profiles. Although Grohse was investigating a different regime of fluidization, he does give explicit information as to the type of equipment used, the system calibration and the determination of the absorption coefficient u. Note that the energy levels at which he worked, 150KV and 3mA, were too low for obtaining instantaneous densities. Moreover, the 0.1 - 10 second exposure times used confirm this fact. What is not obvious from the experimental description is whether the x-ray beam was collimated or not. The geometry of the beam is unknown. His detector was a point measuring photomultiplier tube which measured absorption through the diameter of the column. Grohse does, however, point out the distinct advantage in using x-rays as an analytical tool in that they are absorbed by inner electrons and are therefore not dependent on the chemical or physical state of the absorbing medium. Considering the many phases in which alumina can exist this is a distinct advantage.

2. Rowe used x-rays to measure the interaction of

bubbles with surfaces [22] 2,3-D bubbles [23], bubble size [24], and number, solids mixing in bubbles [25], cloud formation [26], bubble formation [27][28][29] and most of all, photographing bubbles [30]. What all of the above studies have in common are x-rays and bubbling beds. Although we are operating in a different regime, the experimental techniques may have much in common.

Rowe provides a survey of the types of x-rays units available and equipment recommendations. Quoting from his work [22], p. 42:

"There are broadly three kinds of x-ray sets commercially available. Flash x-ray units are made with voltages up to 300kV of nano-second duration. Because they depend on condenser discharge, there is a delay of several seconds between successive flashes which makes them unsuitable for studying movement. Industrial and medical therapeutic machines are in the range above 150kV but the tube rating is usually less than 10mA anode current. It would require several seconds to produce any blackening of film through a typical fluidized bed under these conditions. Finally, medical diagnostic units are made to operate up to 130kV at anode currents as great as 400mA. These peak conditions can only be maintained for brief periods, but long enough to obtain a picture of a moving bubble with good definition and with a succession of exposures to follow its passage over some ten centimeters of travel. It is this last class of machine that is most suited for our purpose."

The unit used in this work falls into this last category with a target potential of 150 and 300kV (depending on tube used) and a maximum current of 30mA. It will be seen that this unit is suitable to get sufficient resolution of bed density. We have, just as Rowe does, an image intensifier which assists with the resolution. Remember that Rowe was x-raying a bed voidage of 0.5-0.6, while this work is more in the range of 0.80-0.95.

3. At the Lensovet Leningrad Technological Institute x-rays were used to evaluate the distribution function of solid particle velocities as well as other statistical functions [36][37]. The bed used was 72mm (2.83in.) diameter and particle diameter was 7.0mm (ρ_p=0.49g/cc)(Ug=1-5m/s). Particles were made visible by their difference in ability of absorbing x-rays (tracer). This was done by covering expanded polystyrene particles with lead foil. It is not at all clear how it was possible to obtain a higher integrated value for electron density without simultaneously using a higher mass density. This technique if feasible may be used to rexamine the solid mixing experiments of Avidan [2].

As a matter of interest to us, Chesnekov et al. [8] were concerned with the porosity (voidage) distributions measured by their predecessors, Taganov et. al. [36,37], due to the insufficient accuracy obtainable from the background exposure of motion picture negatives. As a result Chesnekov used medical x-ray film 35.6 cm square which was replenished as in a motion picture camera on roller devices. His

replacement time was 0.3 seconds, assumed to be also his exposure time. What is not known about the above studies are the x-rays emanated from the two x-ray generators. It is assumed that the image translators they used are ordinary image intensifiers.

4. Gajdos and Bierl [6] carried out an x-ray density study of a 3 inch diameter fast fluidized bed. A core annular-structure can be observed from their photographs. However, although they presented a method of calibrating their absorption spectra to yield densities, a radial density profile was never calculated. They did give an estimate for density in the core and annulus as being 3 lbm/ft^3 and 22 lbm/ft^3 respectively (ϵ = 0.97, 0.76). See profile Figure 6.1. Their x-ray unit was kept at 100 KV, exposure times 0.25 second and a Kodak x-omatic intensifying screen was used instead of an image intensifier. Just as with the Russians the film here was a large plate type (cassettes replaced manually after each exposure). Among some of the conclusions drawn by these authors was that the core annular interface was neither smooth nor axisymmetric [6,p. 44]. They seem to have forgotten a fundamental fact about x-ray photography. As pointed out by both Grohse and Rowe, the x-ray source has a periodicity of its own due to its mode of generation. In fact, Rowe took this into consideration in estimating the physical boundary of his bubbles. The underlying perodicity should be kept in mind when examining the plate film exposures of this work.

5.2 - X-Ray Density Studies: Experimental

The center of the x-ray system is a Norelco MG 150/300 x-ray generator. It is an industrial unit designed to be operated with either 150 kV or 300 kV tubeheads. Its features are high continuous output and high intensity of operation. The maximum output of the system with the 150 kV head which was used in this study is given as:

30 mA at 100 kV

20 mA at 150 kV

The double focus tube limits the maximum operating current for a given operating potential. The double focus allows for a choice in the size of the focal spot from which the x-rays are generated. The particular tubehead used for this study has focal spots of 1.5 mm and 4 mm. Selection of the focal spot can be made by simply turning the dial on the control console. The current value for this tubehead at 65 kV, which can only be operated with the smaller focal spot, was limited to 10 mA. Overall image density could be controlled through variation in exposure times.

The MG 150 installation consists of the control console, one generator tank with a constant potential to ground of -150 kV, one high tension cable and the water cooled x-ray tubehead. From the control console all the control functions can be performed. These include setting exposure time, kV, mA, tube type, focal spot and on-off functions. The console is positioned in the control room

which also houses a video monitor and recorder as well as the x-ray carriage position and camera on-off controls.

The x-ray tubehead and the three cameras used in recording images are mounted on opposing sides of the fluidized bed. A carriage supports and positions all the components. The shroud enclosing the carriage is lead lined so that minimal external lead shielding is required. The entire carriage assembly rides up and down a 12 foot center section of the fluidized bed. It rests on two support arms which are attached to guidewheels that roll along the adjacent support column. A winch lifts and lowers the carriage by a chain attached to it.

The imaging cameras include a cassette holder for plate film, and video and cine cameras for motion picture recording. Figure 5.2-1 is a scale drawing of the carriage assembly with the side panel removed. The figure shows how the cameras and tubehead are arranged. Note that the video and cine cameras are filming off an image intensifier whereas the cassette holder is not. Since the plate film does not benefit from the amplification of the image intensifier longer exposure times are needed to produce an image on this film.

Figure 5.2-2 is a schematic showing the geometry of the various components of the carriage. In the figure can be seen the position, to scale, of the x-ray point source, the fluidized bed cross section, the plate film cassette and image intensifier and the lens position of the video and

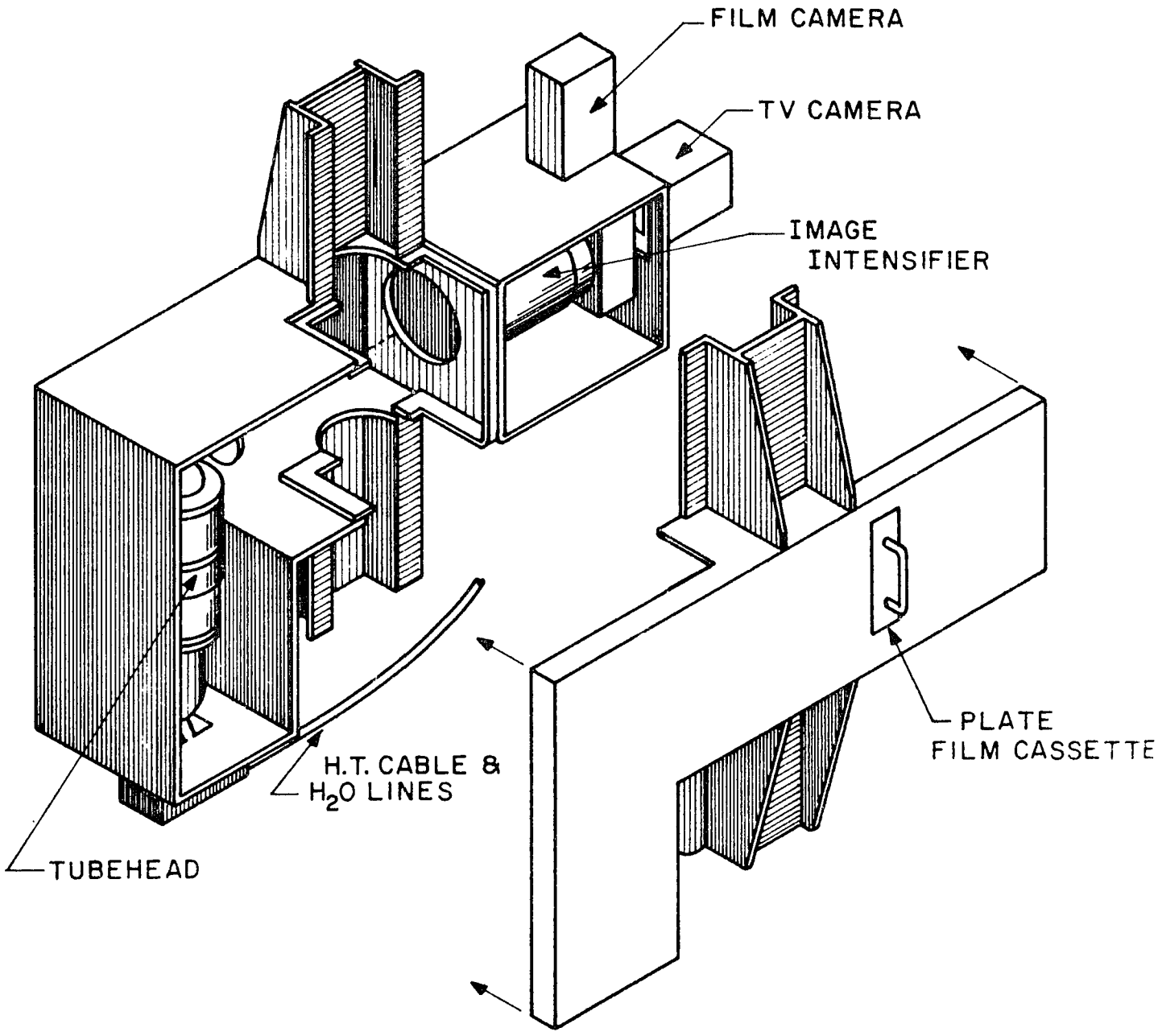

Figure 5.2- 1 Scale drawing of the x-ray carriage assembly - the fluidized bed fits into the slot on the assembly.

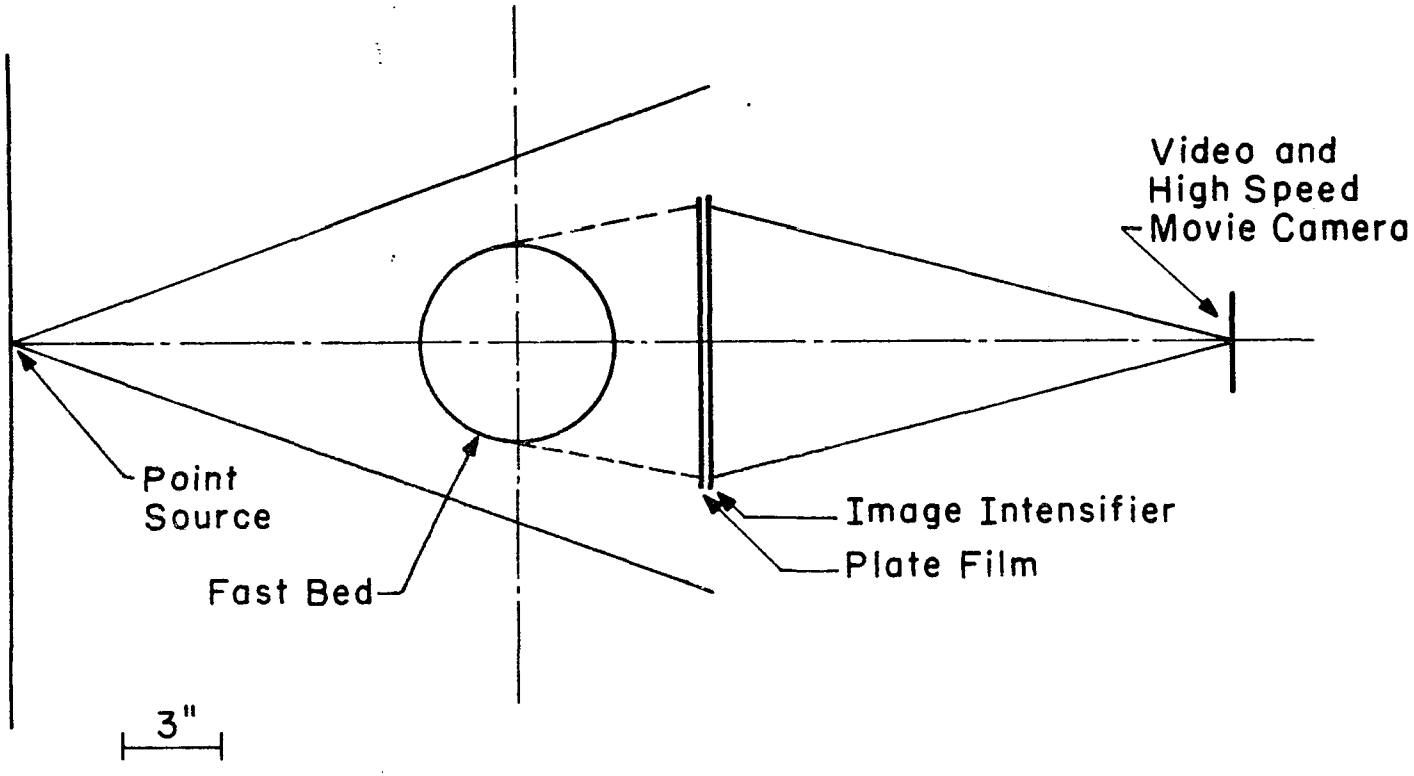

Figure 5.2-2 Geometry of the x-ray beam and of the ancillary photographic equipment relative to the fluidized bed cross section.

cine cameras. The x-ray system focal spots of 1.5 mm and 4 mm were considered small enough for the x-rays to be considered emanating from a point source. The lens angle shown is actually for the 37.5 mm cine camera and can be seen to be just sufficient to capture the entire 9 inch image intensifier field. The 25 mm video camera had a wider pickup angle and is not shown. Notice how the emerging x-ray beam does not limit the field of view either. The dashed lines shown represent the magnification of scale of the fluidized bed by the divergent x-ray beam. Also note that the 9 inch image intensifier is just sufficient to capture the magnified 6.5 inch O.D. column. On the video recordings of the x-ray images one column wall can barely be distinguished. During initial start up runs 0.5 inch washers were placed at 3.0 inch intervals to ascertain the orientation and size of the image. The image is oriented upright with correct left to right positioning as seen by the video camera from the back of the bed.

8 by 10 inch plate film (Kodak Industrex type M) is positioned in the plate film cassette holder. Initial test exposures at various tubehead potentials gave a clear image at the intermediate voltage, -65 kV. 25 kV gave essentially no image while 90 kV and above masked much of the details. The resolution appeared to be optimal at the lower end of the voltage range that gave a clear image. For plate film exposures, operating conditions were limited to 10 mA by the focal spot chosen and overall image density had to be

controlled by adjusting exposure time. It was reccomended by the film manufacturer, Eastman Kodak Co., Rochester, N.Y., that for best image resolution kV was to be kept low and adjustments to exposure could be made by varying mA and/or time.

The safety precautions employed for the x-ray system were approved by the City College radiation safety committee and safety reports were filed with the city and state of New York. The entire fluidization laboratory was scanned with a geiger counter at the maximum 150 kV output and less than 0.5 mR was found at the highest leakage point. To prevent exposure due to unauthorized entry into the laboratory warning lights and power disconnects were installed at each entrance. All personnel involved with the experiments wore radiation film badges which were monitored on an approved schedule.

5.3 X-Ray Density Studies: Radial Profiles

The x-ray system is capable of filming the fluidized bed on three time scales. The plate film records the bed behavior averaged over a time of about 3-10 seconds. Although swirl like patterns can be discerned on these films it is not certain what they represent. As discussed earlier they may in part represent the underlying periodicity in intensity of the x-rays. On a shorter time scale of 1/30 to 1/60th second the video camera shows the bed behavior with a dynamic response approximately equivalent to the human eye. As such, vortices can clearly be seen forming and collapsing in a fast bed and bubbles can be tracked in a bubbling fluidized bed. Movement on the time scale of 1/300th second can be captured by the high speed cine camera. However, for the present work, photographs with this camera were not taken.

Figures 5.3-1a,b,c,d are contact prints made of the plate film negatives. These prints correspond to the three different axial positions in the bed plus an empty tube. Fluidized bed operating conditions for these pictures are 2.0 m/s and 85 kg/m^2-sec and were so chosen as to have an inflection point at the center of the x-ray carriage traverse. X-ray tube operating conditions were at 65kV and 9mA throughout the entire 15 second exposure. The three photographs show strong evidence for lower solids concentration in the tube core as opposed to the annular region. They also clearly show how the axial traverse of the

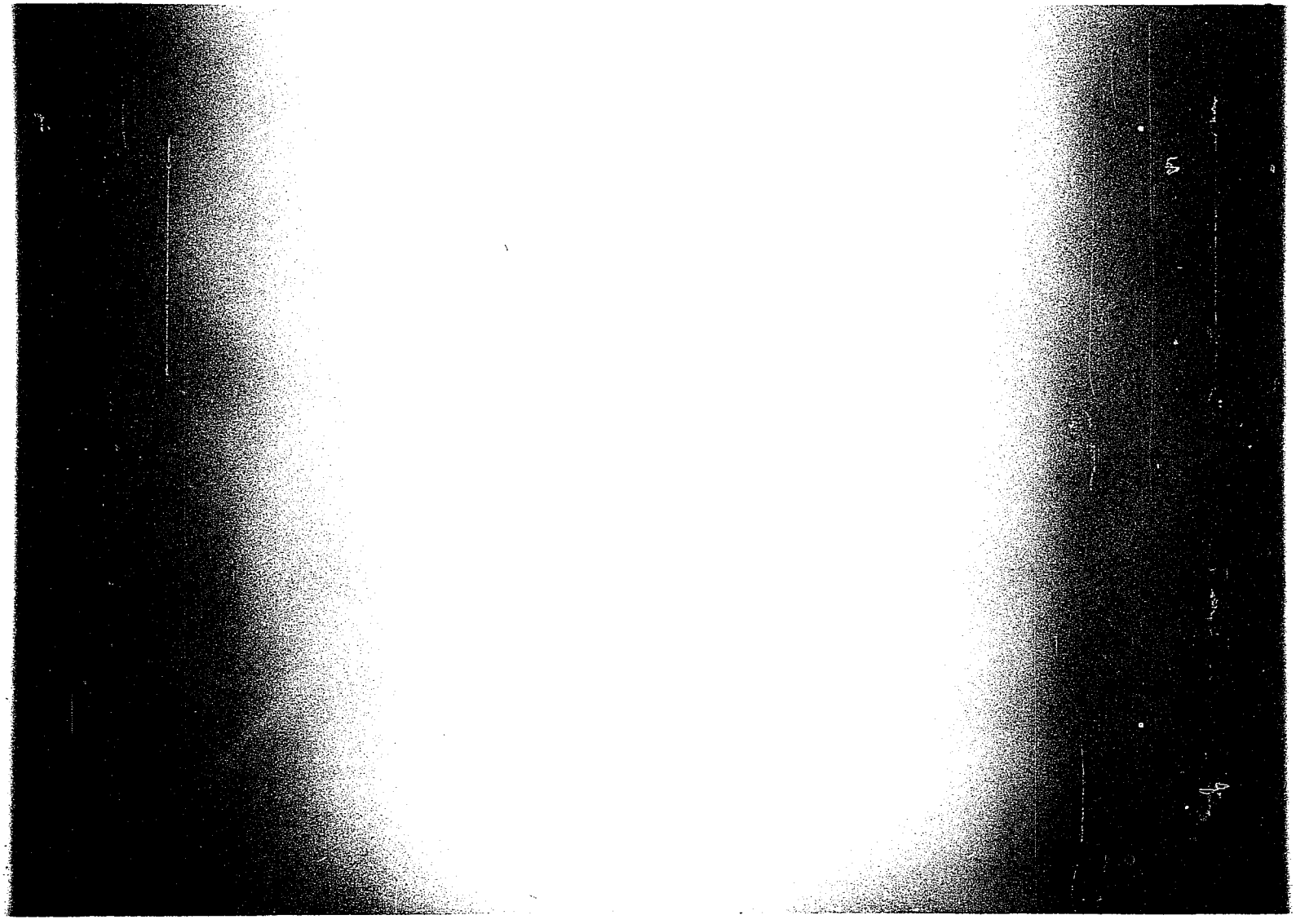

Figure 5.3-1a Contact print of the x-ray plate film negative exposed at the lowest bed position.

Figure 5.3-1b Contact print of the x-ray plate film negative exposed at the inflection point position.

Figure 5.3-1c Contact print of the x-ray plate film negative exposed at the highest bed position.

Figure 5.3-1d Contact print of the x-ray plate film negative exposed with no solids in the bed.

bed passes through regions of succesively lower solids concentration.

Table 5.3-1 Densitometer Measurements

Experimental Conditions: 85 kg/m²-s, 2 m/s, 65kV, 9 mA, 15s.

	α	0°	2.05°	4.1°	6.13°	I_o
empty	I	5.45	5.44	5.43	5.42	5.45
	ln I/I_o	0.0	-0.002	-0.004	-0.006	
	-1/2ln I/I_o					
bottom	I	2.72	2.56	2.17	1.80	5.47
	ln I/I_o	-0.6986	-0.75755	-0.9209	-1.0894	
	-1/2ln I/I_o	0.3493	0.3787	0.4604	0.5447	
middle	I	3.84	3.75	3.20	2.54	5.46
	ln I/I_o	-0.352	-0.377	0.531	-0.760	
	-1/2ln I/I_o	0.176	0.187	0.265	0.579	
top	I	5.40	5.32	4.77	3.76	5.46
	ln I/I_o	-0.011	-0.027	-0.131	-0.368	
	-1/2ln I/I_o	0.006	0.012	0.066	0.184	
bubbling	I	0.53	0.51	0.51	0.65	5.44
	ln I/I_o	-2.33	-2.37	-2.37	-2.13	
	-1/2ln I/I_o	1.17	1.19	1.19	1.06	

The distance on each contact print from outer wall to wall is 8.8 inches. This is the magnified image of the 6.5 inch O.D. bed due to the divergent x-ray beam. For each plate, measurements of I_o and I, the plate film density, for values of the angle α, 0.0°, 2.38°, 4.75°, and 7.10° were made. These angles were chosen by taking the intensity, I, measurements at equally spaced 3 cm. intervals from the centerline. Due to some distortion near the wall the closest measurements to the wall was taken at a distance of 2.18 cm. I_o measurements were made on the portion of the film which protruded beyond the bed, directly in line with the x-ray source. Although the chord along which the x-rays had to travel to reach this point on the film was longer than any other, and therefore had a lower I reading due to geometry, this error was estimated at less than 0.8%. Table 5.3-1 contains all the optical density measurements.

For each plate the second line of the table contains the natural logarithm of the optical density ratio for each chord. Each such chord value is corrected for x-ray absorption of the plastic. This was done by subtracting the empty tube absorption for each corresponding chord. As can be seen from Figure 5.3-1, and the measurements of Table 5.3-1 the corrections become more important with increasing angle α. Figure 5.3-2a, is a plot of the plastic thickness each chord must pass through as a function of the source angle α. It can be seen to vary from 1.3 cm. - the wall

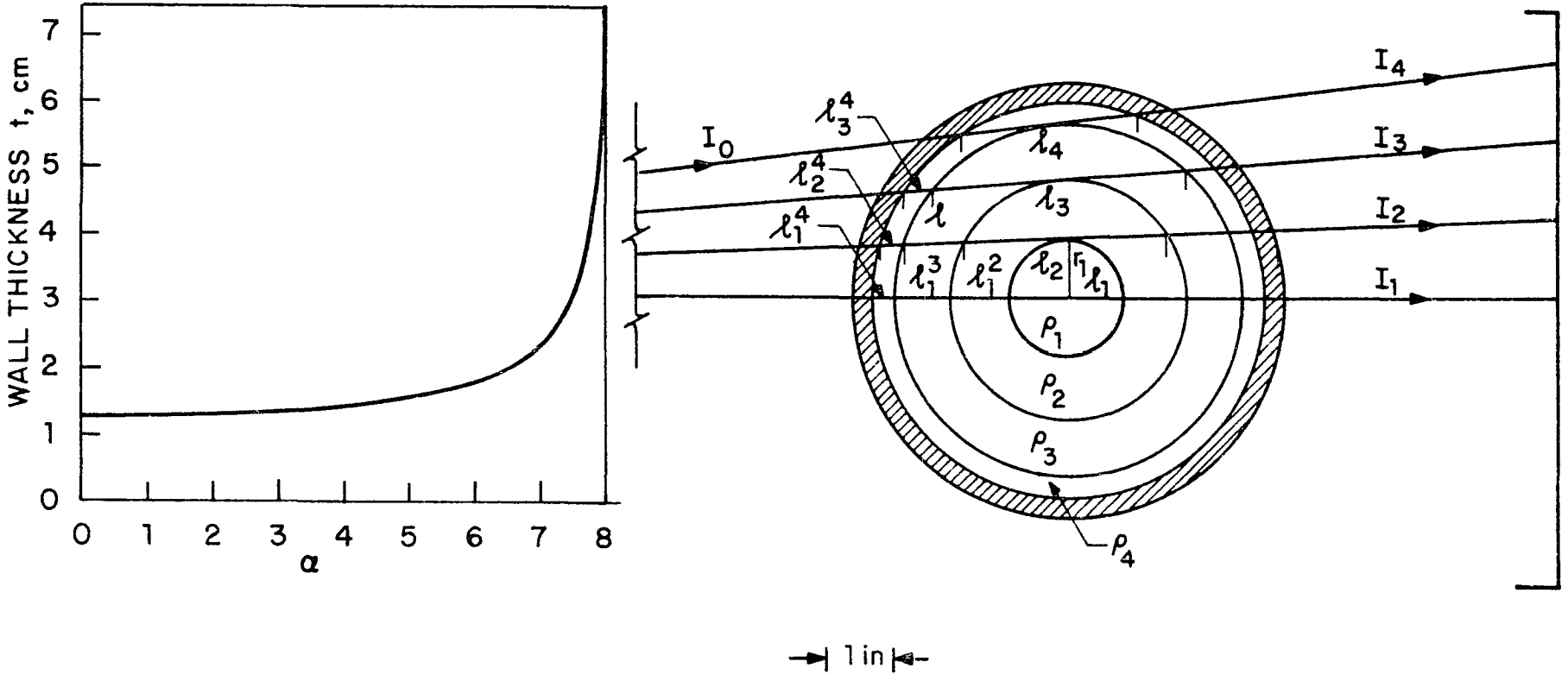

Figure 5.3-2 a. Plastic thickness through which the x-ray beam must pass vs. the source angle. b. Geometry of "ring method" for deconvoluting side-on absorption measurements (see text).

thickness - at a= 0.0 to 7.0 cm. at maximum a.

Figure 5.3-3 is a plot of the radial optical density profile for the three positions; bottom, top and inflection point positions in the fast fluidized bed. At the time these measurements were taken video monitoring of the bed in operation showed the middle position to correspond approximately to the inflection point height. Simultaneous differential pressure measurements showed a drop in solids holdup at this position. As can be seen from Figure 5.3-3 the gas velocity was 2 m/s and the solid rate 85 Kg/m^2-sec for this run. These conditions are well within the fast fluidized bed regime for this equipment. From the figure one can see quite clearly the relatively dense annular region for all three bed positions. Also one can easily see how the solids holdup in the segment of bed being measured, as given by the stippled area under the curve, decreases with increasing bed height. In the discussion section, Chapter 6, it will be shown how assuming the densest annular region to correspond approximately to a bubbling bed will predict a pressure drop very close to that experimentally measured.

The video monitor and recorder gave a direct means of observing the fluidized bed in operation. Although no calculations were performed on the video recordings, they are valuable for flow visualization. Figure 5.3-3 is a set of eight photographs of the monitor screen exposed while the video tape was paused. They correspond to increasing values of superficial gas velocities. The first one, bubbling

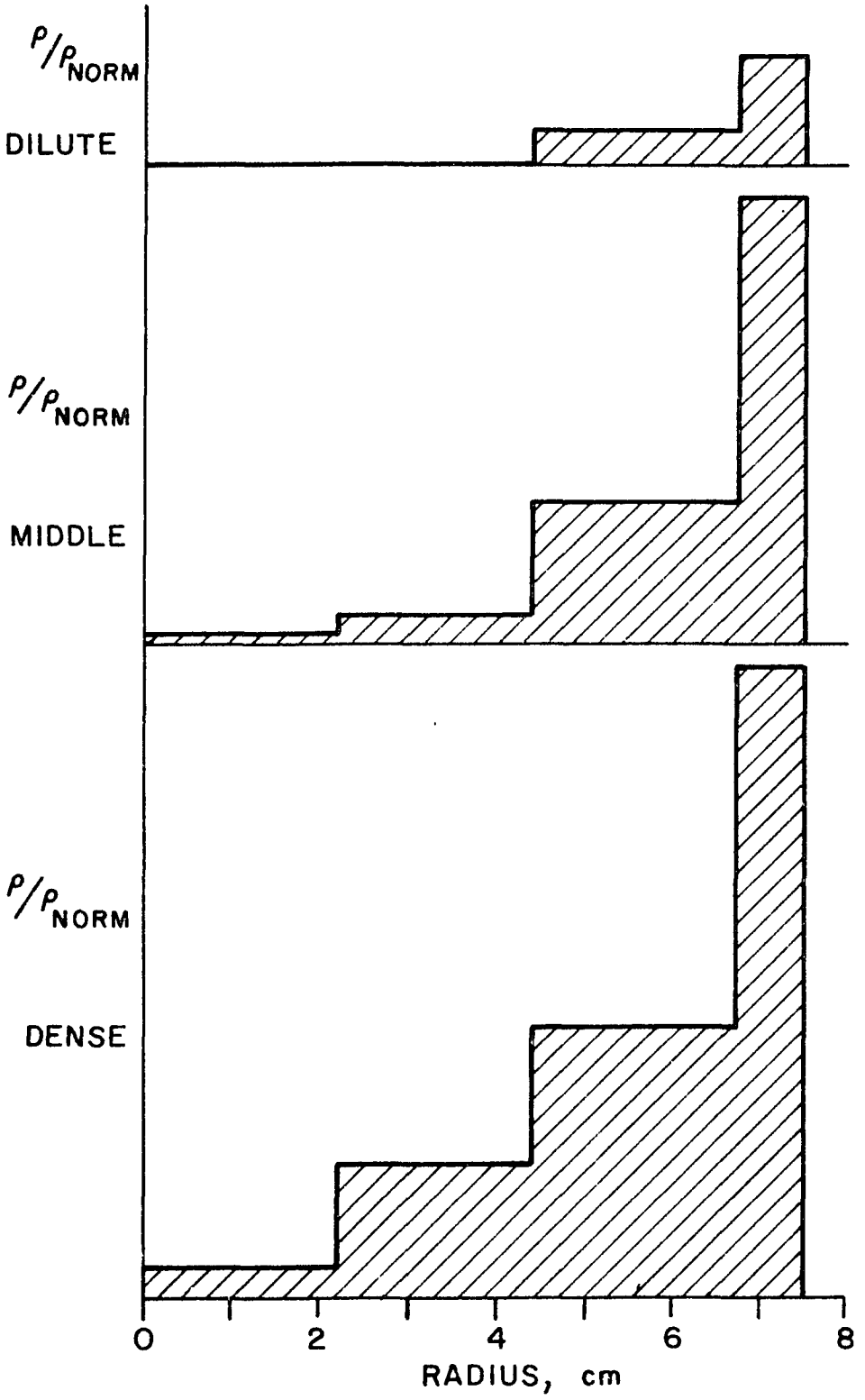

RELATIVE SOLIDS DENSITY

HFZ-20, $U_g \cong 2$ m/s, $G_s \cong 85$ kg/m^2-s

Figure 5.3-3 Optical density profile for a fast fluidized bed for each of three bed positions corresponding to above, below and level with the inflection point.

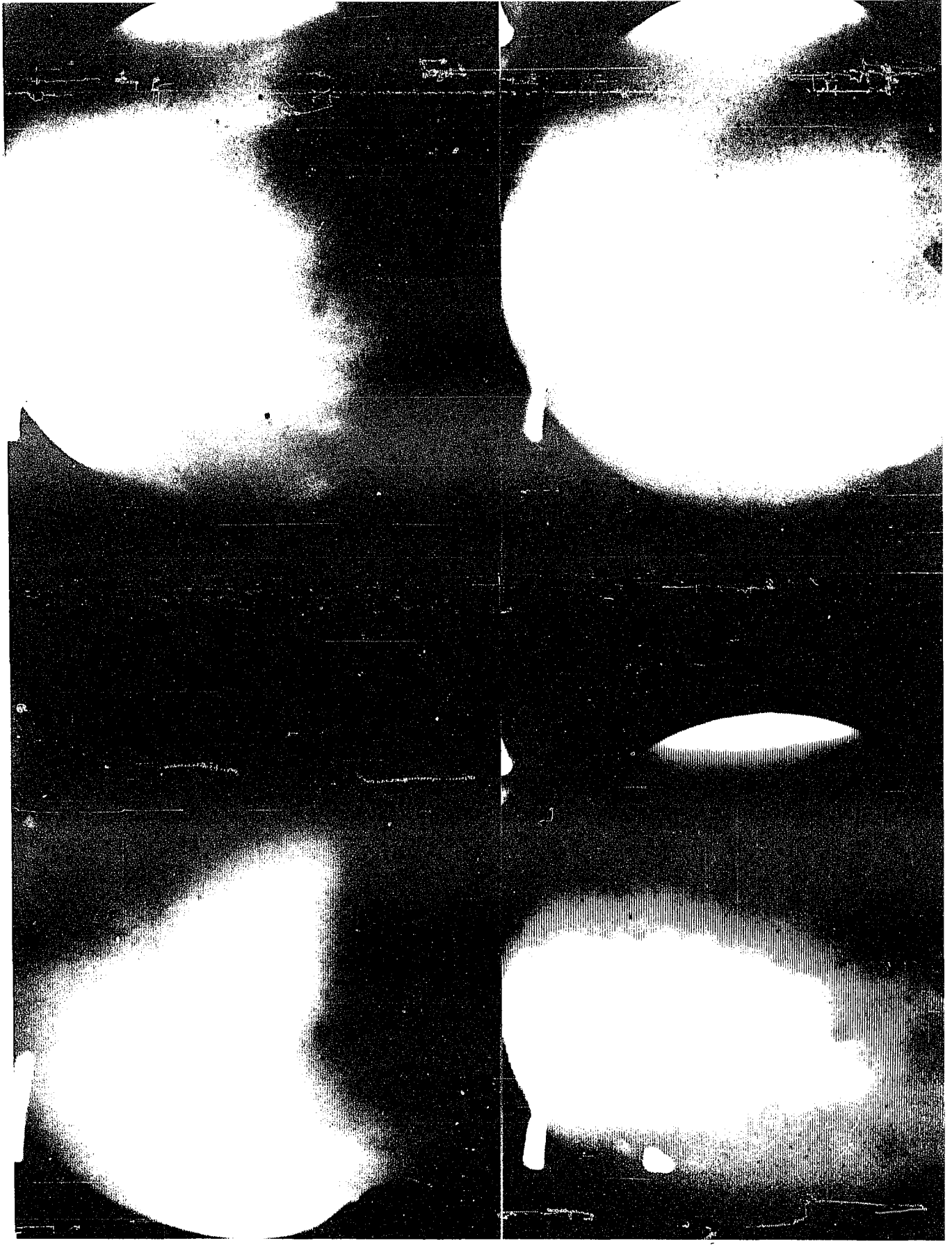

Figure 5.3-4 Photographs of the video screen (view page sidewise).
a. upper left - bubbling, b. lower left turbulence, c. upper right - slugging
d. lower right - fast fluidization.

clearly shows a bullet nosed bubble. In later photographs we see the tube split axially in half with one side full and the other side empty indicating a slugging bed with a slug just having broken. In the more homogenous higher gas velocities regions one can still distinguish between photographs which contrast the solid filled regions very sharply from those that show solid filled regions as mere shadings on the photograph. These latter photographs can be associated with dilute phase pneumatic transport.

	$\ln I_4/I_o$	ρ_4	$\ln I_3/I_o$	ρ_3	$\ln I_2/I_o$	ρ_2	$\ln I_1/I_o$	ρ_1
Bottom	1.0894	0.1472	0.9209	0.0609	0.7574	0.0301	0.6987	0.0062
Middle	0.7598	0.1027	0.5306	0.0311	0.3739	0.0065	0.3520	0.0001
Top	0.1838	0.0248	0.1314	0.0078	0.0241	0.0072	0.0111	-0.0079

6 - Discussion

The axial pressure gradient in a fast fluidized bed often exhibits a variation from a relatively high value in the bottom section of the bed, (dense phase) through a transition region in the middle of the bed which contains an inflection point, to a low value (dilute phase) in the top section of the bed. The axial pressure gradient has been shown to be almost equivalent to the fluidized density which justifies the reference to this gradient profile as a solid density profile. The type of profile being discussed can be demonstrated for either of the two solids investigated although the magnitude of the variation is more pronounced for the heavier HFZ-20 catalyst. Data taken over the entire range of fluidization, from bubbling through pneumatic transport , indicate that this type of variation is in no way unique tc fast fluidization or to high velocity fluidization for that matter. It is reasonable to believe that the dense annular region, shown by the x-ray density measurements to be more pronounced below the inflection point, is responsible for the overall higher density gradient in this region. This same core-annular structure was discussed earlier as having been recognized by Shumkov and Ivanov for bubbling beds, recently measured by Abed for turbulent beds and is evident for fast fluidization from the radial density profiles of chapter five. The particular value of solid fraction in the dense and dilute regions tended towards 0.2 and 0.04 respectively for either of the

two solids examined. Whether these particular values are governed by the particle size, size distribution, equipment dimensions or some other factor is uncertain.

Not all the density profiles shown in chapter four have an inflection point in the column. It is still not possible to predict a priori when a profile of this sort exists rather than a relatively flat one at either the typically dense phase or dilute phase of solids loading. For flat profiles, the potential for an inflection point exists but the operating conditions are such that the entire column is filled in either the fast fluidization or pneumatic transport mode. When the solid rate is high enough or the gas rate low enough the point of inflection moves to the top of the column so that the entire column is filled in the fast fluidization mode. Conversely, if the solid rate is low enough or the gas rate high enough, the inflection point merges with the acceleration zone and the bed exhibits the pneumatic conveyance mode.

The height of the solids acceleration zone has been the subject of some speculation. Avidan has calculated the length for solids acceleration to be greater than for pressure gradient equilibration and in fact occupies about 1/3 of the column length. The length for pressure gradient equilibration can clearly be seen on all the pressure gradient profiles of chapter four except when dealing with bubbling beds. It is therefore believed that this higher pressure gradient at the entrance region is due to solids

decelerating in this region. Gajdos and Bierl have experimented with a number of different inlet configurations and concluded that although the entrance pressure gradient varied slightly for each the remaining profile was unchanged. The remaining profile must be set by the prevailing imposed pressure as well as gas and solid rates as is discussed below. The high pressure gradient in the entrance region as well as some ELR calculations for the entire column indicate that the the internal solid recirculation superimposed on the external solid recirculation renders the entire column an acceleration zone.

That the inflection point type of profile is possible for FCC as well as HFZ-20 catalyst can be most clearly seen from Figure 4.3-1a, run 143. In this run the gas velocity of 1.75 m/s is clearly in the fast fluidization regime and yet an inflection point exists in the axial density profile.

Although the criteria for the onset of high velocity fluidization, i.e. Uc and UK, were measured in a 2-D bed, careful monitoring of the experimental pressure fluctuations indicated that these values were approximately correct for the 15 cm I.D. bed as well. The reverse situation, that flat profiles are possible for HFZ-20 can be seen from any number of the higher velocity runs, Figure 4.3-3b.

For a once through system of gas and solid the inflection point position varies, as mentioned previously with gas and solid rate. The imposed pressure drop on this

system is set by the degree of hold up that the bed experiences. For systems in which solids are recirculated, the inflection point cannot set itself independently but is forced to assume a position which yields a given degree of solid holdup depending on the solid inventory in the slow bed. Specifically, raising the solid inventory has the effect of raising the inflection point in the bed as well. In summary, raising the solid rate, lowering the gas rate, or raising the solid inventory have the effect of raising the inflection point in the bed.

That gas and solid rate alone do not uniquely define a recirculating fluidized bed system can be discussed with reference to the Leung diagram Figure 2.1. In this diagram the regimes of fluidization are traversed by varying the gas velocity, Ug. What is implied in this plot is that for a recirculating system I is being held constant. Conversely, it should be possible to keep Ug constant and traverse the various regimes by varying I alone. Transitions from fast fluidization to pneumatic transport as well as to a lesser degree transitions to other regimes by variation in I can be seen in the data of chapter four. Until now the profiles reported by various investigators did not include the values of imposed pressure drop under which they were measured.

Neglecting the effects of imposed pressure drop even for the same solids in the same diameter equipment has caused disagreement in the shape of the axial density profiles reported by various investigators. Compare for

example the data of Li and Kwauk, Figure 6-1; Gajdos and Bierl, Figure 6-2, and the data of this thesis. The data of Li and Kwauk, and Gajdos and Bierl were taken in three inch diameter beds while this work was done in a six inch diameter bed. The heights of all three units were comparable. An explanation is necessary as to why the dense voidage of this work is centered about 0.8, that of Li and Kwauk about 0.9 and Gajdos and Bierl at 0.95. In chapter four it was shown, for either solid investigated, that the voidage in the dense phase only increases for extremely high gas velocities or when the inflection point has merged with the acceleration zone.

Examining the data of Li and Kwauk four sets of axial profiles can be seen for four different solid rates. In each set the inflection point height decreases with increasing gas velocity. The solid rate for each solid given varies greatly, with the lowest value given for FCC (ρ_p = 1.78) Gs = 16 Kg/m^2-s up to the highest value given for iron concentrate (ρ_p = 4.51) Gs = 135 Kg/m^2-s In order to eliminate the effects of varying solid density the volumetric solid rates, mass rate divided by particle density were compared.

Vs (m^3/m^2-s) : Pyrites = 42.3, Iron = 30.0, FCC = 9.0, Alumina = 23.1,

Examining the data of Gajdos and Bierl shows that unlike most of the Li and Kwauk profiles no inflection point in the profiles is seen except for the highest density, 0.1

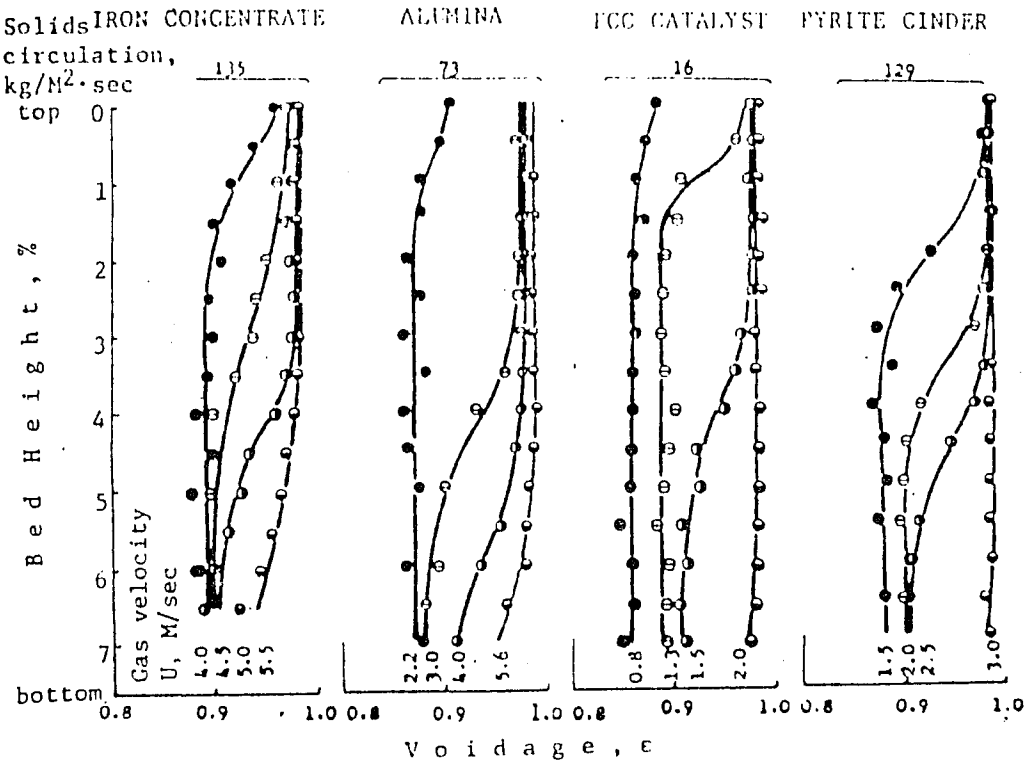

Figure 6-1 Voidage ε distribution along bed height z
(data from Li and Kwauk, reference 44)

	ave.dia. $\bar{d}_p$, μ	density ρ_s, g/cm^3	term.vel. U_t, m/sec	Archimedes number	$\bar{d}_p(\rho_s-\rho_f)$ g/cm^2
FCC catalyst	58	1.78	0.368	12.39	103
Coarse alumina	81	3.09	0.712	58.59	250
Fine alumina	54	3.16	0.485	17.75	170
Pyrites cinder	56	3.05	0.509	19.11	171
Iron ore conc.	105	4.51	1.155	186.3	473

Figure 6-2 Riser Pressure Gradient vs. Height
(data from Gajdos and Bierle, reference 6)

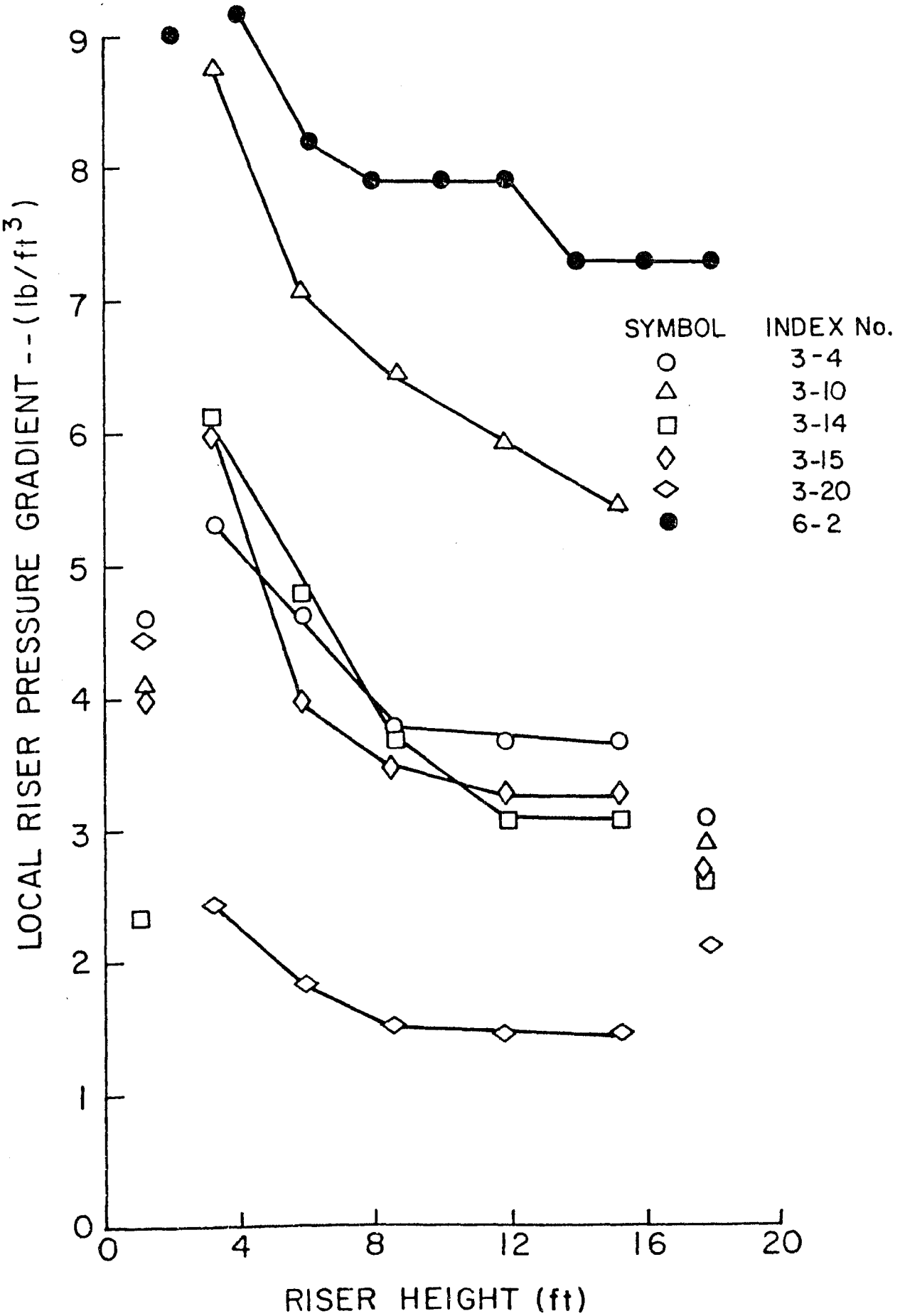

solid fraction case.

The variable which has been omitted from all of the above reported studies is imposed pressure drop. In cases of gravity feed of solids the solid feed valve appears not to decouple the fast bed from the slow companion bed as was previously thought to be the case [33]. Further explanations of the differences in the reported profiles cannot be made unless imposed pressure drop information is given.

Inflection point position also controls to a large degree the bed -average solid holdup in a recirculating fast fluidized bed. This can most clearly be seen for HFZ-20 catalyst, Figure 4.3-9b, where the the upper bed density position (1-)13-14 is shown to straddle the 0.04 solid fraction position for all values of solid inventory except for the two runs at the highest I and Gs. Similarly the lower bed density as given by position (1-)3-4, beyond the acceleration region tends towards 0.2 solid fraction. The bed-average solid holdup is then given by:

$$hi/L(0.2) + (1-hi/L)0.4$$

and depends upon inflection point height.

In an effort to try and collapse the dependence of hi/L on a single variable a number of runs were used to plot hi/L vs. ΔPs, the slow bed pressure drop regardless of solid inventory level. If the fluidization conditions were kept identical for all inventories ΔPs should increase with solid inventory. Such a trend does occur and the indicated plot is given in Figure 6.3.

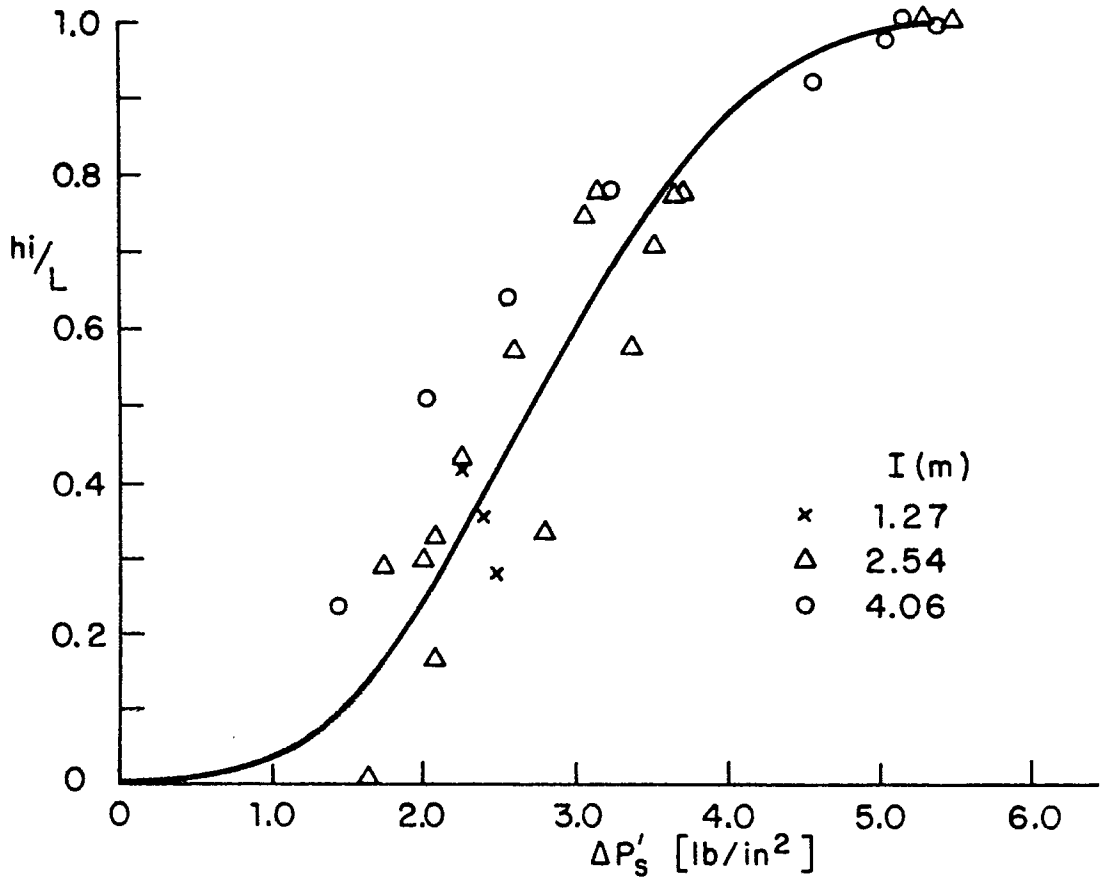

Figure 6. 3 Dimentionless inflection point height vs. slow bed pressure drop.

To remove the dependence of particle density on the value of void fraction in the bed the solid rates were divided by particle densities to yield solid volumetric rates. When voidages are plotted against Vs, the solid volumetric rate, it is shown that both solids exhibit about the same bed-average solid holdup when compared at the same values of gas velocity and imposed pressure drop. The reasoning for this behavior can be given as follows:

Consider the two different solids each in a fast bed system at the same gas velocity, solids volumetric flow rates and slow bed inventory. If there were no losses or pressure drops through the cyclones and solid valves which are not proportional to particle density, the two solids should have identical fast bed solids fractions - assuming of course that the less tangible fluidization characteristics of both solids were the same. This is because the same height of solids in the slow bed for each solid would yield pressure drops in the ratio of their particle densities. The solids energy gains on the fast bed side as well as the energy inputs from the compressor would also all be in the ratio of the solids particle densities. The frictional loss terms, however, should not be in the same ratio. It would therefore be expected that the solids fractions in the fast bed would be close for the two different solids but not identical.

X - ray Density Studies

X - rays have proven to be suitable for non-disruptive

solid density variation measurements in a 15.2 cm I.D. fast fluidized bed filled with HFZ-20 catalyst. Although rays were used on much larger diameter risers, and a radial profile calculated, these were averaged over long periods of time, several hours, and results reported for only a few parameter values. The x-ray measurements that were taken on a 3 inch I.D. bed were never used to calculate a radial profile.

The equipment used in this thesis is suitable for density measurements on three time scales. 1/300 second exposures can be recorded on high speed motion pictures, 1/30 second can be recorded on video tape, both via an image intensifier, while longer time exposures can be made directly on standard medical x-ray film. Video recordings are used for flow visualisation studies while plate film images are used to quantify radial density measurements.

Measurements of the radial profiles at three axial positions in the fast fluid bed, corresponding to the dense, dilute and inflection point positions, confirmed the conclusions of axial pressure gradient measurements. At each of these bed locations a dilute core - dense annular wall region conformation appears to exist.

Radial Solid Distribution

The side-on x-ray absorption data has been converted, using the chordal absorptometry technique discussed in chapter three, into a radial optical density profile. Thus the ordinate for the radial profile given in Figure 5.3-3 is

plotted by what is the equivalent, relative solid density. Mass density values can be gotten from this distribution if one assumes a constant value for the attenuation coefficient μ and has knowledge of a single value of ΔP_s. Such a point can be given for example by the assumption that the densest part of the bed (the annulus) has a density in the range of that in a bubbling bed.

From the data of the lowest bed position the profile yields a mean bed density of 0.11. This value is within the range given by axial pressure gradient measurements for these fluidization conditions.

$$0.3/7.6(1 + .061/.147(2.6) + .031/.147(2.6) + .006/.147(2.6)) = 0.11$$

Another estimate for solids density can be gotten by calculating a radial optical density profile for a bubbling bed. In this case assuming the mean bed voidage to be 0.7, the maximum solid density in the bed can be calculated to be about 0.5.

$$0.3 = X/7.6(1 + .177/.288(2.6) + .146/.288(2.6) + .082/.288(2.6))$$

From which X, the maximum density in a bubbling bed, can be calculated to be X = 0.49. This corresponds to a solid density, ρ_4, of 0.288 For the data of the lowest bed position discussed earlier the voidage corresponding to a ρ_4 of 0.147 is $(1-\epsilon) = 0.248$ which seems reasonable.

The most direct method of correlating optical and solids density is through a calibration curve. Apparently

the attenuation coefficient is not constant and as such poses a problem in such a calibration.

When examining the optical density of an x-ray plate film it must be remembered that the specific exposure is the result of two related effects, solid density and bed geometry. For the chord through the diameter, for instance, it might be expected that the transmitted x-ray intensity be lowest due to the great path length through which the x-rays pass. The fact that the transmitted x-ray intensity for this chord is highest, the optical density recorded on the film is greatest, is testimony to the extremely low solid density in the core. Gajdos and Bierl plot two hypothetical x-ray density absorption profiles and show how for a constant density bed the optical density is lowest on the centerline. That plot is essentially a graphical description of the above two competing effects.

Energy Loss Ratio

The work of Sandy et al. served to distinguish between the energy consumption of dense phase transport and dilute phase pneumatic transport. In fact the ramifications of such calculations are far greater in that they provide insight into the flow patterns of the fluidized bed system. In this work, exchanges of energy between gas and solid, as well as the total energy gained by the solid or lost by the gas in traversing the column are evaluated. These calculations aid in the reconstruction of the flow patterns responsible for such changes.

Earlier work done on calculating energy loss ratios in a fluidized bed led to the tentative conclusion that ELR increases with solid rate. The ELR for FCC catalyst was calculated to be about 2.0 with HFZ-20 at about twice this amount. An estimate of the energy requirements to accelerate the solids , gotten from the acceleration pressure gradient times gas velocity, failed to account for this loss. It was therefore assumed that internal recirculation consumed 1/2 -3/4 of the gas kinetic energy.

Subsequent experiments extended the range of solid rates, examined the effects of varying gas velocities as well as solid inventories. In these experiments as well, the ELR was calculated. An attempt was made to calculate the local energy loss ratio to examine variations in a single column above and below the inflection point. In this data ELR's as high as 9 - 10 were calculated while considerable scatter in the data began to appear. Statements about the trends relating ELR to each of the system variables, gas velocity and solid rate as well as inventory can be made.

Raising the solid inventory, with all else held constant, has the effect of increasing the ELR. This fact can be seen from the defining equation where if Ug and Gs are held constant raising the inventory raises ΔPf and therefore ELR. Although this data has not been included experimental measurements have confirmed these results. On a plot of ELR vs. Gs, raising the solid inventory serves to raise the whole family of ELR curves. It should be noted

that the actual increase in ELR is not quite as large as might be given by direct increase in ΔP_f because the feed valve is being closed to maintain the same solid rate.

Intuitively the effect of raising the solid inventory might be thought to be reversed. Consider the high solid holdup in a fast bed adjoining a high inventory companion bed. In this case the potential energy of the solids is higher both due to the higher amount of solids in the bed as well to their higher average position. It might therefore be thought that to maintain the same Gs as for the comparably lower inventory case would require less energy input. Nevertheless the higher imposed pressure drop requires larger pressure drop on the gas which consumes more energy.

For each value of solid rate it is believed at least two values of ELR exist. These two values correspond to some forms of dense phase and dilute phase transported beds. In a static dense bed ΔP is set by the height of solids while Ug is set arbitrarily. Gs, however, is almost zero making the ELR approach infinity. Energy incoming with the gas is consumed in recirculating the solids in the bed. In contrast, a transported bed ΔP is small and Ug may be many times that for bubbling while Gs has a comparably large value. The resulting ELR is not infinite but rather has some small value.

From the defining equation of ELR, if Gs is held constant more than one combination of ΔPUg must exist for a multiplicity to exist. Although a choking plot (ΔP vs. Ug)

does predict such double values one of these values is given for the case where gas-wall friction is high. This was not a case considered in this work. Although at least one other $\triangle$PUg value must exist for the same Gs in the denser transported bed, how to explain such behavior in terms of the flow model presented in this thesis is uncertain.

For the system under consideration, varying Ug and evaluating ELR is difficult because changing this variable alters Gs and ΔP as well. The data trends are not clear cut. From the defining equation for ELR what is expected is an increase in ELR with increasing Ug. This did not happen and further analysis must be undertaken. Nevertheless, the inconsistencies in this respect do not detract from the usefulness of ELR as a qualitative tool and portray the complexity of the solid flow patterns which must be treated in the analysis.

7 - Conclusions

1. The axial solid fraction profile in high velocity fluidization often exhibits a variation from a relatively high value in the bottom section of the bed, (dense phase) through a transition region in the middle of the bed which contains an inflection point, to a low value (dilute phase) in the top section of the bed. This type of profile can be demonstrated for either of the two solids investigated although the magnitude of the variation is more pronounced for the more dense HFZ-20 catalyst.

2. The position of the point of inflection has been shown to depend upon imposed pressure drop as well as gas and solid rates. Raising the imposed pressure drop, raising the solid rate or decreasing the gas rate all have the effect of raising the inflection point in the density profile. Under extreme conditions the inflection point can be made to move beyond the bed top or to merge with the solids acceleration zone at the bottom of the bed.

3. Disagreements in the shape of the axial density profile given by various investigators even for the same solids was often attributed to the geometric differences in process equipment. This work points out the importance of considering the imposed pressure drops and particle densities when displaying such profiles.

4. The bed-average solids holdup in a recirculating

fluidized bed is controlled by the imposed pressure drop across it as well as the gas and solid rates. Values for mean solid fraction in the bed vary from about 0.20 at large imposed pressure drops to less than 0.05 at low values for either of the two solids considered. The imposed pressure drop is given by the sum of the cyclone, slow bed inventory and solid valve pressure drops. These pressure drops are given by the portion of the recirculating system which is parallel to the fast bed.

5. It is shown that for the same values of superficial gas velocity, imposed pressure drop and volumetric solids rate, the bed-average solids holdup is almost independent of particle density for the two cracking catalysts used in this study.

6. X - rays have proven to be suitable for nondisruptive solid density variation measurements in a 15.2 cm I.D. fast fluidized bed filled with HFZ-20 catalyst. Although γ-rays were used on much larger diameter risers, and a radial profile calculated, these were averaged over long periods of time, several hours. The x-ray measurements that were made previously on three inch I.D. were never used to calculate radial profiles.

7. X - ray density studies reveal an annular radial density distribution with a dilute core and denser annular region near the wall. This profile is similar to the profile measured in turbulent beds with capacitance probes.

8. Measuring the radial profiles at three axial positions in the fast fluid bed, corresponding to the dense, dilute and inflection point positions, confirm the conclusions of axial pressure gradient measurements. The dilute core-denser annulus configuration persists in all three regions, but the size of the annulus is greater below the inflection point - leading to a higher pressure gradient.

1. Abed, R., "The Characterization of Turbulent Fluid Bed Hydrodynamics", Procedings of the IV-th International Conference on Fluidization, KashikKajima, Japan; May, 1983.

2. Avidan, A. A., "Bed Expansion and Solid Mixing in High Velocity Fluidized Beds", PhD Dissertation, The City University of New York, (1980)

3. Bakker, P. J. and P.M. Heertjes, CES, 12, (1960).

4. Bakker, P. M. and P. M. Heertjes, Brit. Chem. Engng. No. 5 p. 240 (1958)

5. Bartholomew, R. N. and R. M. Casagrande, "Measuring Solids Concentration in Fluidized Systems by Gamma-Ray Absorption", I.&E.C., 49, No. 3, March, 1957, p.428

6. Bierl, T. W., and L. T. Gajdos, "Studies in Support of Recirculating Bed Reactors for the Processing of Coal", DOE/FE-2449-8

7. Bierl, T. W., and L. T. Gajdos, "Phenomenological Modelling of Reaction Experiments in Risers", DOE/MC/14249-1149.

8. Chesnokov, Yu. G., Protod'yakonov, I. O., and V. A. Glinskii, "Investigation of the Motion of the Solid Phase of a Fluidized Bed with the Aid of Two-Projection High-Speed X-Ray Photography", Translated from: Zhurnal Prikladnoi Khimii, Vol. 54, No. 2, pp. 456-459 (February, 1981), Plenum Publishing Co., UDC 66.021.33:543.422.8

9. Enos, J. L., Petroleum Progress and Profits: A History of Process Innovation, The MIT Press, Cambridge, Massachusettes (1962).

10. Frazer, T. and H. F. Yancey, "Artificial Storm of Air-Sand Floats Coal on its Upper Surface, Leaving Refuse to Sink", Coal Age, 29, No. 9, p. 325-327.

11. Geldart, D. "Types of Gas Fluidization", Powder Tech., 7, p. 285-292 (1973).

12. Gohr, E. J., "Bachground, History and Future of Fluidization", in Fluidization in Practice, Polytechnic Institute of Brooklyn, (February 2, 1955).

13. Grohse, E. W., "Analysis of Gas Fluidized Solids Systems by X-Ray Absorption", AIChE J., 1, p. 358-365 (1955).

14. Jahnig, C. E., Cambell, D. L. and H. Z. Martin, "History of Fluidized Solids Development at Exxon", in Fluidization, J. R. Grace and J. M. Matsen, ed., Plenum Press, New York p.3 (1980).

15. Kunii, D. and O. Levenspiel, Fluidization Engineering, Robert E. Krieger Publ. Co., Huntington, N.Y. (1977).

16. Lanneau, K. P., "Gas-Solid Contacting in Fluidized Beds", Trans, Inst. Chem. Eng. 38, 125 (1960).

17. Leung, L. S., Verticle Pneumatic Conveying: A Flow Regime Diagram and a Review of Choking versus Non-Choking Systems", Powder Tech., 25, 185-190, (1980).

18. Lewis, W. K. and E. R. Gilliland, "Conversions of Hydrocarbons with Suspended Catalyst", U. S. Patent No. 2,490,088 (1950)

19. Lewis, W. K., Gilliland, E. R. and W. C. Bauer, "Characteristics of Fluidized Particles", I.& E. C., 41, No. 6, 1104-1117.

20. Massimilla, L., "Behavior of Catalytic Beds of Fine Particles at High Gas Velocities", AIChE Symposium Series, 128, Vol. 69, 11-13.

21. Odell, W. W., U. S. Patent No. 2,091,892 (August 31, 1937).

22. Rowe, P. N. and D. J. Everett, "Fluidised Bed Bubbles Viewed by X-Rays: Part 1 - Experimental Details and the Interaction of Bubbles with Solid Surfaces", Trans. Instn. Chem. Engrs., Vol. 50, 42-48 (1972).

23. Rowe, P. N. and D. J. Everett, "Fluidised Bed Bubbles Viewed by X-Rays: Part 11 - The Transition from Two to Three Dimensions of Undisturbed bubbles", Trans. Instn. Chem. Engrs., Vol. 50, 49-54, (1972).

24. Rowe, P. N. and D. J. Everett, "Fluidised Bed Bubbles Viewed by X-Rays: Part 111 - Bubble Size and Number When Unrestrained Three Dimensional Growth Occurs, Trans. Instn. Chem. Engnrs., Vol. 50, 55-60, (1972).

25. Rowe, P. N., Partridge, B. A., Cheney, A. G., Henwood, G. A. and E. Lyall, " The Mechanism of Solids Mixing in Fluidised Beds", Trans Instn. Chem. Engrs., Vol. 43, T271-T286, (1965).

26. Rowe, P. N., Partridge, B. A. and E. Lyall, "Cloud Formation Around Bubbles in Gas Fluidised Beds", Chem. Eng. Sci., Vol. 19, 973-985, (1964).

27. Rowe, P. N., Macgillivray, H. J. and D. J. Cheeseman, "Gas Discharge from an Orifice into a Gas Fluidised Bed", Trans Instn. Chem. Engrs., Vol. 57, 194-199,(1979).

28. Rowe, P. N. and C. X. R. Yacono, " The Bubbling Behavior of Fine Powders When Fluidised", Chem. Eng. Sci., Vol. 34, 1179-1192, (1976).

29. Rowe, P. N. and R. Matsuno, "Single Bubbles Injected into a Gas Fluidised Bed and Observed by X-Rays", CES, Vol. 26, No. 6-1, 923-935.

30. Rowe, P. N. and B. A. Partridge, "An X-Ray Study of Bubbles in Fluidised Beds", Instn. Chem. Engrs., Vol. 43, T158-T175, (1965)

31. Sandy, C. W., Daubert, T. E. and J. H. Jones, "Verticle Dense-Phase Gas-Solids Transport", Chem Eng. Symposium Series, 66, No. 105, p.133-143.

32. Saxton, A. L. and A. C. Worley, "Modern Catalytic Cracking Design", Oil and Gas J., 82-89, May 18, 1970.

33. Shinnar, R., Personal Communication.

34. Shumkov, Kh. S. and D. G. Ivanov, " Axial and Radial Density Profiles in Fluidized Beds With and Without Electromagnetic Fields", International Chemical Engineering, Vol. No. 3, July 1977.

35. Squires. A. M., "Contributions Toward a History of Fluidization", presented at the joint meeting of AIChE and Chemical Industry and Engineering Society of China, in Beijing, September 20-22, 1982.

36. Taganov, I. N., Malkhasyan, L. G. and P. G. Romankov, "Investigation of the Motion of Particles in a Fluidized Bed by X-Ray Film", translated from, Teoretiche Osnovy Khimicheskoi Technologii, Vol. 1, No. 2, p. 259-263, March-April 1967, UDC 66.096.5:778.53:537.531.

37. Taganov, I. N., Galkin, O. A. and P. G. Romankov, "Statistical Characteristics of Particle Motion in a Polydispersed Fluidized Bed", translated from, Teoretiche Osnovy Khimicheskoi Technologii, Vol. 1, No. 6, p. 825-830, November-December 1967, UDC 532.529.5.

38. Turner, D., "Turbulent and Fast Fluidization", PhD Dissertation, The City University of New York, December 1978.

39. van Swaaij, W. P. M., Buurman, C. and van Breugel, J. W., "Shear Stresses on the Wall of a Dense Gas-Solids Riser", CES, 25, 1818-1820 (1970).

40. Yang, Wen-ching, "A Criterion for Fast Fluidization", Pneumotransport 3 - third international conference on the pneumatic transport of solids in pipes, April, 7-9, 1976, paper E5.

41. Yerushalmi, J. and N. T. Cankurt, "High Velocity Fluidized Beds", Chemtech, 8, p. 564, (1978).

42. Yerushalmi, J., Turner, D. H. and A. M. Squires, "The Fast Fluid Bed", I.&E.C. Proc. Des. & Dev., 15, 47, (1976).

43. Yerushalmi, J., Memo to: Prof. A. Squires, Prof. R. Graff, Mr. A. Avidan, Mr. N. Cankurt. Subject: CMU's report on "Studies in support of recirculating bed reactors for the process of coal", October 27, 1978. ref. (6).

44. Youchou, L. and M. Kwauk, "The Dynamics of Fast Fluidization", in Fluidization, J. R. Grace and J. M. Matsen eds., Plenum Press, New York (1980).

45. Zenz, F. A., "Graphical Analysis of Fluid-Solids Systems in the Process Industries", in Fluidization, D. F. Othmer ed., 285-282, (1973).